



# NAVAL POSTGRADUATE SCHOOL

MONTEREY, CALIFORNIA

## THESIS

**PRELIMINARY DESIGN, SIMULATION, AND TEST OF THE ELECTRICAL  
POWER SUBSYSTEM OF THE TINYSCOPE NANOSATELLITE**

by

Chad William Melone

December 2009

Thesis Advisor:

Marcello Romano

Thesis Co-Advisor

Jim Horning

Second Reader:

Jim Newman

**Approved for public release; distribution is unlimited**

## REPORT DOCUMENTATION PAGE

Form Approved OMB No. 0704-0188

Public reporting burden for this collection of information is estimated to average 1 hour per response, including the time for reviewing instruction, searching existing data sources, gathering and maintaining the data needed, and completing and reviewing the collection of information. Send comments regarding this burden estimate or any other aspect of this collection of information, including suggestions for reducing this burden, to Washington Headquarters Services, Directorate for Information Operations and Reports, 1215 Jefferson Davis Highway, Suite 1204, Arlington, VA 22202-4302, and to the Office of Management and Budget, Paperwork Reduction Project (0704-0188) Washington DC 20503.

1. AGENCY USE ONLY (Leave blank)	2. REPORT DATE December 2009	3. REPORT TYPE AND DATES COVERED Master's Thesis
4. TITLE AND SUBTITLE Preliminary Design, Simulation, and Test of the Electrical Power Subsystem of the TINYSCOPE Nanosatellite		5. FUNDING NUMBERS
6. AUTHOR(S) Chad William Melone		
7. PERFORMING ORGANIZATION NAME(S) AND ADDRESS(ES) Naval Postgraduate School Monterey, CA 93943-5000		8. PERFORMING ORGANIZATION REPORT NUMBER
9. SPONSORING /MONITORING AGENCY NAME(S) AND ADDRESS(ES) N/A		10. SPONSORING/MONITORING AGENCY REPORT NUMBER
11. SUPPLEMENTARY NOTES The views expressed in this thesis are those of the author and do not reflect the official policy or position of the Department of Defense or the U.S. Government.		
12a. DISTRIBUTION / AVAILABILITY STATEMENT Approved for public release; distribution is unlimited		12b. DISTRIBUTION CODE

## 13. ABSTRACT (maximum 200 words)

Agile warfighter support, restrictive budgets, and complex adversaries are potential drivers for the United States to shift to smaller, simpler space payloads. Recent progress in miniaturized space system technologies may make it possible for nanosatellites to complement today's large, extremely high reliability, single mission satellites with smaller, less costly platforms that greatly reduce development, integration, and launch timelines. To fully realize this transition, Academia and Industry must make additional technological advances in all supporting satellite subsystems. This thesis focuses on the design, simulation, and hardware testing of a nanosatellite electrical power subsystem.

Thesis efforts centered on investigating the feasibility of using commercial off the shelf power management and distribution systems in a CubeSat-based design for a tactically useful earth-imaging satellite. Criteria were developed to select one power system from among those considered. Extensive analytical simulation, electrical testing, and environmental testing was conducted in the context of TINYSCOPE's mission parameters. Tactical Imaging Nano-sat Yielding Small-Cost Operations and Persistent Earth-coverage (TINYSCOPE) is an ongoing collaborative project of the Nanosatellite Advanced Concepts Laboratory and the Small Satellites and CubeSat Laboratory both at the Naval Postgraduate School in Monterey, California.

14. SUBJECT TERMS Electrical Power Subsystem, EPS, CubeSat, TINYSCOPE, solar cell, solar panel, IBPS, depth of discharge, power management and distribution , PMAD, vibration test, thermal-vacuum test		15. NUMBER OF PAGES 203
		16. PRICE CODE
17. SECURITY CLASSIFICATION OF REPORT Unclassified	18. SECURITY CLASSIFICATION OF THIS PAGE Unclassified	19. SECURITY CLASSIFICATION OF ABSTRACT Unclassified
		20. LIMITATION OF ABSTRACT UU

NSN 7540-01-280-5500

Standard Form 298 (Rev. 8-98)  
Prescribed by ANSI Std. Z39.18

THIS PAGE INTENTIONALLY LEFT BLANK

**Approved for public release; Distribution is unlimited**

**PRELIMINARY DESIGN, SIMULATION, AND TEST OF THE ELECTRICAL  
POWER SUBSYSTEM OF THE TINYSCOPE NANOSATELLITE**

Chad W. Melone  
Major, United States Air Force  
B.S., University of Central Florida, 1999

Submitted in partial fulfillment of the  
requirements for the degree of

**MASTER OF SCIENCE IN ASTRONAUTICAL ENGINEERING**

from the

**NAVAL POSTGRADUATE SCHOOL**  
**December 2009**

Author: Chad William Melone

Approved by: Marcello Romano  
Thesis Advisor

Jim Horning  
Thesis Co-Advisor

Jim Newman  
Second Reader

Knox Millsaps  
Chairman, Department of Mechanical and Astronautical  
Engineering

THIS PAGE INTENTIONALLY LEFT BLANK

## ABSTRACT

Agile warfighter support, restrictive budgets, and complex adversaries are potential drivers for the United States to shift to smaller, simpler space payloads. Recent progress in miniaturized space system technologies may make it possible for nanosatellites to complement today's large, extremely high reliability, single mission satellites with smaller, less costly platforms that greatly reduce development, integration, and launch timelines. To fully realize this transition, Academia and Industry must make additional technological advances in all supporting satellite subsystems. This thesis focuses on the design, simulation, and hardware testing of a nanosatellite electrical power subsystem.

Thesis efforts centered on investigating the feasibility of using commercial off the shelf power management and distribution systems in a CubeSat-based design for a tactically useful earth-imaging satellite. Criteria were developed to select one power system from among those considered. Extensive analytical simulation, electrical testing, and environmental testing was conducted in the context of TINYSCOPE's mission parameters. Tactical Imaging Nano-sat Yielding Small-Cost Operations and Persistent Earth-coverage (TINYSCOPE) is an ongoing collaborative project of the Nanosatellite Advanced Concepts Laboratory and the Small Satellites and CubeSat Laboratory both at the Naval Postgraduate School in Monterey, California.

THIS PAGE INTENTIONALLY LEFT BLANK

## TABLE OF CONTENTS

I.	INTRODUCTION.....	1
A.	PURPOSE.....	1
B.	PROJECT TINYSCOPE.....	2
1.	Mission Description.....	2
2.	Project Description.....	2
3.	Novel EPS Requirements.....	3
C.	PREVIOUS EPS WORK IN CUBESATS .....	5
II.	PRELIMINARY ELECTRICAL POWER SUBSYSTEM DESIGN .....	9
A.	EPS MODEL .....	9
B.	POWER REQUIREMENTS OF COMPONENTS.....	12
C.	LOAD PROFILES .....	17
1.	Normal Operations .....	17
2.	Launch.....	21
3.	Contingency Operations .....	22
D.	SOLAR ARRAY DESIGN .....	23
1.	Solar Array Size .....	23
2.	Cell Alternatives.....	26
3.	Radiation Impacts.....	27
4.	Thermal Impacts .....	29
5.	Manufacturing Impacts and Final Adjusted Efficiencies....	33
6.	Series and Parallel Requirements .....	34
E.	POWER MANAGEMENT AND DISTRIBUTION.....	36
1.	Alternatives Considered.....	36
2.	Selected System .....	41
3.	Solar Array Power Control.....	42
F.	BATTERY DESIGN.....	45
1.	PMAD Battery Requirements .....	45
2.	Alternative Batteries .....	48
3.	Depth of Discharge and Number of Cycles .....	49
G.	MASS BUDGET .....	52
III.	SIMULATION.....	55
A.	TOP LEVEL DESCRIPTION .....	55
B.	BASIC ORBIT .....	57
C.	SOLAR INTENSITY .....	61
D.	SOLAR ARRAY ORIENTATION & SOLAR CELL CONSTANTS....	62
E.	LOADS.....	63
F.	POWER MANAGEMENT AND DISTRIBUTION, EFFICIENCIES, AND BATTERY .....	64
G.	PARAMETER FILE .....	67
H.	RESULTS.....	67
I.	SIMULATION CONCLUSION .....	71

<b>IV.</b>	<b>HARDWARE TESTING .....</b>	<b>73</b>
A.	INTRODUCTION.....	73
B.	DETAILED HARDWARE DESCRIPTION.....	74
C.	SOLAR PANEL COMPATIBILITY TEST.....	82
D.	BATTERY COMPATIBILITY TEST.....	85
E.	IBPS EFFICIENCIES .....	92
F.	BASELINE FUNCTIONAL TEST AND CONTROL SOFTWARE DESCRIPTION.....	95
1.	Overview.....	95
2.	Procedure and Timeline .....	97
3.	Proper Operation .....	100
G.	ENVIRONMENTAL TESTING.....	101
1.	Overview.....	101
2.	Vibration Testing .....	104
3.	Thermal-Vacuum Testing.....	110
H.	HARDWARE TESTING SUMMARY .....	124
<b>V.</b>	<b>RECOMMENDATIONS AND CONCLUSIONS.....</b>	<b>127</b>
<b>APPENDIX A.</b>	<b>SOLAR ARRAY POWER EQUATION .....</b>	<b>131</b>
<b>APPENDIX B.</b>	<b>EPS LOAD DETAIL .....</b>	<b>133</b>
<b>APPENDIX C.</b>	<b>SOLAR CELL SPECIFICATION SHEETS .....</b>	<b>145</b>
<b>APPENDIX D.</b>	<b>SOLAR CELL PREDICTED TEMPERATURE .....</b>	<b>149</b>
<b>APPENDIX E.</b>	<b>SUMMARY OF UNITED NATIONS T-TESTS .....</b>	<b>151</b>
<b>APPENDIX F.</b>	<b>EPS SIMULATION PARAMETER FILE .....</b>	<b>153</b>
<b>APPENDIX G.</b>	<b>SOLAR INTENSITY VERSUS BETA MATLAB CODE.....</b>	<b>157</b>
<b>APPENDIX H.</b>	<b>EFFICIENCY MEASUREMENTS.....</b>	<b>159</b>
<b>APPENDIX I.</b>	<b>FUNCTIONAL TEST SOFTWARE &amp; EQUIPMENT .....</b>	<b>163</b>
<b>APPENDIX J.</b>	<b>VIBRATION TEST RESULTS .....</b>	<b>165</b>
<b>APPENDIX K.</b>	<b>THERMAL-VACUUM TEST PROCEDURES .....</b>	<b>167</b>
<b>APPENDIX L.</b>	<b>THERMAL-VACUUM TEST NOTES.....</b>	<b>173</b>
<b>LIST OF REFERENCES.....</b>		<b>175</b>
<b>INITIAL DISTRIBUTION LIST .....</b>		<b>181</b>

## LIST OF FIGURES

Figure 1.	Notional CubeSat Mechanical Drawing From [8].....	4
Figure 2.	Possible TINYCOPE configurations: 5U on far left; 2U x 3U on far right, From [2] and [5] .....	4
Figure 3.	Conceptual drawing of QuakeSat, From [12].....	6
Figure 4.	Simplified EPS Equivalent Circuit From [16].....	10
Figure 5.	TINYSCOPE EPS Equivalent Circuit.....	12
Figure 6.	TINYSCOPE Representative Power Profile .....	20
Figure 7.	TINYSCOPE Imaging Power Profile, 0 to 650 Seconds .....	20
Figure 8.	TINYSCOPE Sun Soak & Warm-up Power Profile, 586 to 5283 Seconds .....	21
Figure 9.	P-POD, Post Deployment From [17].....	22
Figure 10.	TINYSCOPE, Preliminary Structural Design Modified After [5] .....	25
Figure 11.	Exploded View of TINYSCOPE Preliminary Structural Design After [5] .....	25
Figure 12.	Solar Panel V-I Characteristic vs. Irradiance From [23].....	44
Figure 13.	Solar Panel V-I Characteristic vs. Temperature From [23] .....	44
Figure 14.	IBPS OEM Batteries With 18650 Cell.....	46
Figure 15.	Depth-of-Discharge versus Cycle Life for NiCd & NH <sub>2</sub> From [15] .....	50
Figure 16.	Integrated Matlab/Simulink© EPS Model After [16] .....	56
Figure 17.	Geometric Relationship Between Earth and Spacecraft.....	58
Figure 18.	Illustration of Beta Angle.....	59
Figure 19.	Solar Intensity and Beta Angle versus Day of Year .....	60
Figure 20.	Solar Unit Vector in Spacecraft Body Frame After [16].....	63
Figure 21.	Contents of “orientation” Block .....	63
Figure 22.	Contents of Load Subsystem Block.....	64
Figure 23.	EPS Simulation Output, Case 1 .....	68
Figure 24.	EPS Simulation Output, Case 2 .....	69
Figure 25.	IBPS Components After [33] .....	75
Figure 26.	Base board Power Controller, BB-04FR, Top Down View .....	77
Figure 27.	BB-04 Drawing From [33] .....	78
Figure 28.	DC to DC Converter, DC-123SR, Top Down View .....	79
Figure 29.	DC-123 Drawing From [33].....	79
Figure 30.	Solar Panel Test Setup.....	83
Figure 31.	Detail View of Solar Panel Test Setup, IBPS on Left.....	83
Figure 32.	Battery Current During Solar Panel Test .....	84
Figure 33.	Graphical Battery Comparison .....	86
Figure 34.	Representative Load Bank .....	87
Figure 35.	Custom Battery Harness .....	88
Figure 36.	Battery Compatibility Test, Top-Level Setup .....	88
Figure 37.	Battery Compatibility Test, NH2054HD26 “Medium Battery” .....	90
Figure 38.	Battery Compatibility Test, ND2054HD26 “Small Battery” .....	91
Figure 39.	TINYSCOPE EPS Equivalent Circuit With Efficiency Measurements.	93

Figure 40.	Baseline Functional Test Overview Diagram.....	96
Figure 41.	Baseline Functional Test Physical Setup.....	97
Figure 42.	OS_Tester1.py Control Software Screen Shot .....	98
Figure 43.	Flow of Qualification Testing for Components After [15].....	101
Figure 44.	Minimum Random Vibration Spectrum, Vehicle Acceptance Tests From [42] .....	105
Figure 45.	Component Minimum Workmanship Random Vibration Test Levels From [41] .....	106
Figure 46.	IBPS on Vibration Test Stand, Top Down View.....	107
Figure 47.	IBPS on Vibration Test Stand, Side View .....	108
Figure 48.	Post Vibration Functional Test, 23 October 2009 .....	109
Figure 49.	Unit Test Temperature Ranges and Margins From [42] .....	110
Figure 50.	Payload Test Temperature Ranges From [42] .....	111
Figure 51.	Thermal-Vacuum Temperatures From [41] .....	112
Figure 52.	IBPS in Thermal-Vacuum Chamber .....	114
Figure 53.	Temperature Profile, 28 October 2009 TVAC Test.....	115
Figure 54.	Functional Test Results, First Thermal-Vacuum Test.....	117
Figure 55.	Functional Test Results, First Thermal-Vacuum Test, 0 to 2,000 Seconds .....	118
Figure 56.	Functional Test Results, First Thermal-Vacuum Test, 9,500 to 12,000 Seconds .....	120
Figure 57.	Temperature Profile, 17 November 2009 TVAC Test.....	121
Figure 58.	IBPS in Thermal-Vacuum Chamber, Second Test .....	122
Figure 59.	Functional Test, Second Thermal Vacuum Test.....	123
Figure 60.	Solar Panel Configuration From [16] .....	149

## LIST OF TABLES

Table 1.	TINYSCOPE Equipment Summary .....	16
Table 2.	Available Solar Cells.....	27
Table 3.	Summary of 1 MeV Equivalent Electron Fluence (cm <sup>-2</sup> ) at Solar Max.....	28
Table 4.	Summary of 1 MeV Equivalent Electron Fluence (cm <sup>-2</sup> ) at Solar Min.	28
Table 5.	Predicted Solar Cell Temperatures.....	31
Table 6.	Solar Cell Adjusted Efficiencies .....	32
Table 7.	Final Adjusted Solar Cell Efficiencies .....	34
Table 8.	Series and Parallel Requirements .....	35
Table 9.	TINYSCOPE EPS Mass Budget.....	53
Table 10.	IBPS Component Operating Temperature Limits .....	81
Table 11.	Test Solar Panel Specifications .....	82
Table 12.	Battery Data Comparison .....	86
Table 13.	EPS Efficiencies .....	94

THIS PAGE INTENTIONALLY LEFT BLANK

## LIST OF ACRONYMS AND ABBREVIATIONS

$A_{sa}$	Area of a solar array
$F_a$	The product of multiple radian measured angles describing how much of the solar array's area is pointing at the earth's albedo
$F_e$	The product of multiple radian measured angles describing how much of the solar array's area is pointing at the earth
$f_p$	Packing factor of the solar array
$p_0$	Power per unit area of a solar array at beginning of life
$P_1$	Power of load 1.
$P_2$	Power of load 2.
$P_3$	Power of load 3.
$P_{bc}$	Power of the battery in charge
$P_{bd}$	Power of the battery in discharge
$p_{EOL}$	Power per unit area of a solar array at end of life
$P_L$	Power of the load.
$P_{Lc}$	Power of the load during charging.
$P_{\max}$	Maximum power rating of test solar panel
$P_{sa}$	Power of the solar array
$T_d$	Time of battery in discharge
$T_c$	Time of battery in charge
$\alpha_B$	Absorptivity of backside of solar array
$\alpha_F$	Absorptivity of front side of solar array
$\beta$	Beta angle; angle between a satellite orbit plane and the subsolar point
$\Delta T$	Temperature difference
$\varepsilon_B$	Emissivity of backside of solar array
$\varepsilon_F$	Emissivity of front side of solar array

$\lambda$	Earth flux incidence angle on a solar array; typically on the backside of a solar array
$\eta$	Solar cell nominal efficiency
$\eta_1$	Solar array to load line efficiency
	Base board charge efficiency.
$\eta_2$	Solar array to load line efficiency.
	Base-board discharge efficiency.
$\eta_3$	DC to DC converter efficiency for load voltage 1.
$\eta_4$	DC to DC converter efficiency for load voltage 2.
$\eta_5$	DC to DC converter efficiency for load voltage 3.
$\eta_6$	DC to DC converter efficiency for load voltage 4.
$\eta_c$	Charge efficiency of the battery.
$\eta_{cell}$	Nominal efficiency of a solar cell
$\eta_d$	Discharge efficiency of the battery.
$\eta_p$	Nominal efficiency of the power controller base board.
$\mu$	A constant with the value 398,600 km <sup>3</sup> /s <sup>2</sup>
$\nu$	Angular measure of a satellite's position in orbit
$\rho$	Angular radius of the earth at a particular altitude
$\sigma$	Stefan-Boltzman constant
$\phi$	Sun incidence angle on solar array
$\omega$	Angular velocity of a rotating satellite
$\Omega$	Symbol for Ohms, a measure of resistance
$^\circ$	A measure of temperature or angle
\$	United States Dollar
£	Great British Pound
1U	One Cube (1 x 1) CubeSat
2U x 3U	Six Cube (2 x 3) CubeSat
3U	Three Cube (3 x 1) CubeSat
5U	Five Cube (5 x 1) CubeSat
A	Ampere

a	Earth albedo factor; multiplied by Earth power flux
ADCS	Attitude Determination and Control Subsystem
$a_g$	Gravitational acceleration
Ah	Ampere-hour
AM0	Air Mass Zero
$a_r$	Radial component of linear acceleration of a satellite
As	Ampere-second
ATJ	Advanced Space Solar Cell manufactured by Emcore
ATJM	Advanced Space Solar Cell manufactured by Emcore
ATX	Advanced Technology Extended; standard pin definition for personal computer motherboards
BOL	Beginning of Life; used in describing solar cell efficiency
BTJ	Space Solar Cell manufactured by Emcore
BTJM	Space Solar Cell manufactured by Emcore
C	Celsius
	Charge Rate
C&DH	Command and Data Handling Subsystem
cm	Centimeter
COTS	Commercial Off The Shelf
CS	Communications Subsystem
CubeSat	Cube Satellite
dB	Decibel
DC	Direct Current
DET	Direct Energy Transfer
DOD	Depth of Discharge
E	Earth power flux; 326 W/m <sup>2</sup>
e	Eccentricity of a satellite's orbit
ELF	Extremely Low Frequency
EMC	Electromagnetic Compatibility
EOL	End Of Life; used in describing solar cell efficiency
EPS	Electrical Power Subsystem
ESA	European Space Agency

<b>g</b>	Grams
	Acceleration of gravity at sea level; 9.8m/s <sup>2</sup>
<b>G</b>	Gravitational Constant
	Acceleration of gravity at sea level; 9.8 m/s <sup>2</sup>
<b>GaAs</b>	Gallium Arsenide
<b>GEVS</b>	General Environmental Verification Standards
<b>GHz</b>	Gigahertz (1 x 10 <sup>9</sup> cycles per second)
<b>GPS</b>	Global Positioning System
<b>g<sub>rms</sub></b>	Root mean square value of the acceleration of gravity at sea level
<b>h</b>	Hours
	Altitude of a satellite's orbit above R <sub>E</sub>
<b>Hz</b>	Hertz or cycles per second
<b>i</b>	Inclination of a satellite's orbit
<b>IBPS</b>	Integrated Battery and Power System
<b>IC</b>	Integrated Circuit
<b>I<sub>mp</sub></b>	Current of a solar cell at its maximum power point
<b>IMU</b>	Inertial Measurement Unit
<b>Inc</b>	Incorporated
<b>IPDR</b>	Integrated Power and Data Ring
<b>I<sub>sc</sub></b>	Solar cell current at short circuit condition
<b>ITJ</b>	Improved Triple Junction solar cell manufactured by Spectrolab
<b>J</b>	Used to specify a particular pin on a printed circuit board
<b>K</b>	Kelvin
<b>km</b>	Kilometers
<b>LBS</b>	Pounds
<b>LCDR</b>	US Navy Lieutenant Commander
<b>LLC</b>	Limited Liability Corporation
<b>LT</b>	US Navy Lieutenant
<b>Ltd</b>	Limited
<b>m</b>	Meter
	Mass of a body orbiting the earth
<b>M</b>	Mass of the earth

mA	milli-ampere
MeV	Million electron volts
min	Minutes
mm	Millimeter
MPT	Minimum Predicted Temperature Maximum Predicted Temperature
mW	milli-watt
NH <sub>2</sub>	Nickel Hydrogen
NiCd	Nickel Cadmium
NPS	Naval Postgraduate School
NVRAM	Non Volatile Random Access Memory
OCV	Open Circuit Voltage
OEM	Original Equipment Manufacturer
PCB	Printed Circuit Board
PMAD	Power Management and Distribution
P-POD	Poly Picosatellite Orbital Deployer
PPT	Peak Power Trackign
PV	Photovoltaic
r	Orbit radius of a satellite
RAAN	Right Ascension of the Ascending Node
R <sub>E</sub>	Average radius of the earth; 6378.15 km
S	Solar constant; 1,322 W/m <sup>2</sup> at summer solstice, 1,414 W/m <sup>2</sup> at winter solstice
S.A.	Société anonyme; a type of corporation in Europe
SA	Solar array
SACI	Charge Control & Solar Array Interface Card manufactured by Broadreach Engineering
sec	Seconds
SEU	Single Event Upset
SMS	Structures and Mechanisms Subsystem
SOC	State of charge of a battery, i.e. how much charge a battery has
SPA	Space Plug and Play

SPENVIS	Space Environment Information System
SSTL	Surrey Satellite Technology, Ltd.
TCS	Thermal Control Subsystem
TINYSCOPE	Tactical Imaging Nano-sat Yielding Small-Cost Operations and Persistent Earth-coverage
T-Test	A series of battery tests prescribed by the governing body of the UN
TVAC	Thermal-vacuum
UN	United Nations
UTJ	Ultra Triple Junction solar cell manufactured by Spectrolab
V	Volt
Vibe	Vibration
$V_{mp}$	Voltage of a solar cell at its maximum power point
$V_{oc}$	Solar cell voltage at open circuit condition
W	Watt
Wh	Watt-hour
XTJ	NeXt Triple Junction solar cell manufactured by Spectrolab
ZTJ	Space Solar Cell manufactured by Emcore
ZTJM	Space Solar Cell manufactured by Emcore

## ACKNOWLEDGMENTS

The author would like to thank the following:

- The National Reconnaissance Office for financial support by way of Professor Marcello Romano.
- Professor Marcello Romano for your patience, understanding, and support throughout this thesis work. It was a pleasure to be on the TINYSCOPE team!
- Professor Rudy Panholzer for the outstanding support of your Small Satellite Laboratory. The Space Systems students are very lucky to have such an ardent supporter...thank you!
- Jim Horning, Ron Phelps, Dan Sakoda, and David Rigmaiden...without your tireless assistance and guidance I would have produced exactly squat. You guys added immensely to my learning.
- Professor Barry Leonard for your energy, encouragement, and effort. I thoroughly enjoyed your classes. Thank-you for your invaluable feedback on this thesis.
- Professor Jim Newman for your very thorough review of my thesis drafts...it is much better as a result!
- Beki, Dylan, Tyler, and Connor...it is hard to put into words how much you mean to me and how much inspiration you gave me throughout our time at NPS. You are all very special. Even though our time in Monterey has ended, I know truly amazing things await us in the future.

THIS PAGE INTENTIONALLY LEFT BLANK

## I. INTRODUCTION

### A. PURPOSE

The purpose of this thesis is to advance the design of an Electrical Power Subsystem (EPS) for a very small satellite project. Under the auspices of Dr. Marcello Romano's Nanosatellite Advanced Concepts Laboratory, TINYSCOPE (Tactical Imaging Nano-Satellite Yielding Small Cost Operations for Persistent Earth Coverage) was first proposed by [1] and further studied by [2] and [3] as a three-axis stabilized, low earth orbiting, electro-optical imager based on an extension of the CubeSat form factor. The project's design and operations philosophy centers on potentially using a constellation of many relatively inexpensive satellites in lieu of a few or one large, expensive satellite. This approach relies heavily on simple design, readily available commercial off the shelf (COTS) components, and inexpensive launch on a per satellite basis.

This strategy presents several unique challenges to the EPS portion of the project. First, TINYSCOPE has much higher power requirements than any previous CubeSat system. This has obvious implications for all facets of the EPS including power collection, energy storage, and power management and distribution (PMAD). Second, detailed market research revealed that no space rated COTS power management and distribution components exist for a CubeSat with TINYSCOPE's power requirements. That could lead to an expensive new design that could slow down the entire project.

This thesis endeavors to answer the challenges laid out above through design, simulation, and hardware component testing. The design and simulation portions are primarily an analytical-numerical effort while the testing portion details the rationale, physical setup, resulting data, and conclusions from testing actual hardware. The intent is to establish whether the selected hardware can

meet the requirements laid out in design and simulation. The outcome of this work can then be extended to increasing levels of detail to support a prototype unit in the very near future.

## **B. PROJECT TINYSCOPE**

### **1. Mission Description**

The overall mission concept of TINYSCOPE is to provide useful imagery directly to in-theater war fighters using a very small and relatively inexpensive satellite. An argument is made by Blocker in [2] that high-demand, low-density space-based imagers are not readily available to small tactical units. Furthermore, it is suggested that the very high-resolution imagery national assets can provide is not generally required by tactical field units. Because of these reasons, tactical units would benefit from more regular access to “good enough” imagery. While the threshold of quality for tactically useful imagery is debatable, the overall idea is that many, perhaps hundreds of, TINYSCOPE satellites could provide a near real-time stream of battlefield imagery thus affording tactical combat units a decisive upper hand. In particular, according to the preliminary study reported in [2], about 350 TINYSCOPE satellites would be needed to obtain persistent coverage of the world from 500 km of altitude, while about 60 would provide an average revisit time of about 30 minutes in daylight.

### **2. Project Description**

Beyond the debate surrounding the definition of the term “tactically useful,” implementing the mission described above presents several budgetary and technical challenges. These challenges are highly interrelated, i.e. as budget is increased, technical challenges become more solvable. The intent of Project TINYSCOPE is to design, build, test, and operate a low earth-orbiting (LEO) proto-flight unit using the following guiding principles:

- Use COTS components or slightly modified COTS to the maximum extent possible.
- Plan on a short mission life (one year or less).
- Use a very small, very inexpensive CubeSat spacecraft bus (described in more detail below).
- Use a bulk launch system to populate the constellation (the satellite's small mass and volume enable launching many satellites simultaneously).

Project TINYSCOPE is currently in Phase 2 of 4 phases. Phase 1 consisted of two feasibility studies performed by two NPS students, LCDR J. Allen Blocker and LT Chance Litton. LCDR Blocker showed that the concept for the bus and attitude control subsystem was viable while LT Litton demonstrated that the optical payload was feasible in the context of the current state of technology. Phase 2 will culminate with an engineering design unit demonstrating the form, fit, and function of the individual subsystems integrated together. A proto-flight unit will be designed, built, tested, launched, and operated in Phase 3. The proto-flight unit may or may not be in the final intended TINYSCOPE orbit because of available launch opportunities. The Department of Defense's Space Test Program launch service will be used since TINYSCOPE is Space Experiment Review Board approved [4]. Finally, Phase 4 could be the full deployment of a constellation of about 60 individual TINYSCOPE satellites. TINYSCOPE's notional operational orbit will be sun-synchronous at 500 km in altitude with a threshold mission life of one year [5].

While this thesis focuses on the EPS, [6] extends the work of [3] on payload design, [7] develops critical elements of the attitude determination and control subsystem, [5] concentrated on overall systems engineering, and as of this writing Army Major Christopher Turner is working as the student project manager.

### **3. Novel EPS Requirements**

TINYSCOPE's design is based on the Cube Satellite (shortened to "CubeSat") standard [8]. This standard sets volume, mass, structural, electrical,

operational, and testing requirements. A so-called 1U configuration is shown in Figure 1. The 1U has dimensions of 10 cm x 10 cm x 10cm and a mass of less than 1 kg. A 3U configuration is also described in the standard. The 3U is 10 cm in length and width and 30 cm in height – this is essentially three 1Us stacked on top of each other.

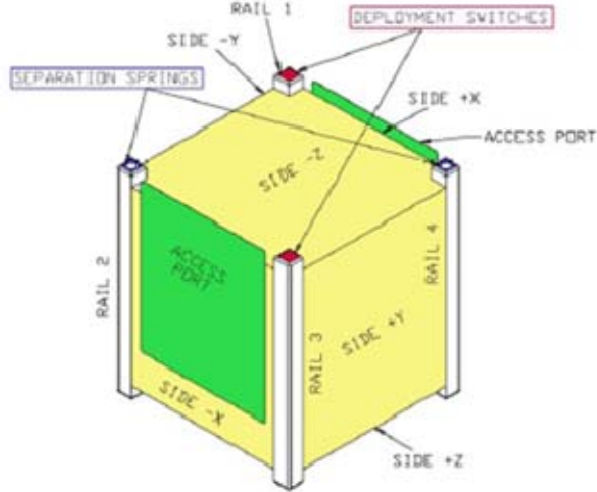


Figure 1. Notional CubeSat Mechanical Drawing From [8]

While TINYSCOPE's present design cannot fit in a 3U form factor, there are several members of the nano-satellite community pushing for a 5U and a 2U x 3U configuration consistent with TINYSCOPE's proposed configuration. The 5U would be 10 cm x 10 cm x 50 cm and the 2U x 3U would be 10 cm x 20 cm x 30 cm (also known as the "Six Pack"). Figure 2 shows several candidate configurations.



Figure 2. Possible TINYSCOPE configurations: 5U on far left; 2U x 3U on far right, From [2] and [5]

The most important design implications for a satellite of this size are the limited mass, volume, and power generation capabilities of a five to six liter right rectangular cylinder. The solar power collection capabilities will be limited and the thermal environment for the solar cells and the batteries may be a concern.

Another important design consideration is the radiation environment. While displacement damage is not expected to be a significant concern for solar cells or integrated circuits in the design, expected LEO single event effects and their impacts to COTS, typically designed for terrestrial applications, must be managed.

### C. PREVIOUS EPS WORK IN CUBESATS

A fair amount of work has been accomplished in the field of electrical power subsystems for CubeSats. While the CubeSat standard was first introduced in 1999 [9], [10] documented that there had been 24 launches by November 2008. Since that time, [11] documents several more launches. Not all of these systems are pertinent for TINYSCOPE's EPS design, however, because many previous CubeSats are in a 1U configuration that tumbles at unknown rates in multiple axes. These CubeSats are not three axis stabilized and subsequently are not able to support demanding load requirements.

Several 3U CubeSat systems that are important to consider in the design of TINYSCOPE's EPS are QuakeSat, GeneSat, MAST, Delfi-C3, CanX-2, and Cute 1.7+APD II. Particularly interesting are QuakeSat and Delfi-C3 because of their deployable solar arrays. Within this subset, QuakeSat additionally had a rudimentary form of passive stabilization using the Earth's magnetic field lines to maintain attitude [12]. While not as sophisticated as TINYSCOPE's planned use of reaction wheels or possibly control moment gyroscopes, QuakeSat's design and configuration can provide several insights into overall EPS design.

QuakeSat was designed and built as a joint university and commercial collaboration between Stanford University's Space Systems Development Laboratory and QuakeFinder LLC. Its primary mission was to detect, record, and

downlink extremely low frequency (ELF) radio waves caused by earth's shifting plates immediately surrounding an earthquake [12]. Figure 3 shows QuakeSat's basic configuration.

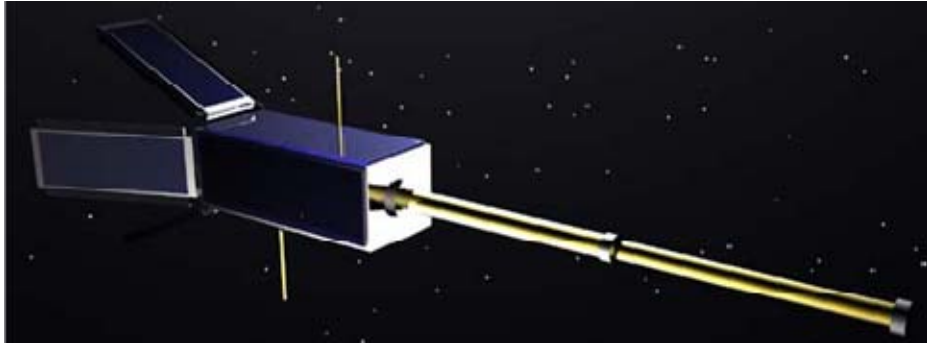


Figure 3. Conceptual drawing of QuakeSat, From [12]

As indicated in Figure 3, QuakeSat had body mounted, as well as deployable solar arrays. The wings, each having solar arrays on both sides, are offset by 150 degrees to maximize solar collection. The twelve 22.9% nominal efficiency GaAs solar arrays (four on body, eight on wings) were expected to provide between 7.9 W and 19.05 W of power depending on the season. Together with the two series, two parallel strings of lithium ion batteries, QuakeSat's EPS supported loads between 2.8 W at minimum and 12.6 W at maximum.

QuakeSat's EPS was wholly derived from COTS components. Of particular note is the fact that none of QuakeSat's components were space-rated or space-qualified [13]. To partially mitigate this limitation, several reset mechanisms were incorporated to deal with single event effects. These mechanisms were successfully used during QuakeSat's approximately two year mission (June 2003 to June 2005) [14].

QuakeSat's success with unmodified COTS components led to discussion among those on the TINYSCOPE team when this approach would be appropriate and what steps could be taken to mitigate some of the risk associated with this strategy. This discussion led to the work documented in the subsequent

chapters of this thesis. Chapter II documents the overall design of TINYSCOPE's EPS, Chapter III investigates a simulation based on Chapter II's design, and Chapter IV documents the hardware characterization and testing accomplished to mitigate some of the risk related to using a COTS approach for the EPS.

THIS PAGE INTENTIONALLY LEFT BLANK

## II. PRELIMINARY ELECTRICAL POWER SUBSYSTEM DESIGN

### A. EPS MODEL

A simplified EPS model based on constant loads developed by [15] is used as the starting point from which TINYSCOPE's model is created. The equations in the following discussion are taken from [15] while [16] elaborated on these equations by developing Figure 4. The EPS model is predicated on a single orbit energy balance equation. In this arrangement, the amount of energy taken out of the batteries in a single orbit must be replaced on that same orbit during the satellite's non-eclipse period. This is stated mathematically as,

$$P_{bd} \times T_d \leq P_{bc} \times T_c \quad (1)$$

Equation 1 states that the product of charge time ( $T_c$ ) and the power of the battery during charge ( $P_{bc}$ ) must be greater than or equal to the product of the discharge time ( $T_d$ ) and the power of the battery during discharge ( $P_{bd}$ ). Because the batteries may be in a net state of either charge or discharge, but not both, the sum of  $T_d$  and  $T_c$  is the total orbit time. A basic steady-state EPS model assumes that the power collected during the satellite's daylight period provides all the power necessary to supply the loads during the daylight period as well as fully charging the batteries from their use during eclipse. With this assumption, Figure 4 represents a general simplified equivalent circuit for an EPS.

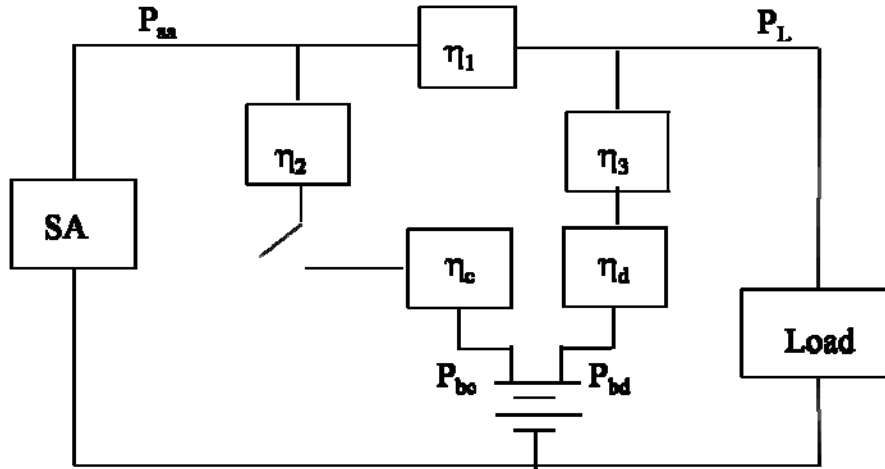


Figure 4. Simplified EPS Equivalent Circuit From [16]

The power to the load is denoted  $P_L$  while the power from the solar array is denoted  $P_{sa}$ . The efficiencies represented on the diagram are battery charge efficiency ( $\eta_c$ ), battery discharge efficiency ( $\eta_d$ ), line efficiency from the solar array to the loads ( $\eta_1$ ), line efficiency from the solar array to the battery ( $\eta_2$ ), and line efficiency from the battery to the load ( $\eta_3$ ). Efficiencies resulting from regulation and switching are not included at this time. Recalling the earlier assumption that the power collected by the solar array ( $P_{sa}$ ) must be sufficient to simultaneously charge the batteries ( $P_{bc}$ ) and supply the load during charging ( $P_{Lc}$ ), Equation 2 applies,

$$P_{sa} = \frac{P_{Lc}}{\eta_1} + \frac{P_{bc}}{\eta_2 \eta_c} \quad (2)$$

One interpretation of Equation 2 is that the solar array must provide a higher level of power than just the sum of the power of the load and the power to charge the battery. The solar array power must actually be higher than this sum because of the power that is lost due to current flowing in resistive lines and the power that is lost putting energy into and taking energy out of batteries. Solving for  $P_{bc}$  results in,

$$P_{bc} = P_{sa}\eta_2\eta_c - P_{Lc} \frac{\eta_2\eta_c}{\eta_1} \quad (3)$$

From Figure 4 it can be seen that the power of the load during discharge flows from the battery and is written as,

$$P_{bd} = \frac{P_{Ld}}{\eta_d\eta_3} \quad (4)$$

Equation 4 assumes that the batteries discharge only in eclipse, i.e. when no sunlight is available to partially offset the power required from the batteries. This assumption will be relaxed later. Substituting Equations (3) and (4) into Equation (1) and solving for  $P_{sa}$  results in the required power of the solar arrays,

$$P_{sa} = \frac{\left( \frac{P_{Ld}T_d}{\eta_2\eta_c\eta_d\eta_3} + \frac{P_{Lc}T_c}{\eta_1} \right)}{T_c} \quad (5)$$

Much of this thesis focuses on finding higher resolution estimates for each of the parameters in Equation 5. Chapter II, Sections B and C, go into detail regarding the power required by the load. Chapter III develops justification for the time in discharge and charge. These values are not the same as the time in eclipse and sunlight for TINYSCOPE because of the slewing and subsequent reduced solar collection during its ten-minute imaging period. The efficiencies shown in Equation 5 depend upon the structure of the EPS equivalent circuit shown in Figure 4. Figure 5 was developed to show a more accurate representation of TINYSCOPE's equivalent circuit. Regulation and switching efficiencies are now included as  $\eta_1, \eta_2, \eta_p, \eta_3, \eta_4, \eta_5$ . The only line efficiency is now  $\eta_s$ . Because the DC to DC converter is very close proximity to the DC to DC converter, no line efficiency is necessary. Additionally, although line efficiencies are not shown in Figure 5, they are assumed to be 0.90. Justification for the efficiency values chosen are more fully in Chapter IV, Section D.

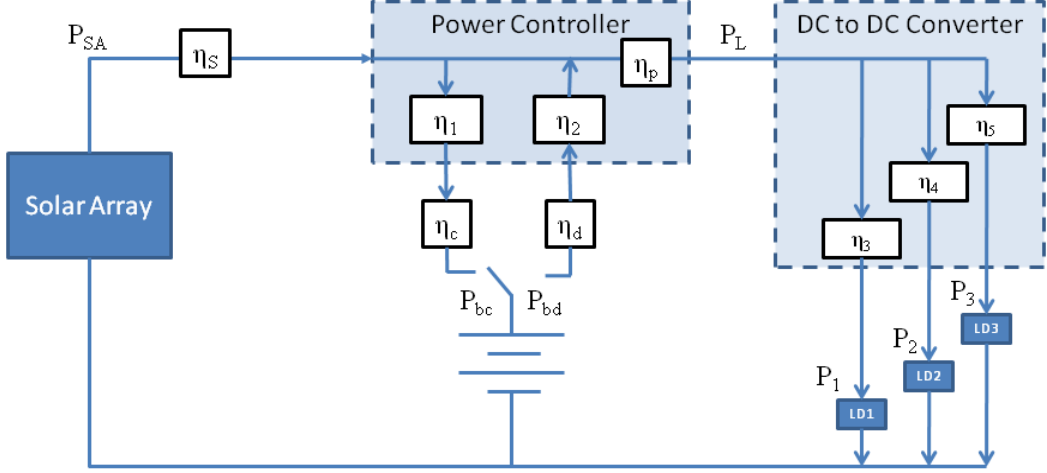


Figure 5. TINYSCOPE EPS Equivalent Circuit

Chapter II, Sections E and F present rationale for Figure 5. Following a similar process as outlined for translating Figure 4 to Equations (2) through (5), Equation 6 can be derived from Figure 5. A full development is shown in Appendix A.

$$P_{SA} \geq \frac{P_L T_d}{\eta_p (\eta_s \eta_1 \eta_c \eta_d \eta_2 T_c + \eta_s T_d)} + \frac{P_L T_c}{\eta_p \left( T_c + \frac{\eta_s}{\eta_1 \eta_c \eta_d \eta_2} T_d \right)}; \quad \text{where } P_L = \frac{P_1}{\eta_3} + \frac{P_2}{\eta_4} + \frac{P_3}{\eta_5} \quad (6)$$

Equation 6 still assumes single orbit energy balance but it allows for multiple efficiencies present in a regulated EPS and it relaxes the requirement that the batteries are only discharged during eclipse. However, Equation 6 does not account for the detrimental effects of shadowing, thermal impacts, radiation impacts, or sun incidence angle on solar cells. Subsequent sections expand upon these issues with a complete model presented in Chapter III.

## B. POWER REQUIREMENTS OF COMPONENTS

The power requirements of TINYSCOPE as a whole depend upon the power requirements of the individual components and how the components are used together for operations as depicted graphically in a load profile. Together with the efficiency information of the EPS components, this data is used to determine critical elements of the EPS design, like required solar array and

battery size. It is important to note that the list of components, their associated power requirements, and load profiles are all subject to change based on TINYSCOPE's evolving design and verification of manufacturers' reported specifications. Component and subsystem power requirements, including level of voltage and current, must be kept up to date throughout the design process so that accurate information can be input into the simulation on an iterative basis.

TINYSCOPE will have the standard set of satellite subsystems: payload, structures and mechanisms subsystem (SMS), communications subsystem (CS), electrical power subsystem (EPS), thermal control subsystem (TCS), attitude determination and control subsystem (ADCS), and command and data handling subsystem (C&DH). While some subsystem designs are advanced to the point where components have been chosen, other subsystems are not as advanced. In the latter case, representative voltages and currents are used.

As of the time of this writing, the exact set of payload equipment had not been chosen. However, so that a preliminary EPS design could proceed, the power requirements of a scientific/industrial camera were used as an approximation for the payload. The SMS consists of the main 2U by 3U CubeSat structure along with the deployable solar arrays. At this time, the SMS has no power requirements. A Microhard 2.4 GHz radio model number IP2421 makes up the CS. The radio manufacturer recommended using power requirements of a similar radio (model number Nano920) because the IP2421 is a new design. A small beacon may be included in the CS in the future but is not presently included in the EPS power baseline. Unlike the other subsystems, EPS power requirements are not static. They vary as the load varies. For this reason, efficiencies are used in lieu of set numbers. Efficiencies of the EPS depend on the components used and will be discussed in detail in Chapter IV, Section D. Similar to the payload, a final set of equipment has not been determined for the TCS. However, a Texas Instruments (TI) Mixed Signal Processor (MSP) model number 430 (MSP430) and a 2.5 W Minco commercial grade polyimide heater

strip are used as representative components. As of the time of this writing, the ADCS subsystem was baselined with the following set of components:

- (1) Novatel Global Positioning System (GPS) model number OEMV-1
- (1) Analog Devices Inertial Measurement Unit (IMU) model number ADIS16400.
- (1) AeroAstro Miniature Star Tracker
- (1) Sinclair Interplanetary sun sensor model number SS-411
- (3) Sinclair Interplanetary Nanosatellite Reaction Wheels model number RW-0.03-4
- (1) TI MSP430 microcontroller

The C&DH will use a TI MSP430 similar to the TCS and ADCS. Table 1 shows a summary of the power requirements of the above components.

Name	Model	Manufacturer	Voltage (V)	Current (A)	Power (W)	Note
C&DH Controller	MSP430	TI	3.3	$336 \times 10^{-6}$	$1.11 \times 10^{-3}$	Active Mode. Calculated from formula on page 13 of data sheet.
				$70 \times 10^{-6}$	$2.31 \times 10^{-4}$	Low-power Mode 0. Current at 3 V.
ADCS Controller	MSP430	TI	3.3	$336 \times 10^{-6}$	$1.11 \times 10^{-3}$	Active Mode. Calculated from formula on page 13 of data sheet.
				$70 \times 10^{-6}$	$2.31 \times 10^{-4}$	Low-power Mode 0. Current at 3 V.
IMU	ADIS16400	Analog Devices	5	0.07	0.35	Normal Mode
				$600 \times 10^{-6}$	$3 \times 10^{-3}$	Sleep Mode
Star Tracker	Miniature Star Tracker	AeroAstro	5	0.4	2	Voltage & current estimated from given power
GPS Receiver	OEMV-1	Novatel	3.3	$303 \times 10^{-3}$	1	Current estimated from given voltage and given power.
Sun Sensor	SS-411	Sinclair Interplanetary	5	$5 \times 10^{-3}$	$25 \times 10^{-3}$	Average power. Voltage assumed.
				$15 \times 10^{-3}$	$75 \times 10^{-3}$	Peak power
Reaction Wheels	RW-0.03-4	Sinclair Interplanetary	5	0.4	2	Full Torque. Current estimated from given voltage and given power.
				0.02	0.1	2000 RPM Steady State

Name	Model	Manufacturer	Voltage (V)	Current (A)	Power (W)	Note
TCS Controller	MSP430	TI	3.3	$336 \times 10^{-6}$	$1.11 \times 10^{-3}$	Active Mode. Calculated from formula on page 13 of data sheet.
				$70 \times 10^{-6}$	$2.31 \times 10^{-4}$	Low-power Mode 0. Current at 3 V.
TCS Heater	HK5951	Minco	12	$209 \times 10^{-3}$	2.5	Area is 2.54 cm x 2.54 cm.
Transceiver	IP2421	Microhard	12	$1 \times 10^{-3}$	$12 \times 10^{-3}$	Sleep Mode
				$95 \times 10^{-3}$	1.14	Receive Only
				$545 \times 10^{-3}$	6.54	Send & receive simultaneously.
Camera	CSC12M25BMP19	Toshiba Teli Corp	12	$417 \times 10^{-3}$	5	Current estimated from given power and given voltage.
Frame Grabber			5	0.8	4	Estimated by payload engineer

Table 1. TINYSCOPE Equipment Summary

## C. LOAD PROFILES

Simplified standard modes were developed for TINYSCOPE to facilitate the EPS modeling in this thesis. The intent of this section is to establish the notional capacity requirements for each of the modes. Additional work will need to be accomplished to ensure the operational feasibility of these modes. The modes were developed based on the spacecraft's mission with the power requirements of each mode assembled from the individual component power requirements. The three modes discussed in this report are normal operations, launch and checkout, and contingency operations. A summary of power requirements for each of the modes is presented below with a detailed accounting of voltage, current, power, and timing shown in Appendix B.

### 1. Normal Operations

The standard concept of operations for TINYSCOPE is currently an approximately ten minute imaging period that is preceded by a ten-minute payload warm-up period. It is assumed in this discussion the warm-up period ends just as the satellite rises above the horizon and establishes communications with an in-theater ground station. TINYSCOPE will be in a sun soak orientation at all times other than when it is in an active imaging period or in eclipse. At the conclusion of the warm-up period, TINYSCOPE will receive a command load for the upcoming imaging period. Once the command load is received, TINYSCOPE will slew to the first ground target and take an image. Once the first image is taken, the satellite slews to the second ground target and takes another image. TINYSCOPE then slews back to the ground command center to downlink the image data before dropping below the horizon. The following several paragraphs present a detailed description of equipment turn on and turn off times. Refer to Figures 6, 7, and 8 below to follow along graphically with the textual description. Figure 6 shows a top-level depiction of an entire

orbit while Figures 7 and 8 show detailed views of portions of the orbits. The portions highlighted are annotated in the figure title. EPS efficiencies are not included.

The C&DH, ADCS controller, IMU, star tracker, GPS, and sun sensor are always on (3.43 W). At 0 seconds, TCS heaters are on to help warm-up the payload (2.50 W), the transceiver is in sleep mode (12 mW), two reaction wheels are in high rate slew and one is in low rate to attain lock with the ground station (4.1 W), the payload camera and frame grabber are full on for warm-up (5 W and 4 W respectively). This is a total of about 19.0 W.

At 20 seconds, the reaction wheels drop to an average slew load to maintain lock with ground station (1.2 W) while the transceiver increases to its transmit and receive simultaneously load (6.54 W). The transceiver is downloading the previous orbit's payload data (if it was missed on the last orbit) while simultaneously receiving the command load for the current orbit. This net increase of 3.628 W increases the total load to 22.7 W.

At 90 seconds, two reaction wheels increase to the full rate slew load of 4.1 W to attain the first target. This net increase of 2.9 W increases the total satellite load to 25.6 W.

At 110 seconds, all reaction wheels decrease to their average slew load to maintain payload nodding while imaging the first target. This is a net decrease of 2.9 W reducing the total satellite load to 22.7 W.

At 115 seconds, two reaction wheels again increase to the full rate slew load of 4.1 W causing a net increase of 2.9 W. The purpose of this slew is to attain the second target. The total satellite load is now 25.6 W.

At 135 seconds, all reaction wheels decrease to their average slew load to maintain payload nodding while imaging the second target. This is a net decrease of 2.9 W reducing the total satellite load to 22.7 W.

At 140 seconds, the payload camera, frame grabber, and heaters turn off reducing the load by 11.5 W. Two reaction wheels increase to high rate slew to maximize the transceiver link margin with the ground station. This increases the total load by 2.9 W. The net total is a load of 14.1 W.

At 160 seconds, all reaction wheels decrease to average slew loads to maintain maximum link margin. This reduces the overall spacecraft load to 11.2 W.

At 620 seconds, a sun soak period begins. The transceiver goes from its maximum transmit and receive load of 6.54 W to its sleep load of 12 mW. This reduces the overall load to 4.64 W.

Upon entering eclipse at 3,532 seconds, the 2.5 W heaters turn on increasing the total load to 7.14 W.

At 5,216 seconds, the payload camera and frame grabber turn back on for warm-up increasing the load to 16.1 W.

At 5,676 seconds, the process starts over.

Not including EPS efficiencies or the loads during the sun soak period from 620 to 3,532 seconds, the batteries must support 7.78 Wh (or 0.54 Ah) of capacity. The maximum draw is 1.78 A. When efficiencies are included, the numbers rise to 10.9 Wh (or 0.76 Ah) and 2.43 A respectively.

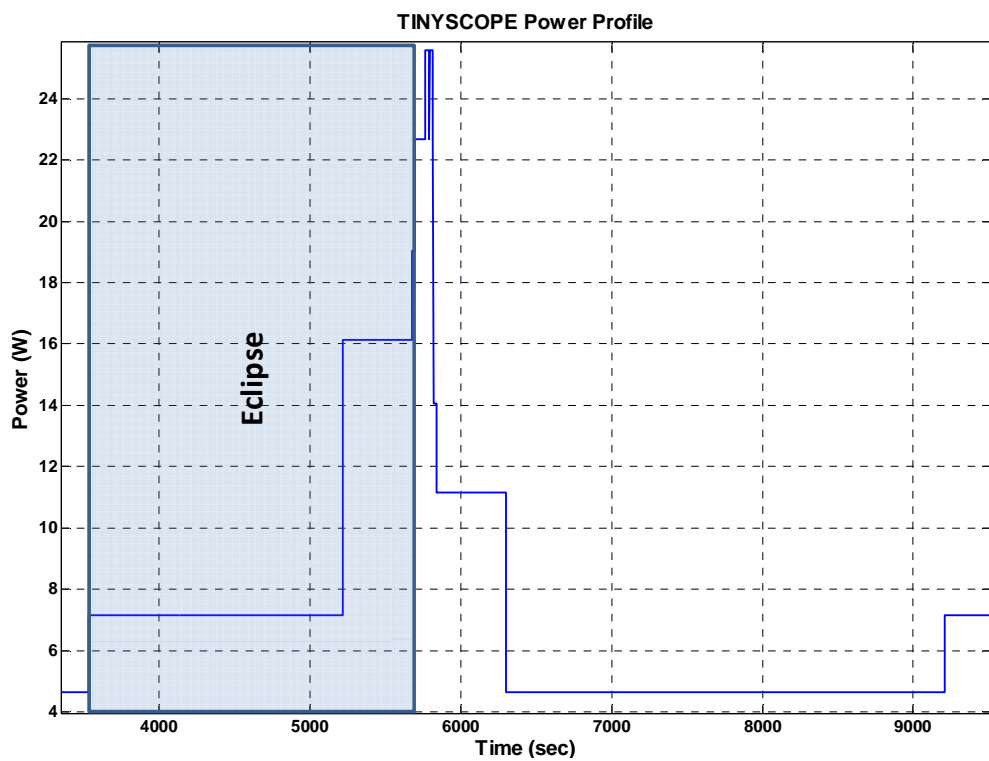


Figure 6. TINYSCOPE Representative Power Profile

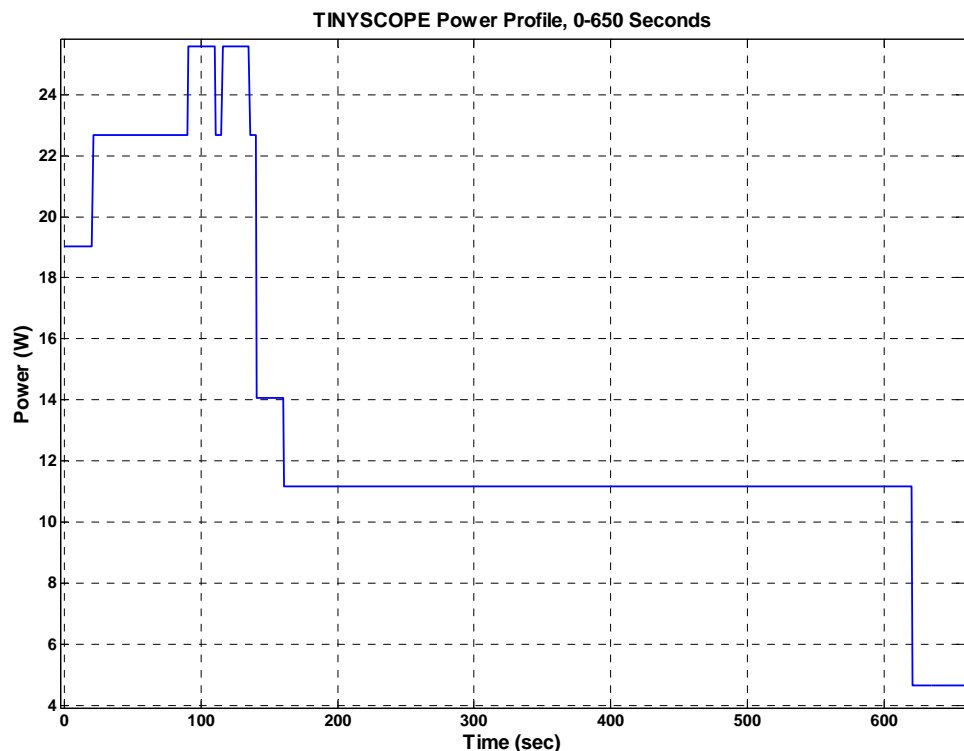


Figure 7. TINYSCOPE Imaging Power Profile, 0 to 650 Seconds

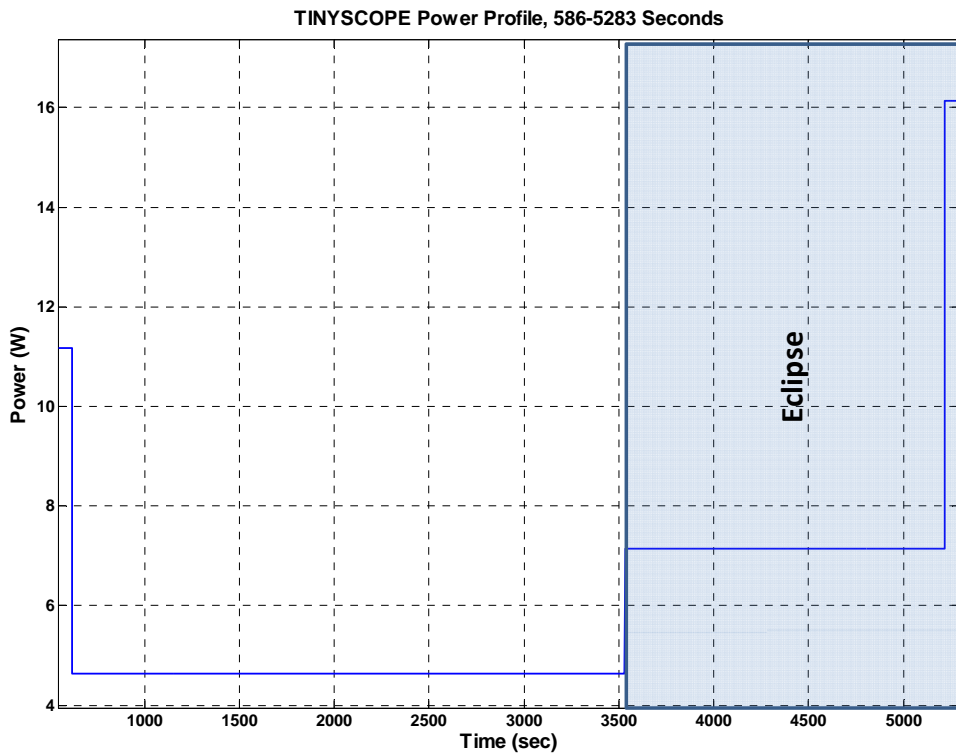


Figure 8. TINYSCOPE Sun Soak & Warm-up Power Profile, 586 to 5283 Seconds

## 2. Launch

A nanosatellite is typically powered off throughout prelaunch integration and transportation to LEO. Before delivery to the launch site for prelaunch integration, TINYSCOPE will be fitted into a launch canister similar to California Polytechnic State University's Poly Picosatellite Orbital Deployer (P-POD) shown in Figure 9, below. To minimize the number of charge, discharge cycles the batteries incur, the flight batteries will be installed as close to launch as practical. Battery installation will likely be just before delivery to the launch canister integrator saving as much of the battery lifetime for operations as possible.



Figure 9. P-POD, Post Deployment From [17]

Depending upon the launch provider but for this discussion at approximately thirty minutes after launch, the transceiver will be turned on and put in its low power mode (12 mW). The GPS receiver, star tracker, and sun sensor will be activated adding 3.08 W. If necessary, the TCS heaters will be on (2.5 W) to compensate for a cold environment. Finally, two reaction wheels will be in their high rate slew and one in low rate slew (4.1 W). The total load is now about 10.0 W. ADCS modeling has shown that this vehicle mode will last no longer than 90 minutes. This results in a total of 15.0 Wh (or 1.05 Ah) with a maximum current draw of about 700 mA.

### 3. Contingency Operations

Recovering from an on-orbit contingency can take many forms depending upon the contingency. One highly likely contingency is a single event upset (SEU) causing a reset of one or more of the subsystems causing the satellite to go into a safe mode. For purposes of this discussion, it is assumed that TINYSCOPE has sustained an SEU causing it to shed as many of its loads as possible and go into a sun-soaking orientation, i.e. a safe mode. Although the

duration of recovery operations is unknown, it is assumed that TINYSCOPE achieves a sun-soaking attitude within one orbit (approximately ninety minutes).

While the state of charge of the batteries will be unknown when an SEU occurs, the loads during a contingency can be approximated. All of the ADCS components will be active: ADCS controller (1.11 mW), GPS receiver (1 W), IMU (0.35 W), star tracker (2 W), sun sensor (7.5 mW), and reaction wheels. To conserve power, the reaction wheels will all be in a low rate slew using 0.3 W. The C&DH and TCS controllers will be on (2.22 mW) as well as the heaters (2.5 W). Finally, the transceiver will be in a receive mode using 1.14 W. The total power required is 7.37 W. Total capacity required for ninety minutes of contingency operations is 0.768 Ah with a maximum current draw of 0.512 A.

Some types of recoveries could take much longer—on the order of days. In that situation, the batteries will be able to support much longer periods of discharge. This will be shown later when the capacity of the batteries is discussed in detail in Chapter II, Section F3.

## D. SOLAR ARRAY DESIGN

Major considerations for how much power TINYSCOPE will be able to collect during its orbit are the size of the solar array, nominal photovoltaic cell efficiency, and length of eclipse periods. These are dependent upon other important factors such as solar intensity variations (earth perihelion versus aphelion), solar incidence angle, thermal considerations, and radiation effects during the satellite's lifetime. These issues are discussed in detail below with important parameters used in the simulations of Chapter III.

### 1. Solar Array Size

Sizing the solar array can take two basic approaches. In the first approach, the result of Equation 6 is divided by the amount of power developed by a particular solar cell per unit area. This value is arrived at through application of Equation 7 [16],

$$P_o = S \cdot \eta_{cell} \left[ \frac{\text{Watts}}{\text{Area}} \right] \quad (7)$$

The amount of power per unit area,  $p_0$ , is the product of solar intensity and the nominal solar cell efficiency. Adjustments are made due to the fact that the solar intensity varies by season<sup>a</sup> and the solar cell efficiency may degrade over time due to, “thermal cycling in and out of eclipses, micrometeoroid strikes, plume impingement from thrusters, and material outgassing. [15]” This results in an end of life (EOL) value for  $p_0$  denoted  $p_{EOL}$ . The required area is then given by Equation 8 [15],

$$A_{sa} = \frac{P_{sa}}{p_{EOL}} \left[ \text{Area} \right] \quad (8)$$

The preceding method is valuable mainly for a satellite design with maximum freedom with regard to the size and orientation of the solar array. A second approach may be used when size, mass, deployment vehicle, e.g. the P-POD, and volume are driving elements of the design. In this case, one may alternatively approach solar array design by investigating and optimizing the maximum area available for solar power collection. The power profile is then limited to this top level of power. Project TINYSCOPE has used a combination of the two approaches with an emphasis on the latter.

Although several different solar array configurations were initially considered, the structural design developed in [5] was used because it offered the most solar array area. Detailed justification for this choice is given in Chapter III. Figure 10 below shows the preliminary structural design and Figure 11 shows an exploded structural design view.

---

<sup>a</sup> Variation in solar intensity is about +/- 4% from the average.

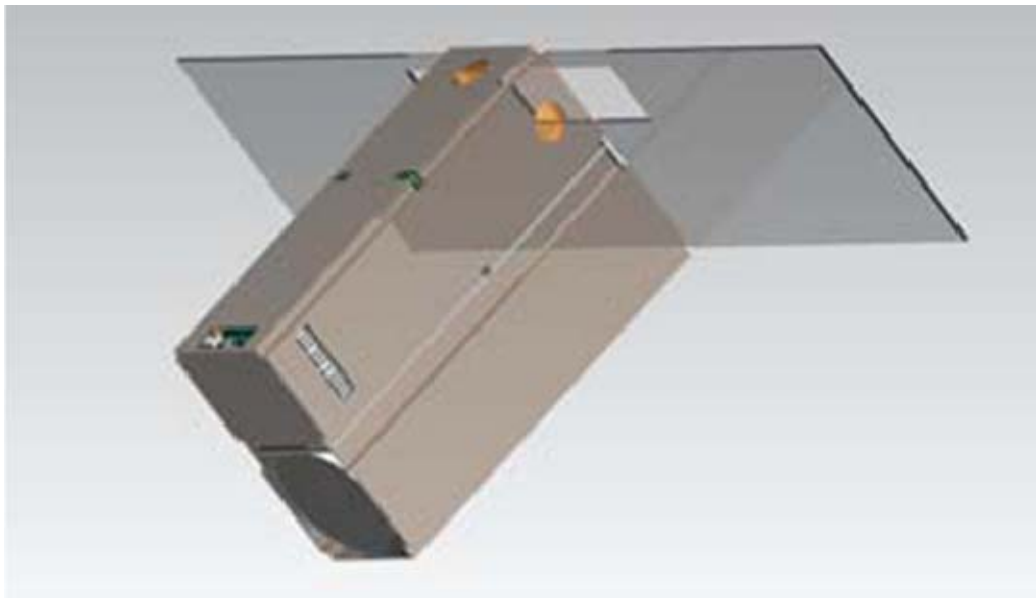


Figure 10. TINYSCOPE, Preliminary Structural Design Modified After [5]

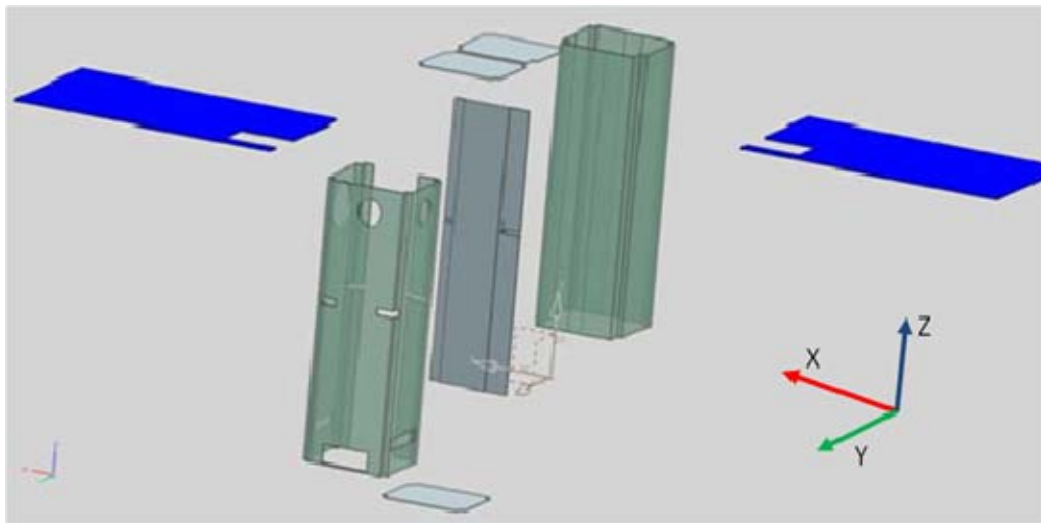


Figure 11. Exploded View of TINYSCOPE Preliminary Structural Design After [5]

The dimensions in the following discussion were taken from NX CAD drawings developed by [5]. These dimensions are not strictly consistent with the dimensions of the 6U because the dimensions of the “six pack” had not been defined as of the time of this writing. Thus, [5] used assumptions upon which this discussion depends. The absolute outer dimensions of the plus and minus X faces are 21.35 cm in width and 34.6 cm in height resulting in a total surface area

for each face of about 740 cm<sup>2</sup>. Doubling this results in about 1,480 cm<sup>2</sup>. This number must be adjusted down by the openings required by the star tracker on the plus X face and the sun sensor on the minus X face. The star tracker's diameter is approximately 2.75 cm and the distance from the top of the structure to the bottom of the star tracker structure is approximately 7.1 cm (surface area of about 19.5 cm<sup>2</sup>). The sun sensor's diameter is approximately 1.6 cm and the distance from the top of the structure to the bottom of the sun sensor structure is approximately 5 cm (surface area of 8 cm<sup>2</sup>). Subtracting out the surface area of the two rectangular shapes (27.5 cm<sup>2</sup>) results in approximately 1,450 cm<sup>2</sup>. The plus Z face dimensions are 9.4 cm by 21 cm. This adds another 197 cm<sup>2</sup> of available area. The total surface area available to place solar cells is about 1,650 cm<sup>2</sup>.

## **2. Cell Alternatives**

Both Emcore Corporation (Albuquerque, New Mexico) and Spectrolab Incorporated (Sylmar, California) manufacture photovoltaic (PV) cells in the United States. Emcore and Spectrolab PV product lines are comparable in nearly every way (nominal efficiency, size, price, radiation degradation, thermal properties, etc.) Table 2 below shows a summary of each manufacturer's product lines. Full specification sheets can be found for Spectrolab's 25.1% efficiency cells and Emcore's 27% efficiency cells in Appendix C.

Company	Solar Cell Name	Nominal Efficiency
Spectrolab	Triple Junction Solar Cell	25.1%
	Improved Triple Junction (ITJ)	26.8%
	Ultra Triple Junction (UTJ)	28.3%
	NeXt Triple Junction (XTJ)	29.9%
Emcore	Advanced Space Solar Cell (ATJM)	27%
	Advanced Space Solar Cell (ATJ)	27.5%
	Space Solar Cell (BTJM)	28%
	Space Solar Cell (BTJ)	28.5%
	Space Solar Cell (ZTJM)	29%
	Space Solar Cell (ZTJ)	29.5%

Table 2. Available Solar Cells

Because of Project TINYSCOPE’s stated goal of keeping costs down, the main criteria for selecting the model of solar cell to be analyzed further was to select the least costly, i.e. the lowest efficiency cell, that maintained single orbit energy balance. The lowest efficiency cell lines from each manufacturer were selected for the remaining portion of this analysis.

### 3. Radiation Impacts

The European Space Agency (ESA) provides an online modeling tool to predict the 1 MeV electron fluence that solar cells will experience for a defined orbit. These values are then compared with a solar cell manufacturer’s stated radiation degradation coefficients to determine an effective solar cell efficiency. The ESA’s Space Environment Information System (SPENVIS) [18] first requires an orbit to be defined, in this case a 500 km circular orbit with an approximate 98° inclination. Then, trapped electrons and protons are modeled with the National Space Science Data Center’s AE-8 and AP-8 models (accessible from

the SPENVIS website). These models contain omnidirectional flux maps for electrons and protons trapped in Earth's radiation belts based on empirical data from more than twenty satellites from the 1960's through the 1970's [19]. Although much of the mapping is extrapolated, it remains a reasonable estimation and the current de facto standard.

SPENVIS outputs fluence levels for up to a maximum thirty-day period. These values were then multiplied by twelve to calculate the fluence levels for TINYSCOPE's one-year mission. Since it is not known at this time if TINYSCOPE will be launched at solar minimum or maximum, Tables 3 and 4 show the 1 MeV equivalent electron fluencies for both cases. All information in the tables is referenced to a thickness of coverglass shown in the leftmost column. Fluence levels are given in terms of the maximum power point of the solar cell  $P_{\max}$ , the open circuit voltage  $V_{oc}$  of the solar cell, and the short circuit current  $I_{sc}$  of the solar cell.

Coverglass Thickness g cm <sup>-2</sup>	mils	micron	Total			Trapped Electrons			Trapped Protons		
			$P_{\max}$	$V_{oc}$	$I_{sc}$	$P_{\max}$	$V_{oc}$	$I_{sc}$	$P_{\max}$	$V_{oc}$	$I_{sc}$
0	0	0	1.127E+15	1.321E+15	1.571E+15	1.566E+12	1.125E+15	1.320E+15	1.568E+15		
0.0056	1	25.41	1.079E+13	1.242E+13	1.035E+13	1.364E+12	9.428E+12	1.105E+13	8.981E+12		
0.0168	3	76.36	4.663E+12	5.268E+12	3.490E+12	1.153E+12	3.510E+12	4.115E+12	2.336E+12		
0.0335	6	152.27	3.431E+12	3.857E+12	2.323E+12	9.538E+11	2.477E+12	2.904E+12	1.369E+12		
0.0671	12	305	2.681E+12	3.019E+12	1.662E+12	7.148E+11	1.966E+12	2.304E+12	9.469E+11		
0.112	20	509.09	2.224E+12	2.515E+12	1.280E+12	5.314E+11	1.692E+12	1.984E+12	7.495E+11		
0.1675	30	761.36	1.901E+12	2.160E+12	9.997E+11	3.912E+11	1.510E+12	1.769E+12	6.086E+11		
0.335	60	1522.73	1.484E+12	1.709E+12	6.782E+11	1.858E+11	1.298E+12	1.523E+12	4.925E+11		

Table 3. Summary of 1 MeV Equivalent Electron Fluence (cm<sup>-2</sup>) at Solar Max

Coverglass Thickness g cm <sup>-2</sup>	mils	micron	Total			Trapped Electrons			Trapped Protons		
			$P_{\max}$	$V_{oc}$	$I_{sc}$	$P_{\max}$	$V_{oc}$	$I_{sc}$	$P_{\max}$	$V_{oc}$	$I_{sc}$
0	0	0	1.142E+15	1.338E+15	1.572E+15	8.006E+11	1.141E+15	1.338E+15	1.571E+15		
0.0056	1	25.41	3.502E+13	4.093E+13	3.448E+13	7.074E+11	3.431E+13	4.024E+13	3.377E+13		
0.0168	3	76.36	1.244E+13	1.448E+13	1.012E+13	6.058E+11	1.184E+13	1.388E+13	9.518E+12		
0.0335	6	152.27	6.832E+12	7.921E+12	4.826E+12	5.071E+11	6.324E+12	7.415E+12	4.320E+12		
0.0671	12	305	4.238E+12	4.903E+12	2.543E+12	3.846E+11	3.854E+12	4.518E+12	2.158E+12		
0.112	20	509.09	3.240E+12	3.750E+12	1.746E+12	2.875E+11	2.953E+12	3.462E+12	1.458E+12		
0.1675	30	761.36	2.687E+12	3.114E+12	1.279E+12	2.116E+11	2.476E+12	2.903E+12	1.068E+12		
0.335	60	1522.73	2.132E+12	2.484E+12	9.060E+11	9.907E+10	2.034E+12	2.384E+12	8.069E+11		

Table 4. Summary of 1 MeV Equivalent Electron Fluence (cm<sup>-2</sup>) at Solar Min

Proton fluence values are highest at solar minimum, while electron fluence levels are highest at solar maximum. The most important values to observe are contained in the “Total” column. Assuming three mil thick cover glass protection, the pertinent values from Table 3 are 4.663E+12 for  $P_{\max}$ , 5.268E+12 for  $V_{oc}$ , and 3.490E+12 for  $I_{sc}$ . From Table 4: 1.244E+13 for  $P_{\max}$ , 1.448E+13 for  $V_{oc}$ , and 1.012E+13 for  $I_{sc}$ . Close inspection of Spectrolab’s specification sheet for the 25.1% efficiency cells shows a radiation degradation coefficient starting at 1E+14 1 MeV equivalent fluence. This is two orders of magnitude higher than the values for solar maximum and one order of magnitude greater than the values for solar minimum. For this reason, no radiation degradation adjustment is made for the Spectrolab cells. Emcore’s specification sheet for its 27% efficient cells shows a radiation degradation coefficient starting at 5E+13 1 MeV equivalent fluence. This level is one order of magnitude higher than the fluence values at solar maximum and approximately five times higher than the values given at solar minimum. Similar to the rationale for Spectrolab’s cells, no radiation degradation adjustment is made for the Emcore cells.

#### **4. Thermal Impacts**

Solar cells are least efficient when hot and most efficient when cold. One can infer that cells are most efficient immediately after a satellite leaves eclipse and least efficient after the satellite’s solar array has been sun soaking the longest. It has been observed in [15] that non-body mounted, flat solar panels in LEO have a typical temperature of 67 °C. Body mounted solar cells are about 5 °C hotter. It is estimated in [15] that solar cell efficiency can degrade by as much as 0.5% per degree above 28 °C. Analytical models can further refine these estimations.

The first analytical model, taken from page 44 of [16], gives a steady state value for deployed solar arrays in a low earth orbiting satellite,

$$T_{OP} = \left[ \frac{\alpha_F S \cos(\phi) + \alpha_b S a F_a + \varepsilon_b E F_e - \eta f_p S \cos(\phi)}{(\varepsilon_f + \varepsilon_b) \sigma} \right]^{\frac{1}{4}}$$

$$F_a = F_e \cos(\beta) \cos(\nu)$$

$$F_e = \sin^2(\rho) \cos(\lambda)$$
(9)

The variables have the following meanings:  $\alpha_F$  and  $\alpha_B$  are the absorptivities of the front side and back side of the array;  $S$  is the solar flux (power per unit area);  $\phi$  is the angle of incidence of sunlight;  $a$  is a factor applied to the Earth thermal flux to approximate the albedo flux;  $F_a$  is the product of multiple radian measured angles describing how much of the solar array's area is pointing at the earth's albedo;  $F_e$  is the product of multiple radian measured angles describing how much of the solar array's area is pointing at the earth;  $\varepsilon_F$  and  $\varepsilon_B$  are the emissivities of the front-side and back-side of the solar array;  $E$  is the earth flux (power per unit area),  $\eta$  is the nominal solar cell efficiency;  $f_p$  is the solar cell packing factor;  $\beta$  is the angle the orbit plane makes with the sun direction unit vector;  $\nu$  is an angle that defines where the satellite is in its orbit relative to the solar sub point;  $\rho$  is the angular radius of the earth at the satellite's altitude;  $\lambda$  is the incidence angle of the earth's thermal flux on the solar array; and  $\sigma$  is the Stefan-Boltzman constant. Several of these parameters are explained more fully in Chapter III when the dynamic simulation is developed.

Upon re-inspection of Figure 10, one can see that this model has some applicability to TINYSCOPE's steady state temperatures if it is assumed that the solar panel "wings" are thermally isolated from the spacecraft body. Strictly speaking, this is not correct since the underside of the solar panels have the spacecraft body within its field of view. Because radiative heat transfer will occur between the body and the solar panel, one should include appropriate margin in the design to compensate for the model's shortcomings.

Packing factor should be set no higher than 93% [20]. A value of 80% is used here. The value for the solar power per unit area varies with the position of

earth in its orbit around the sun. The highest value, at perihelion, i.e. winter, is  $1,414 \text{ W/m}^2$  while the lowest value, at aphelion, i.e. summer, is  $1,322 \text{ W/m}^2$  [21]. Nominal solar cell efficiency, solar cell absorptance, and solar cell emittance are taken from the cell manufacture's specification sheet. Array backside absorptance and emittance is chosen as a design parameter. Values of 0.17 and 0.92 are chosen from Table 11–46 of [15]. The Stefan-Boltzman constant has a value of  $5.67\text{E}-8$  while the sun incidence angle is chosen as zero because TINYSCOPE will be in sun soaking orientation 90% of the time. Standard values of the albedo adjustment factor and the earth's thermal flux are provided [16] in as 0.3 and  $326 \text{ W/m}^2$ . Because Emcore did not make its absorptance and emittance values available, Spectrolab's were used. The beta angle is chosen as zero while the earth thermal flux angle is chosen as  $45^\circ$ . In reality, this value will be constantly changing but  $45^\circ$  is chosen as a reasonable average value. The angular radius of the earth is set by the satellite altitude and a value of zero is chosen for the starting position of the satellite in its orbit relative to the subsolar point ( $v$ ). These values were substituted into an Excel spreadsheet (see Appendix D) to arrive at the values in Table 5.

	Summer Solstice		Winter Solstice	
Manufacturer	Spectrolab, 25.1%	Emcore, 27%	Spectrolab, 25.1%	Emcore, 27%
Temperature	55.7 °C	54.3 °C	60.5 °C	59.0 °C

Table 5. Predicted Solar Cell Temperatures

The second model that was used to predict solar cell temperature comes from Figure 47 of [5]. Although an “apparent” external temperature of  $124 \text{ }^\circ\text{C}$  was predicted on page 95, a more accurate prediction for the internal solar panel “wing” temperature from page 96 and 97 is used here. The internal “wing” temperature is  $317.5 \text{ K}$  or  $44.35 \text{ }^\circ\text{C}$ . This result is of the same order of

magnitude as that given by Equation 9 and the guideline given on page 414 of [15]. In an effort to provide some level of margin, Equation 9's values will be used.

An adjustment to Spectrolab and Emcore's nominal efficiencies can now be made. Specified currents and voltages are adjusted based on the following linear approximation,

$$NewValue = SpecificationValue + (\Delta T \times Temp\ Coefficient) \quad (10)$$

Equation 10 is applied for both Spectrolab and Emcore at the summer and winter solstices and using the maximum power voltage and current at BOL for 28 °C. Table 6 summarizes these calculations, below.

	Summer		Winter		Note
	Spectrolab	Emcore	Spectrolab	Emcore	
1 Predicted Temperature [°C]	55.7	54.3	60.5	59.0	Equation 9
2 Base Temperature [°C]	28	28	28	28	Manufacturer Specification Sheet
3 Temperature Delta [°C]	27.7	26.3	32.5	31.0	Line 1 - Line 2
4 Voltage Coefficient [V/°C]	-0.0067	-0.0059	-0.0067	-0.0059	Manufacturer Specification Sheet
5 Nominal Max Power Voltage [V]	2.28	2.29	2.28	2.29	Manufacturer Specification Sheet
6 Adjusted Max Power Voltage [V]	2.09	2.13	2.06	2.10	Line 5 + (Line 4 * Line 3)
7 Current Coefficient [ $\mu\text{A}/\text{cm}^2/\text{°C}$ ]	9.0E-06	1.1E-05	9.0E-06	1.1E-05	Manufacturer Specification Sheet
8 Nominal Max Power Current [A]	0.0149	0.0160	0.0149	0.0160	Manufacturer Specification Sheet
9 Adjusted Max Power Current [A]	0.0151	0.0163	0.0152	0.0163	Line 8 + (Line 7 * Line 3)
10 Nominal Efficiency	0.251	0.270	0.251	0.270	Manufacturer Specification Sheet
11 AMO [W/cm <sup>2</sup> ]	0.132	0.132	0.141	0.141	Solar constant at Air Mass Zero (AM0)
12 Power [W]	0.032	0.035	0.031	0.034	(Line 6) * (Line 9)
13 Adjusted Efficiency	0.239	0.262	0.221	0.243	(Line 12) / (Line 11)

Table 6. Solar Cell Adjusted Efficiencies

At the summer solstice, solar power per unit area is lowest giving rise to the potential that the least amount of power will be collected. However, the temperature of the cells is lower than at winter solstice. This lower temperature has the effect of slightly increasing the efficiency of the cells offsetting the reduced collection due to the low power per unit area. Conversely, at the winter solstice, solar power per unit area is high giving the potential to collect more

power. However, the higher solar intensity is offset due to the higher solar cell temperature it causes reducing cell efficiency. The final result is that the winter solstice scenario is worst for both types of cells.

## **5. Manufacturing Impacts and Final Adjusted Efficiencies**

Final adjusted efficiencies are calculated as the product of the nominal efficiency, the radiation adjustment, the temperature adjustment, and design and assembly adjustment. Design and assembly activities introduce losses attributable to circuit connections, line losses, and other imperfections. References vary but efficiencies in the range of 77% to 90% are reasonable [15]. A value of 85% was chosen for TINYSCOPE's EPS design. Table 7 summarizes the final adjusted efficiencies. Lines one through five calculate the overall efficiency while lines six through 11 focus on the specific impacts to voltage and current. One must calculate the individual voltage and current impacts so that a subsequent series and parallel calculation can be made.

To maintain an overall 0.85 adjustment to the power of the solar cell for design and assembly, the square root of 0.85 was applied to both voltage and current, i.e. lines seven and ten. While this probably does not represent the actual physical adjustment that will occur, it is a reasonable engineering approximation. Final efficiencies are listed in Line 14. Observe that Spectrolab cells in the Winter are the least efficient. This is due to the fact that the cells will be at a higher temperature which is reflected in the lowest efficiency listed on Line three.

	Summer		Winter	
	Spectrolab	Emcore	Spectrolab	Emcore
1 Nominal Efficiency	0.251	0.27	0.251	0.27
2 Radiation Adjustment	1	1	1	1
3 Temperature Adjustment	0.954	0.972	0.881	0.899
4 Design and Assembly Adjustment	0.85	0.85	0.85	0.85
5 Final Adjusted Efficiency	0.204	0.223	0.188	0.206
6 Temperature Adjusted Voltage [V]	2.09	2.13	2.06	2.10
7 Square Root of Design & Assy	0.92	0.92	0.92	0.92
8 Final Adjusted Voltage [V]	1.93	1.96	1.90	1.94
9 Temperature Adjusted Current [A]	0.015	0.016	0.015	0.016
10 Square Root of Design & Assy	0.922	0.922	0.922	0.922
11 Final Adjusted Current [A]	0.014	0.015	0.014	0.015
12 Fin. Adj. Voltage * Fin. Adj. Current	0.027	0.029	0.027	0.029
13 Solar Constant at Air Mass Zero [W/cm <sup>2</sup> ]	0.132	0.132	0.141	0.141
14 Final Adjusted Efficiency	0.204	0.223	0.188	0.206

Table 7. Final Adjusted Solar Cell Efficiencies

## 6. Series and Parallel Requirements

The number of solar cells required in series is determined by the level of voltage required by the power management and distribution (PMAD) system. The number of parallel strings of series cells is dependent upon the overall current requirement of the entire satellite. Adjusted values for voltage and current must be used so that an EOL series and parallel requirement is calculated. A general purpose spreadsheet was developed to calculate the number of series and parallel strings required. The spreadsheet also makes it easy to compare the area required by this calculation to the area available on the satellite. To demonstrate the use of the spreadsheet in Table 8, the pertinent values for TINYSCOPE were used.

Lines 1 and 2 are set to the values listed because the PMAD system that will be discussed in Chapter II, Section E2 requires this level of voltage to charge

the batteries. Line 3 lists an adjustable margin level set by engineering judgment to increase the overall voltage level. The overall power requirement listed on Line 5 is taken from the Matlab/Simulink<sup>©</sup> model that is explained in detail in Chapter III.

		Summer		Winter		Note
		Spectrolab	Emcore	Spectrolab	Emcore	
1	Battery Nominal Voltage [V]	14.4	14.4	14.4	14.4	Battery Spec Sheet
2	Voltage Required to Charge Battery [V]	16.8	16.8	16.8	16.8	Battery Spec Sheet
3	Margin [%]	3.0%	3.0%	3.0%	3.0%	Engineering Judgement
4	Net Voltage Required [V]	17.3	17.3	17.3	17.3	Line 2 + (Line 2 * Line 5)
5	Average Power [W]	27	27	27	27	From Matlab/Simulink Model
6	Current Required [A]	1.56	1.56	1.56	1.56	Line 5 / (Line 4)
7	Margin [%]	3.0%	3.0%	3.0%	3.0%	Engineering Judgement
8	Net Current Required [A]	1.61	1.61	1.61	1.61	Line 6 + (Line 6 * Line 7)
9	Area of Solar Cell [cm <sup>2</sup> ]	30.0	30.0	30.0	30.0	From solar cell spec sheet
10	EOL Voltage [V]	1.93	1.96	1.90	1.94	Table 7, Line 8
11	EOL Current Density [A/cm <sup>2</sup> ]	0.014	0.015	0.014	0.015	Table 7, Line 11
12	Series	9	9	10	9	Ceiling (Line 4 / Line 10)
13	Parallel	4	4	4	4	Ceiling [Line 8 / (Line 9 * Line 11)]
14	Cells Required	36	36	40	36	Line 12 * Line 13
15	Cell Area Required [mm <sup>2</sup> ]	1080	1080	1200	1080	Line 9 * Line 14
16	Total Area Available on "Wings" [mm <sup>2</sup> ]	1450				From [Ortiona]
17	Packing Factor	0.8				Prescribed
18	Effective Area Available [mm <sup>2</sup> ]	1160				Line 16 * Line 17

Table 8. Series and Parallel Requirements

Line five's value of 27 W is an adjusted value from the Matlab/Simulink<sup>©</sup> model. The model shows that about 30 W is developed when the satellite is pointing directly at the sun. Because the series and parallel calculation include margin for both voltage and current, some portion of the 30 W must be used for this margin. Engineering judgment was used to apportion approximately 10% power margin evenly between voltage and current (10% of 30 W is 3 W). The current required was simply calculated as the power developed divided by the Net Voltage Required. Similarly to the voltage, a margin was included.

Line nine is taken directly from the solar cell manufacturer's specification sheet. Although Emcore does not state what sizes its solar cells are available in, Spectrolab's 25.1% cells are available in sizes up to 30 cm<sup>2</sup>.

Lines 10 and 11 were taken directly from Table 7 as the fully adjusted values that are expected to be seen from the solar cells. The required string voltage is then divided by Line 10 and rounded up to calculate the number of cells required in series. Similarly, the required overall current is divided by the product of Line 11 and Line nine and then rounded up to calculate the number of parallel strings required. Line 14 is the product of Lines 12 and 13 while Line 15 is product of Line 14 and Line nine. This number, the cell area required, must be smaller than the area available after the total area available has been adjusted by the planned packing factor.

Lines 16 through 18 show the method used to arrive at an available area of 1,160 cm<sup>2</sup>. One can observe that this number is larger than all columns of Line 15 except for Spectrolab in the Winter. The requisite number of cells are listed in Lines 12 and 13. Spectrolab in the Winter requires one more cell in series due to the negative impacts that a higher temperature have on the cells at perihelion.

## E. POWER MANAGEMENT AND DISTRIBUTION

### 1. Alternatives Considered

Although several COTS products were carefully assessed for feasibility as part of TINYSCOPE's EPS design, custom designs built by students or space system manufacturers were ruled out from the start. The primary reason was to stay consistent with Project TINYSCOPE's stated goal of using COTS or slightly modified COTS. The following readily available systems were evaluated:

- CubeSat Power, NanoSat Power, SmallSat Power, Clyde Space Ltd. (<http://www.clyde-space.com/products>)
- Small Satellite Power System, Surrey Satellite Technology Ltd. (SSTL)

(<http://www.sstl.co.uk/assets/Downloads/Datasheet%20Powersystem%20contact%20sheet%20%5BNovember%202008%29.pdf>)

- Integrated Power Electronics, Broad Reach Engineering (<http://www.broadreachengineering.com/eps06.html>)
- Integrated Battery and Power System (IBPS), Ocean Server Technology Inc. (<http://www.ocean-server.com/smallbattery.html>)
- Integrated Power and Data Ring (IPDR), Sierra Nevada Corporation (<http://www.spacedev.com/>)

Clyde Space, based in Glasgow, Scotland, manufactures several power systems that have wide applicability to small and very small satellites. In order of output power, these are CubeSat Power, NanoSat Power, and SmallSat Power lines. The CubeSat Power line is designed for use with spacecraft that have average orbit loads from 1 W to 20 W. Although there are 1U and 3U variants, only the 3U variant is addressed here. The system provides regulated voltages of 3.3 V and 5 V at up to 1.2 A and unregulated battery voltage up to 10 V with a maximum of 2.9 A. The maxima cannot be supplied simultaneously. There is also an option to provide 12 V at 300 mA and 50 V at 1 mA from the unregulated battery bus. The solar array input uses a peak power tracking scheme where up to 9 V may be provided by the solar arrays. Clyde Space also makes a 3U lithium polymer battery system at 8.2 V and up to 7.5 ampere-hours (Ah) of capacity. The main EPS system has a mass of 86 g to which 204 g for the two series, three parallel battery packs is added, resulting in a total mass of 290 g. The EPS board has dimensions of 9.5 cm by 9 cm by 1.5 cm. The battery portion has similar dimensions as it stacks on top of the main EPS boards. The total cost is £2,050 for the batteries and £2,600 for the EPS board. At current currency conversion rates, this is about \$7,700.<sup>b</sup>

The NanoSat Power system is also compatible with average orbit power up to 20 W. It provides 5 V at up to 1.5 A on the 5 V bus and 7 V to 10 V at up to 10 A on the battery bus. The maxima cannot both be supplied simultaneously. It

---

<sup>b</sup> Google Finance currency converter was used on 15 Nov 2009. Entered “4650 GBP in USD” in input field.

uses a peak power tracking scheme with a 10 V to 20 V input. Batteries must be selected separately that meet the maximum charge current (1.5 A) and voltages (12.5 V) supplied by the NanoSat Power system. The system dimensions are 23 cm by 12.2 cm by 2 cm with a mass of approximately 500 g. The manufacturer reports that the NanoSat Power system has been used successfully in space on two previous missions. Unlike the CubeSat EPS, the cost of the NanoSat EPS was not readily available.

The SmallSat Power system is designed for slightly larger spacecraft with an average orbital power requirement of about 20 W to 300 W. Accordingly, it is much larger at 30 cm by 15 cm by 7 cm with a mass of about 1.5 kg. Its battery bus runs from 16 V to 35 V at a maximum of 15 A current and the 5 V bus runs at a maximum current of 2 A. Separately selected batteries can be charged from 30 V to 60 V with a maximum current of 2.5 A. The manufacturer reports that over twenty previous space missions have successfully used the SmallSat Power system. Unlike the CubeSat EPS, the cost of the SmallSat EPS was not readily available.

SSTL, headquartered in Guildford, United Kingdom, is a manufacturer of complete satellites as well as satellite subsystems. Its focus is on small satellites but not nano- and picosatellites. Its Small Satellite Power System is designed for average orbital load requirements up to 1.6 kW. The concept of the design is similar to that used by Clyde Space with an unregulated battery bus as well as a fully conditioned 5 V and 28 V bus. The unregulated bus provides 28 V +/- 6 V with each battery charge regulator able to handle 80 W. The smallest system would consist of two modules, a battery charge regulator module and a power conditioning module, each with dimensions of 30 cm by 30 cm by 3 cm. The battery charge regulator has a mass of 2.25 kg while the power conditioning module has a mass of 1.65 kg. The system would be able to provide upwards of 240 W of power (there are six charge regulators per module). Twenty-eight volt batteries would have to be purchased separately. The manufacturer reports that

its power system has extensive space flight heritage and has an expected design life of seven years. Unlike the CubeSat EPS, the cost of the Small Satellite Power System was not readily available.

Broad Reach Engineering with facilities in Tempe, Arizona and Golden, Colorado focuses mainly on integrated avionics products but also provides systems engineering services. Both the integrated and standalone versions of its EPS provide for solar array switching, power distribution, regulation, and control. Up to 14 solar array strings with inputs of 6.9 A may be controlled. The Charge Control & Solar Array Interface Card (SACI) provides three voltages at 5 V and +/-15 V with a total current output of up to 20 A. The physical dimensions of the basic system are 11.2 cm by 21.8 cm by 3.6 cm with a total mass of approximately 320 g. Batteries must be purchased separately. The manufacturer reports that seven previous space missions have successfully used the SACI power system. Unlike the CubeSat EPS, the cost of the Broad Reach Engineering power system was not readily available.

Massachusetts-based Ocean Server markets its IBPS as a terrestrial based modular system used extensively for autonomous underwater vehicles and remote data collection [22]. The company offers many different power systems with capabilities ranging from supplying a small notebook computer up to 25,000 Wh autonomous submarines. Initial research led to the evaluation of a four channel Mini Battery Controller used in conjunction with a DC to DC voltage converter. Although the controller is designed to be supplied by an AC wall adapter at 18 V and 5.56 A, an appropriately sized solar panel can be used. The controller outputs an unregulated maximum current of 13.25 A at 12 V. This is optionally input to a DC-DC converter board where regulated voltages of 3.3 V, 5 V, and +/- 12 V are provided at up to 10 A, 10 A, and 12 A respectively. The maximum current for each voltage cannot be used simultaneously. The maximum power from the DC board is 144 W. Batteries may be purchased through Ocean Server that are specially designed to work with the IBPS system. The standard batteries are 14.4 V lithium ion in a four series, three parallel

configuration. The 12 cell batteries provide 6.6 Ah or 95 watt-hours (Wh) of capacity.<sup>c</sup> The basic system can use up to four battery packs. The dimensions of the combined base board and DC board are 7.4 cm by 9.1 cm by 4 cm. Its mass is less than 200 g. The standard battery is 22.3 mm in height by 285 mm in length by 58.9 mm in width with a mass of approximately 700 g. The controller and DC converter cost \$532.62 as a pair while a single battery costs \$187.45. The system has no space flight heritage or space rating but has been successfully used for several years in Professor Marcello Romano's Spacecraft Robotics Laboratory at NPS.

Sierra Nevada Corporation, headquartered in Sparks, Nevada, developed the IPDR Space Plug and Play Avionics (SPA) to be modular in design with the capability to manage all aspects of power collection, storage, regulation, and distribution. Because the IPDR is very new, definitive specifications were impossible to obtain. However, enough informal information was gathered to make an informed decision as to the appropriateness of its implementation for TINYSCOPE.

From a hardware perspective, each IPDR is identical. Software and firmware introduces various functionality. The IPDR can simultaneously be used for power control and to support loads. Each IPDR is capable of supporting eight 4 A devices or two 10 A devices at an unregulated voltage of 28 V (+6 V/-4 V). The maximum load current is limited to 32 A. The maximum input current is limited to 40 A. All IPDRs are capable of solar array switching and battery charging and discharging. Thus solar array sections may be connected up to the 40 A maximum and input to the IPDR. The IPDR then controls the solar array input and battery charge, discharge cycle. IPDRs, solar array sections, and batteries can be connected together to support the loads attached to a particular IPDR. As more loads are required, additional pairings of IPDR, solar array

---

<sup>c</sup> To convert between Ah and Wh, multiply the number of Ah by the battery's nominal voltage. In this case, 6.6 Ah X 14.4 V = 95 Wh.

sections, and batteries may be created. The company reports that the system has previous space flight heritage. Unlike the CubeSat EPS and the IBPS, the cost of the IPDR was not readily available.

## 2. Selected System

The above systems were evaluated relative to volume, mass, maximum load power, voltage provided, current provided, and up-front cost. Initially, the EPS was allocated no more volume than one-half of a 1U cube, i.e. 500 cm<sup>3</sup>. Because the spacecraft is intended to conform to the CubeSat standard as much as possible, either the length or the width dimension had to be no more than 10 cm. For example, a board with dimensions of 9 cm by 20 cm was not ruled out but one with a width and height of 20 cm was. This removed Sierra Nevada's IPDR, SSTL's Small Satellite Power System, Broad Reach's SACI system, and Clyde Space's SmallSat and NanoSat power systems.

An initial estimate of the allocated EPS mass was no more than 1 kg for the PMAD and batteries. Both of the remaining systems, Clyde Space's CubeSat power and Ocean Server's IBPS, met this requirement. The complete 3U version of the CubeSat power system has mass of only 290 g. The IBPS has a total mass of 846 g. While this mass is much higher, it still falls well below the initial mass allocation. Additionally, initial review of the IBPS documentation indicated that it might be possible to use much lower capacity batteries giving rise to the hope that the mass could be much lower.

Referencing Figure 6, TINYSCOPE's average orbital load is approximately 7.35 W while its maximum load is 25.6 W. CubeSat Power is rated up to an average required load of 20 W while the IBPS is rated up to 144 W. Both appear to be able to handle the requisite levels of average required power. It is not as clear that both can supply the maximum draw when TINYSCOPE is imaging, slewing, and communicating. Although CubeSat Power states it can output 10 V at 2.9 A, it is unknown if the required level of power can be reached after DC to

DC conversion to the correct voltages. The IBPS, on the other hand, supplies the required voltages at much higher power levels.

From the component descriptions above and electrical requirements listed in Table 1, one can see that the IBPS provides all of the required regulated voltages at adequate current levels. Conversely, CubeSat power supplies 3.3 V and 5 V at sufficient current levels but only a very small current for 12 V.

Finally, the upfront cost of the IBPS is an order of magnitude less than the CubeSat Power system. Additionally, as will be discussed in Chapter II, Section F, several lower capacity, lower cost batteries may be used with the IBPS lowering the overall system cost even more. It should be noted that a detailed trade-off analysis between the IBPS and CubeSat Power was not conducted. This analysis would include the costs associated with hardware testing to reduce mission risk for the IBPS and the costs of modifying the CubeSat Power system to provide the required voltage and current levels.

Careful consideration of the reasons presented above led the EPS engineer and subsequently the TINYSCOPE team as a whole to choose Ocean Server's IBPS power control system. Chapter IV of this thesis details an initial attempt at risk reduction through hardware testing for the IBPS. Detailed observation of the IBPS configuration led to the development of Figure 5, TINYSCOPE EPS Equivalent Circuit, and subsequently Equation 6, the mathematical expression for the required power of the solar array.

### **3. Solar Array Power Control**

The topic of power control relates to the method used to control the transfer of power from a power source to an energy storage device and/or a dissipative load. In this case, the power source is an array of PV cells and the energy storage device is a bank of battery cells. Because batteries are highly sensitive to overcharge and undercharge conditions, PV cells are not normally connected directly to battery cells. In a worst-case scenario, this could cause battery damage and catastrophic failure of a satellite mission. The power source

to energy storage interface can be controlled in many different ways. However, section 11.4.4 of [15] defines two basic methods: peak power tracking (PPT) and direct energy transfer (DET). Both methods are used on modern satellites with DET being much simpler and cheaper whereas a PPT system is designed to extract the maximum amount of power out of the PV array as possible.

The basic method used to allocate power to the load in a DET system is shunt regulation. Current is diverted away from spacecraft loads by shunt resistors, which, along with the load, appear in parallel to the power source. The shunt resistors dissipate power not used by the loads. For thermal reasons, the resistor load bank is typically placed outside the main spacecraft bus, often on the solar panel yoke. TINYSCOPE's very small form factor, with no yoke available, would make an external load bank impossible. An internal load bank could be considered but would greatly complicate the spacecraft thermal analysis.

A PPT system attempts to compensate for the fact that a PV cell's maximum power point varies with operating conditions. The most critical factors are irradiance, i.e. solar intensity, and operating temperature. Decreasing irradiance shifts the current down with little effect on the voltage (reference Figure 12). Increasing temperature shifts the voltage down with little effect on the current (reference Figure 13).

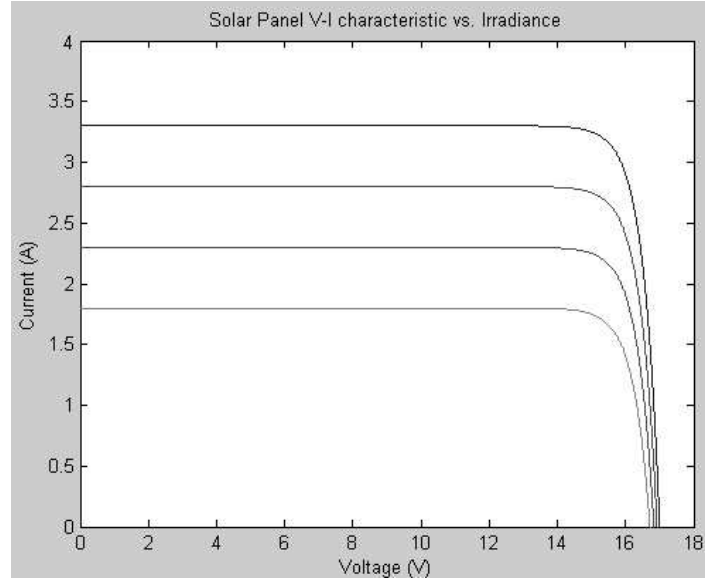


Figure 12. Solar Panel V-I Characteristic vs. Irradiance From [23]

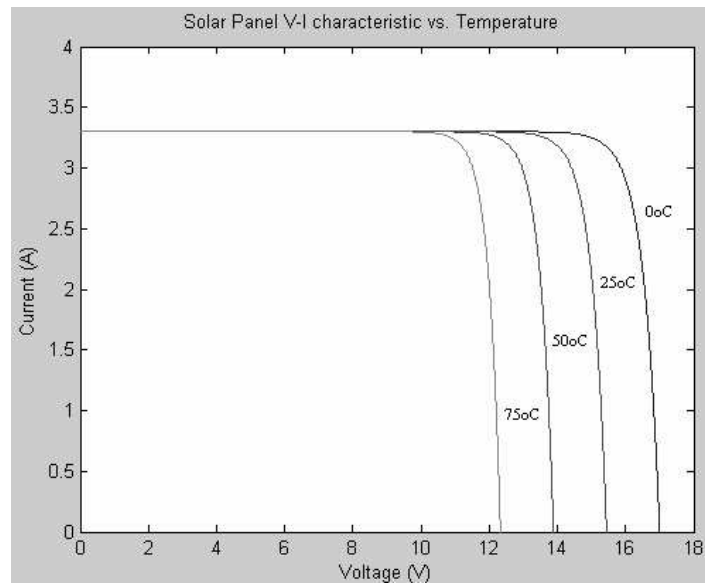


Figure 13. Solar Panel V-I Characteristic vs. Temperature From [23]

The basic idea of a PPT system is to match the continuously varying voltage and current output of a PV cell to that of the energy storage device and/or load. However, since the peak power point cannot be accurately predicted, many different algorithms exist for finding the best approximation. This approximation is then used to tune a DC to DC converter that is placed

between the solar array and the battery and/or load. The efficiency of the PPT depends in large part on how good the PPT system estimates the peak power point of the PV cells along with the circuit efficiency of the components used in the DC to DC conversion. This efficiency is most important from a subsystem level design.

The chosen power management and distribution system is a COTS product that may be modified to operate from a solar panel by following the steps given in a company technical note [24]. However, the documentation does not state if the system is a PPT or a DET. Subsequently, most of the efficiencies shown in Figure 5 are unknown. Chapter IV focuses on characterizing the type of power control used as well as discovering operational efficiencies.

## F. BATTERY DESIGN

### 1. PMAD Battery Requirements

The Ocean Server IBPS is designed around an original equipment manufacturer (OEM) battery provided by Inspired Energy, Inc. of Newberry Florida. The basic battery is 14.4 V, 6.6 Ah in capacity, and 700 g in mass. Two different dimensions are available: 22.3 mm height by 285 mm length by 58.9 mm in width (“long pack”) or 21.7 mm height by 167.5 mm length by 107.3 mm width (“flat pack”). The flat pack will not fit inside TINYSCOPE’s satellite bus because two dimensions exceed 10 cm. However, it is very unlikely that the packs will be used as received from the manufacturer because of out gassing concerns when placed in a vacuum. Both configurations are a twelve cell, lithium ion battery in a four-series, three parallel configuration. Each cell is nominally 3.6 V with 2.2 Ah of capacity. Stacking four cells in series provides 14.4 V, i.e.,  $3.6 \times 4 = 14.4$ . Three of these strings provide 6.6 Ah of total capacity, i.e.,  $2.2 \times 3 = 6.6$ . The cells conform to the standard 18650 cell size with dimensions of 18 mm in diameter and 65 mm in height. Figure 14 shows

both OEM battery sizes one can choose from (“long pack” on top, “flat pack” bottom right) along with a representative 18650 lithium ion cell from inside the case (bottom left).



Figure 14. IBPS OEM Batteries With 18650 Cell

It is common to reference charging and discharging to the Ah capacity of the battery. In the case of the Inspired Energy battery, 6.6 Ah of capacity correlates to a “1 C” rate of 6.6 A. Thus if the battery is capable of discharging at 6.6 A, this is equivalent to saying it is capable of discharging at “1 C.” Under specified temperatures, the batteries are actually capable of discharging at up to 8 A (or 1.2 C) and charging at 4 A (or 0.61 C). The charge and discharge rates are very important to consider when designing load profiles because if they are exceeded, battery damage can occur. As the operating temperature goes below -10 °C or above 50 °C during discharge, the battery current must be derated according to manufacturer’s recommendations. Current derating must also be applied during charge except the following temperatures apply: 0 °C and 45 °C. The battery may be stored between -20 °C and 60 °C. These limitations must be accounted for during the operational concept development and thermal analysis of TINYSCOPE.

Microchips on the batteries work in concert with the IBPS hardware and software to conform to the System Management Bus and Smart Battery Data Specifications [25]. As per the specifications, the batteries communicate dozens of data points to the IBPS which can then be accessed via serial communication with the IBPS. Data like voltage, current, temperature, state of charge, and number of cycles are monitored while other parameters like minimum voltage to shutdown and maximum battery current to shutdown can be commanded.

The BB-04 model of the IBPS can accept up to four 6.6 Ah capacity batteries for a total system capacity of 26.4 Ah. This level of capacity would entail over 2.4 kg of mass just for the batteries and is not practical for TINYSCOPE. The BB-04 autonomously handles all aspects of battery charging and discharging sourcing the power for the load first from the external power supply and then from the batteries when required. In the case of TINYSCOPE, this would mean that the BB-04 would use the batteries during eclipse and when a low amount of solar power is being collected from the solar panels.

Similar to the IBPS itself, the OEM batteries were not specifically designed for operation in space. However, the battery design conforms to the United Nations international transportation regulations for lithium ion batteries. To conform to this standard, each battery's design must pass a series of tests known as the UN T-Tests [26]. Eight separate tests including altitude simulation, thermal shock, vibration, shock, short circuit, impact, overcharge, and forced discharge make up the T-Tests (reference Appendix E for a summary of specific criteria). Analysis of the test criteria show that some of the testing is far beyond what is expected for TINYSCOPE. One example of this is the shock test. The procedure is listed as, "Half sine shock of peak acceleration of 150 G duration 6 ms. 3 shocks in positive direction & 3 shocks in negative direction in each of 3 perpendicular axes: A total of 18." The test is run on a sample size of eight fully charged batteries and then the same eight fully discharged batteries. The pass requirement is, "No mass loss, leakage, venting, rupture, disassembly, or fire and OCV [open circuit voltage] after test  $\geq$  90% OCV before test." Some of the tests

include operational usage of the batteries while others do not. For example, the batteries are not being used during vibration and shock tests but are being used during the short circuit and overcharge tests. While additional on-site battery testing would likely be performed, the T-Tests provide a high degree of risk reduction.

Despite the likelihood that Inspired Energy's batteries will work in TINYSCOPE's application, any batteries that conform to the electrical requirements of the BB-04 IBPS may be used. However, this would require the implementation of SMBus and Smart Battery specifications on separately purchased cells. The TINYSCOPE program may choose to do this if it is deemed too risky to use Inspired Energy's non-space rated lithium ion cells. Two manufacturers are identified here for future reference: Quallion, LLC (Sylmar, California) [27] and Saft S.A. (Bagnole, France) [28]. Both firms market space-rated 3.6 V lithium ion cells that have ample space flight heritage. Many different levels of capacity and charge, discharge rates are available.

## **2. Alternative Batteries**

While the long pack version of Inspired Energy's OEM battery could work for TINYSCOPE, there are several potential shortcomings to this strategy. First, the battery size would be very difficult to integrate into TINYSCOPE's very small satellite bus. At almost 30 cm long, one battery would run almost the entire length of TINYSCOPE's 3U frame. The placement of all other components would be impacted along with the highly undesired effect of increasing the complexity of the thermal properties of the entire spacecraft. Secondly, the long pack's relatively large electrical capacity (6.6 Ah) would be an overall inefficient use of mass and space on the satellite compared to what is required to supply the loads. For example, it is estimated that there would be less than a 5% depth of discharge at this high of a capacity. Lastly, an issue that will be elaborated on in Chapter IV is the single point failure nature of using only one battery port on the BB-04. The BB-04 has inherent redundancy on its printed circuit board

(PCB) with respect to battery control because it has two chips that each control two batteries each. If only one battery is used, a single failure in the microchips on the battery or on the controlling microchip on the BB-04 will cause the EPS to stop functioning. Using one very large battery provides a lot of capacity but no defense against the situation described above. Conversely, using multiple battery ports does provide some protection. However, the use of multiple long pack batteries is impossible on TINYSCOPE.

As mentioned previously, the IBPS product line, including the BB-04, is designed around the use of 14.4 V battery packs. Inspired Energy makes several other model batteries ranging from 7.2 V to 25.2 V and 21.6 Wh up to 95 Wh. Other readily available 14.4 V batteries include capacities of 37 Wh (or 2.6 Ah) and 75 Wh (or 5.2 Ah). The dimensions of these batteries are 22.9 mm in height by 86.4 mm in length by 78.7 mm in width and 22.9 mm in height by 152.4 mm in length by 78.7 mm in height respectively. The 2.6 Ah battery has a mass of 220 g while the 5.2 Ah battery has a mass of 470 g. One string of four series cells make up the 2.6 Ah battery while the 5.2 Ah battery adds an additional string, i.e. four series cells in two parallel strings. While these batteries conform to the UN T-Tests, it is not known if the BB-04 will work properly with them. This is investigated further in Chapter IV, Section C, Battery Compatibility Test.

### **3. Depth of Discharge and Number of Cycles**

A critical aspect of designing a satellite's EPS is the number of charge-discharge cycles a battery can be expected to last. Generally speaking, the higher the depth of discharge (DOD), the lower the number of cycles the battery will last. The exact relationship between these two variables depends on many parameters but most significantly on battery chemistry. Figure 11–11 in [15] shows this relationship for nickel cadmium (NiCd) and nickel hydrogen (NH<sub>2</sub>) batteries. Figure 15, below, reproduces this graph.

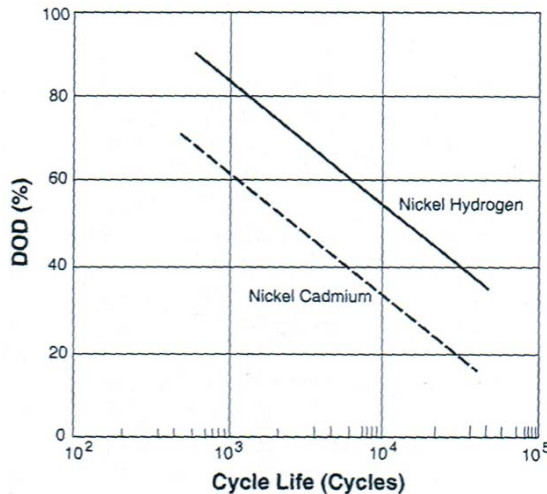


Figure 15. Depth-of-Discharge versus Cycle Life for NiCd & NH<sub>2</sub> From [15]

Because the above data is not readily available in the literature for lithium ion batteries, manufacturer data must be used to estimate battery lifetime. Manufacturers typically report the number of full discharge cycles at which 80% of initial capacity is maintained. For example, Inspired Energy's batteries are all rated at 300 cycles. This means that the manufacturer guarantees that the 6.6 Ah battery will maintain 5.28 Ah, i.e.,  $0.8 \times 6.6 = 5.28$ , after 300 cycles of 100% discharges followed by 100% charge periods. Because 100% discharge cycles will not be used in LEO, the expected number of cycles can be adjusted according the following procedure for Inspired Energy's batteries [29].

$$\begin{aligned}
 (\text{Absolute Number of Cycles}) \times (\text{Nominal Battery Capacity}) &= \text{Total} [\text{Cycle} * \text{Capacity}] \\
 (\text{Number of Cycles}) \times (\text{Capacity Expected To Use}) &= \text{Total} [\text{Cycle} * \text{Capacity}] \quad (11) \\
 \text{Number of Cycles} &= \frac{(\text{Total} [\text{Cycle} * \text{Capacity}])}{(\text{Capacity Expected To Use})}
 \end{aligned}$$

The absolute number of cycles is the point at which the capacity no longer maintains a linear relationship with the number of cycles. For the manufacturer of Inspired Energy's battery cells, from the first charge, discharge cycle through the 300<sup>th</sup>, the capacity falls off from 100% to 80% linearly. Nominally, after the 300<sup>th</sup> charge, discharge cycle, the rate of change of the retained capacity falls off at a faster pace. At some point beyond 300 charge, discharge cycles, the slope

becomes very steep rendering the battery useless. For Inspired Energy batteries, the absolute number of cycles is approximately 450. The nominal battery capacity is the manufacturer's rating for battery capacity. In the case of the 6.6 Ah battery, this value is 6.6. Applying Equation 11 for the example above gives the following results:

$$(450 \text{ cycles}) \times (6.6 \text{ Ah}) = 2,970 [\text{Cycles} * \text{Ah}]$$

$$(Number \text{ of } Cycles) \times (1.2 \text{ Ah}) = 2,970 [\text{Cycles} * \text{Ah}]$$

$$Number \text{ of } Cycles = \frac{(2,970 [\text{Cycles} * \text{Ah}])}{(1.2 \text{ Ah})} = 2,475 \text{ Cycles}$$

It is important to note that this method will only give a rough order of magnitude of the number of cycles the batteries will last. Nonetheless, this estimation is important for predicting spacecraft EPS lifetime. To apply this technique to TINYSCOPE, the expected capacity to be used must be known. Additionally, this number must take into account battery dis/charge, and circuit efficiencies. Chapter II, Section C and Appendix B list the details of the formulation of the expected capacity to be used during normal operations, launch and checkout, and contingency operations. The 0.7553 Ah value for normal operations will be used in this example since this will be TINYSCOPE's long-term mode. Observe that the expected DOD is  $0.7553 \text{ Ah} / 5.2 \text{ Ah} = 14.5\%$  during normal operations.

The last value that must be known (or assumed) is the nominal battery capacity. It has already been stated that the 6.6 Ah long and flat pack batteries will not likely be used. However, one probable configuration is two 2.6 Ah batteries connected to two separate BB-04 battery ports. This gives a total capacity of 5.2 Ah. Equation 11 is now applied:

$$(450 \text{ cycles}) \times (5.2 \text{ Ah}) = 2,340 [\text{Cycles} * \text{Ah}]$$

$$(Number \text{ of } Cycles) \times (0.7553 \text{ Ah}) = 2,340 [\text{Cycles} * \text{Ah}]$$

$$Number \text{ of } Cycles = \frac{(2,340 [\text{Cycles} * \text{Ah}])}{(0.7553 \text{ Ah})} = 3,098 \text{ Cycles}$$

TINYSCOPE has a threshold lifetime of one year and a target lifetime of two years [5]. A 500 km altitude orbit has an orbit period of  $\frac{2\pi}{\sqrt{\mu}} r^{3/2} = 5,676.8$  sec = 94.6 min = 1.577 h. This means that there are  $\frac{24h}{1.577\text{ h}/\text{orbit}} = 15.21$  orbits in each 24-hour day. This equates directly to the number of charge-discharge cycles, i.e. there are 15.21 charge-discharge cycles per day with 5,555 cycles in one year and 11,110 cycles in two years. Thus, it can be seen that Inspired Energy's 3,098 cycles falls about 45% short of the threshold requirement for mission lifetime.

A mitigating factor to this potential shortfall is the fact that the rule-of-thumb presented in Equation 11 produces the same order of magnitude as the required 5,555 cycles. Equation 11 predicts that the batteries will last approximately 200 days or about 6.5 months. This is a substantial amount of time that would definitively show the feasibility of Project TINYSCOPE. Because the estimate produces an order of magnitude calculation, it is feasible that the batteries could last up to 10,000 cycles. This would be longer than one year and eight months. In the end, the Principle Investigator would need to decide if this is a risk that can be accepted or if further testing or other mitigation is needed.

## G. MASS BUDGET

The mass of the entire EPS is made up of the solar cells, the protective cover for the solar cells, the aluminum structure that the solar cells are mounted to, the PMAD electronics, the batteries, and an estimate for the harnessing to interconnect the above components. The solar cell mass per unit area was given by the manufacturer. This value was then multiplied by the product of the packing factor and the overall solar array area to arrive at a mass for the solar cells. The cover was conservatively estimated to be the same mass as the solar cells. The mass for the PMAD electronics was given by Ocean Server. Inspired Energy, the battery manufacturer, gave a value of 220 g for its ND2054 model.

The batteries are discussed in great detail in the following section but notionally two batteries are included here. The density of aluminum was multiplied by 2 mm (notional thickness of solar panel “wings”) to arrive at a mass per unit area. This was multiplied by the total area of the solar array “wings.” Finally, a 4% overhead estimate for harnessing was included. Table 9 summarizes the mass budget of TINYSCOPE’s EPS.

	Unit Mass	Units	Area (m^2)	Number	Total (kg)
Structure	540	mg/cm^2	0.1449895		0.78
Solar Cells	84	mg/cm^2	0.1159916		0.10
Solar Cell Cover			0.1159916		0.10
Batteries	0.22	kg		2	0.44
Regulation & Control	0.2	kg		1	0.20
Subtotal					1.62
Cabling (4% of total)					0.06
TOTAL					1.68

Table 9. TINYSCOPE EPS Mass Budget

THIS PAGE INTENTIONALLY LEFT BLANK

### III. SIMULATION

#### A. TOP LEVEL DESCRIPTION

In order to gain better insight into how the EPS designed in Chapter II will operate in its intended orbit, a detailed Matlab/Simulink<sup>©</sup> model from [16] was customized and extended for TINYSCOPE. To achieve a high level of fidelity, many of the parameters from Chapter II are used in various blocks of the Simulink<sup>©</sup> model. Solar intensity, load levels, power collected, and battery state of charge are plotted versus time and investigated.

It is useful to view the EPS model in terms of seven categories of blocks.

- Basic orbit blocks are depicted in cyan.
- Sun on or off and the intensity of sun when on are depicted in yellow.
- Solar cell physical constants, solar cell orientation, and solar array size are depicted in orange.
- Load power and timing are depicted in green.
- Power management and distribution (PMAD) electronics, efficiencies, and battery parameters are depicted in red.
- Blocks that are for data collection within the model are depicted in gray.

Several blocks of the model depend upon a parameter definition file that is loaded when the simulation is first run. The full model is shown in Figure 16 on the following page. The justification for each of the blocks is discussed in turn below while the full listing of Matlab code is shown in Appendix F.

## EPS Model

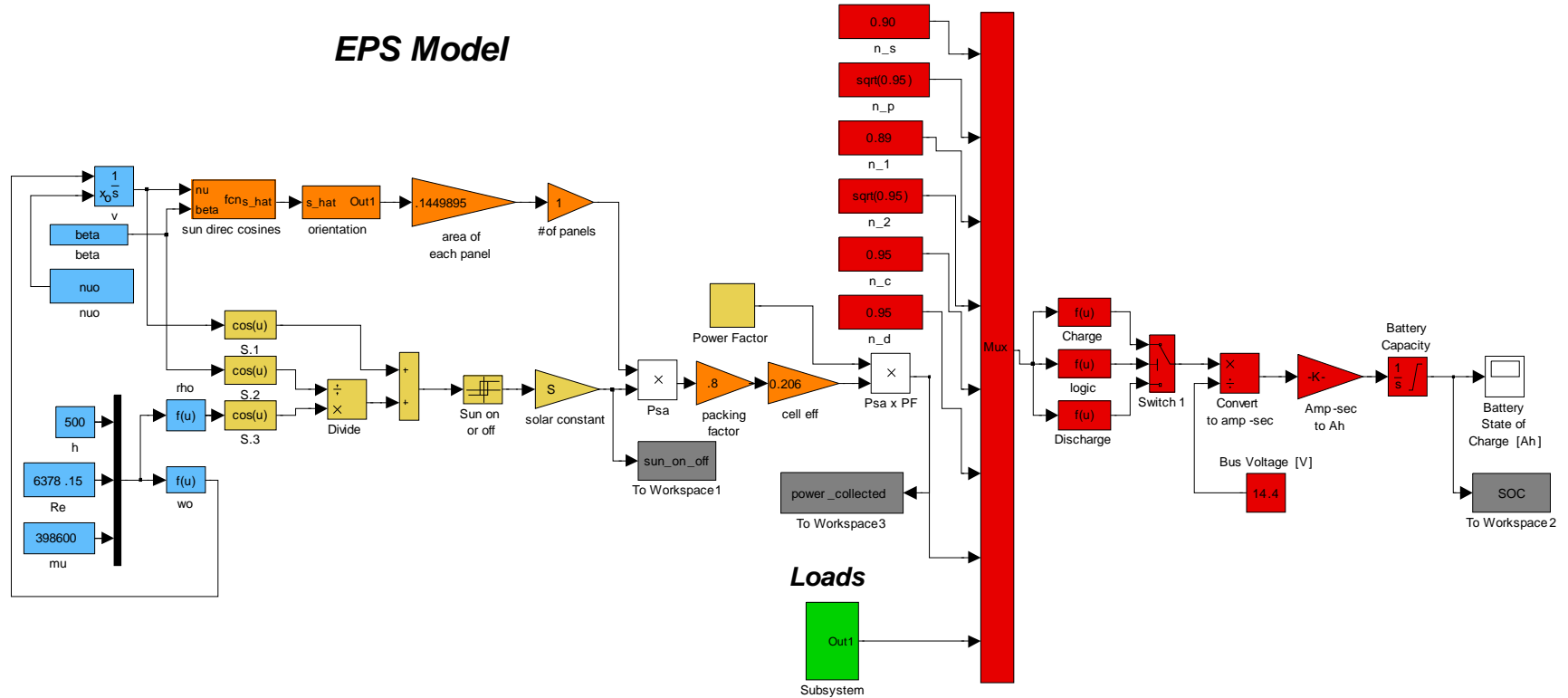


Figure 16. Integrated Matlab/Simulink© EPS Model After [16]

## B. BASIC ORBIT

The cyan blocks have only one varying output—the satellite's angle starting from an arbitrary position around the earth with respect to time. This value is derived for a circular orbit by equating the radial component of acceleration of a rotating body with the gravitational acceleration of the satellite. Equation 11–21 of [30] states that the radial component of linear acceleration  $a_r$  is the product of the square of the angular velocity of a rotating body  $\omega$  and the distance at which that body is from the center of rotation  $r$ .

$$a_r = \omega^2 r \quad (12)$$

Equation 14–12 of [30] states that the gravitational acceleration  $a_g$  is

$$a_g = \frac{GM}{r^2} \quad (13)$$

Where  $G$  is the gravitational constant ( $6.67 \times 10^{-11} N \cdot m^2 / kg^2$ ),  $M$  the mass of the earth ( $5.974 \times 10^{24} kg$ ), and  $r$  is the square of the distance between the orbiting body and the center of the earth.

Setting Equations 12 and 13 equal to each other and solving for the angular velocity  $\omega$  results in,

$$\omega = \sqrt{\frac{\mu}{r^3}} \quad (14)$$

Where  $\mu$  has the value  $398,600 \frac{km^3}{s^2}$  and  $r$  is equal to the sum of earth's radius (6378.15 km) and TINYSCOPE's altitude (500 km). The block labeled "wo" is set to Equation 14. This value, along with the initial position of the satellite in its orbit "nuo," is input to the time integral block labeled "v," i.e. nu. The value for "nuo" is arbitrary and is used in practice only to adjust how long until the TINYSCOPE model enters eclipse.

The two remaining cyan blocks are made up of one block that is prescribed indirectly, “rho,” and one that is prescribed directly, “beta.” The angular radius of the spherical earth as seen from the spacecraft, “rho,” is defined in Equation 5–16 of [15] as,

$$\sin \rho = \frac{R_E}{R_E + h} \quad (15)$$

Equation 15 is formulated using the definition of the sine function and inspection of Figure 17, below,

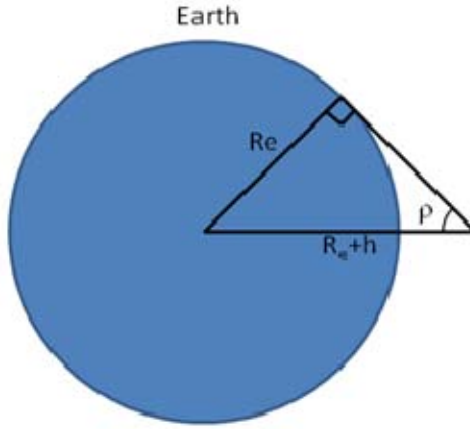


Figure 17. Geometric Relationship Between Earth and Spacecraft

The constant, rho, is used in the determination of when the spacecraft is in direct sunlight.

The final cyan block, “beta,” is critical to accurately predicting the varying length of eclipse periods for LEO satellites as they orbit the earth and as the earth orbits the sun. The beta angle is defined as the angle between the sun’s solar rays and the spacecraft orbit plane. Although a formal development of the definition of beta is beyond the scope of this discussion, one form is given in [31] as,

$$\beta = \sin e \cos i \sin u + \left[ \frac{\sin i (1 - \cos e) \sin(u + w)}{2} \right] - \left[ \frac{\sin i (1 + \cos e) \sin(u - w)}{2} \right] \quad (16)$$

Where  $e$  is the tilt axis of the earth, i.e.  $23.44^\circ$ ,  $i$  is the satellite inclination (discussed below),  $u$  is the right ascension of the sun in the ecliptic plane, and  $w$

is the right ascension of the ascending node of the satellite's orbit. The values for  $e$  and  $i$  are constant while the parameters  $u$  and  $w$  are periodic. Because the terms in Equation 16 are products of sinusoids, one might guess that Equation 16 will produce the rough shape of a sinusoid. The physical interpretation of the beta angle is graphically illustrated in Figure 18. Two bounding cases for eclipse length are useful to observe. A  $90^\circ$  beta, the satellite will never be in the earth's shadow, i.e., it will not enter eclipse. However, as beta approaches  $0^\circ$ , eclipses will be longest.

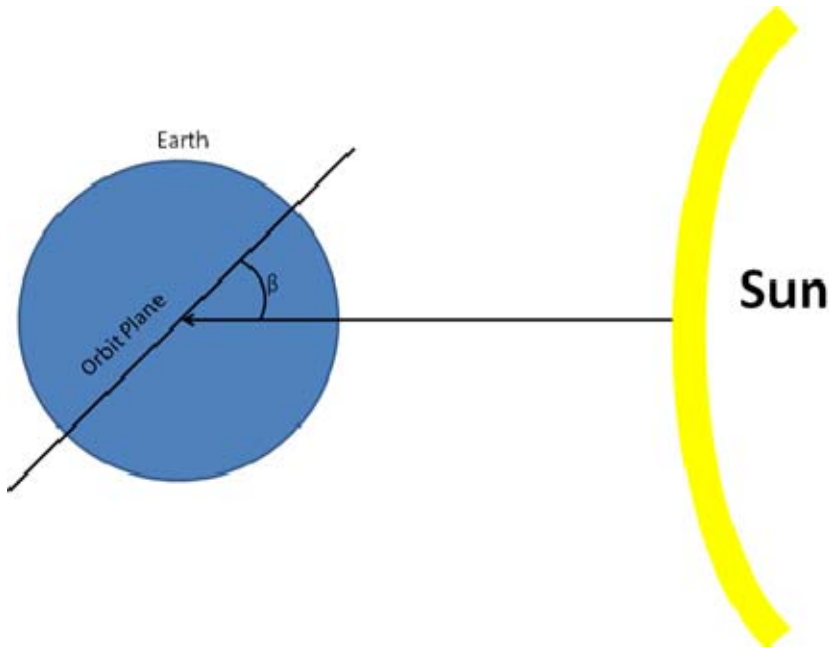


Figure 18. Illustration of Beta Angle

The length of time a satellite spends in eclipse has obvious thermal and power generation implications. If the beta angle is not calculated during the simulation, as depicted in Figure 16, then a realistic value must be carefully chosen. Additionally, since a given beta corresponds to a given position of the earth in orbit around the sun, a realistic value for solar intensity must also be sensibly chosen. Both of these values could be calculated in real-time during the simulation; however, this would add unnecessary complexity. A prudent approach is to choose a worst-case scenario based on the combination of beta

angle, solar intensity, and solar cell adjusted efficiency. Figure 19 uses Equation 16 to plot the beta angle for TINYSCOPE and models the solar intensity at the top of earth's atmosphere as a sinusoid varying from  $1,322 \text{ W/m}^2$  to  $1,414 \text{ W/m}^2$  as described in [21].<sup>d</sup> While TINYSCOPE's sun-synchronous orbit requires an inclination of approximately  $97.4^\circ$ , a right ascension of ascending node (RAAN) of  $0^\circ$  is chosen arbitrarily.

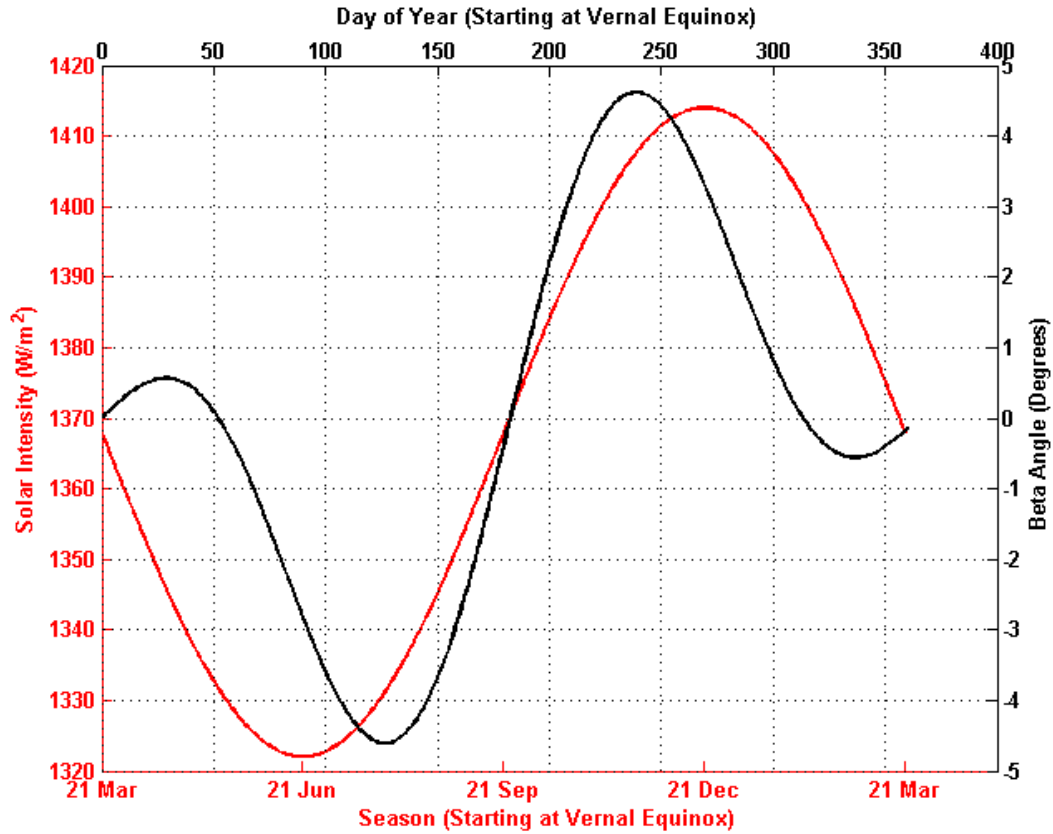


Figure 19. Solar Intensity and Beta Angle versus Day of Year

The graph shows that the smallest beta, i.e., longest eclipses, occur about midway between 21 March and 21 June. At this point, the solar intensity is approximately  $1,335 \text{ W/m}^2$ . Referencing Table 7, one can see that solar cell efficiency at this point is near its highest, however. Conversely, lowest solar cell efficiencies will be near the point where the solar intensity is highest, i.e., at 21

---

<sup>d</sup> Complete Matlab script is contained in Appendix E.

December. At this time, the beta angle is about  $3^\circ$ . The simulation should be run for the two cases listed below to determine which is the worst case scenario.

1. Case 1
  - Solar intensity =  $1,335 \text{ W/m}^2$
  - Beta angle =  $0^\circ$
  - Solar Cell Efficiency = 0.223
2. Case 2
  - Solar intensity =  $1,414 \text{ W/m}^2$
  - Beta angle =  $3^\circ$
  - Solar Cell Efficiency = 0.203

It should be noted that inclination values other than  $97.4^\circ$  will change the shape of the beta function in Figure 19. This implies the above analysis must be accomplished for each specific case considered for TINYSCOPE. The present analysis assumes the above cited conditions. The Matlab code in Appendix G can be used for the general case.

### C. SOLAR INTENSITY

The yellow blocks determine when the spacecraft is in eclipse and thus when the solar array will not be collecting power. The block labeled “S” was just discussed and will be set to the two cases listed above. The “Power Factor” block is a simple way to set solar collection to zero when TINYSCOPE is imaging. This is done to overlap in time with the power profile (developed in Chapter II, Section C). That is, the power factor coefficient is set to zero for the first 620 seconds of the simulation. Thus, regardless of what level of power the model collects during the first 10 minutes and 20 seconds, the product of the “Power Factor” and “ $P_{sa}$ ” blocks is zero. After 620 seconds, the “Power Factor” goes to one to allow any power level collected to pass through to the red PMAD logic blocks.

The remaining yellow blocks relate the current angular position of the satellite on a circle, labeled “nu,” to the point at which the satellite goes into eclipse. Slide 67 of [16] states a satellite is in eclipse if the following condition is true,

$$\cos \nu < -\frac{\cos \rho}{\cos \beta} \quad (17)$$

Thus, as the satellite’s current angular position, nu, is updated during the simulation, Equation 17 is applied to determine if the satellite is in eclipse or not. The physical interpretation is that the satellite is in the shadow of the earth. This results in an “on-off” condition that is then scaled by the “solar constant” value of either 1,335 W/m<sup>2</sup> or 1,414 W/m<sup>2</sup> as discussed above.

#### D. SOLAR ARRAY ORIENTATION & SOLAR CELL CONSTANTS

The orange blocks determine the solar incidence angle on the solar array, which is then scaled by the area of a solar panel and the number of panels. This is further scaled by the packing factor of the solar array and the solar cell efficiency. For the present case, the area is taken from Chapter II, Section D1 and the number of panels is set to one. The packing factor and cell efficiency are taken from Chapter II, Section D4 and D5, respectively.

To find the incidence angle of the sun on the solar panels, the attitude of the solar panel must be compared with the direction of the sun’s rays. The components of the solar unit vector written in the spacecraft body frame are given on slide 69 of [16] as

$$S = -(\cos \beta \sin \nu) X_0 - (\sin \beta) Y_0 - (\cos \beta \cos \nu) Z_0 \quad (18)$$

Where **S** is the unit solar vector and **X<sub>0</sub>**, **Y<sub>0</sub>**, and **Z<sub>0</sub>** are perpendicular axes of the spacecraft body frame. This is illustrated in Figure 20, below,

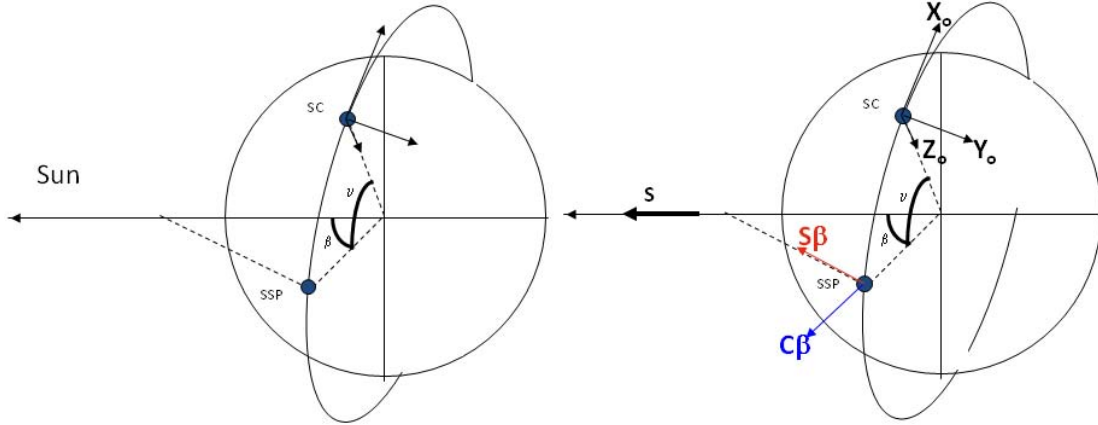


Figure 20. Solar Unit Vector in Spacecraft Body Frame After [16]

The vector dot product is then calculated for Equation 18 and the components of the surface normal vectors of the solar panels. Because TINYSCOPE will be sun soaking except for the 620 second imaging period, the “orientation” block simply contains the unit solar vector dot product with itself. This effectively sets the solar array to be always pointing at the sun. As discussed above, solar power is “turned off” for the 620 second imaging period through the use of the yellow “Power Factor” block. The contents of the “orientation” block are shown below,

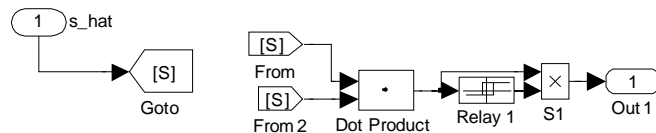


Figure 21. Contents of “orientation” Block

## E. LOADS

The load subsystem block contains the data from Table 1 together with the timing profile of Chapter II, Section C, Normal Operations.<sup>e</sup> This information was used to develop Figures 6 through 8. Additionally, line efficiencies and DC to DC converter efficiencies are also included in the load block. Including these

---

<sup>e</sup> Loads were defined with Matlab repeating table blocks.

efficiencies here treats them as if they are part of the load. When this is done, they are not needed for the PMAD control logic discussed in the next section. Although rough estimates for these efficiencies were used initially, hardware testing provided more accurate values that were incorporated as testing progressed. The contents of the load subsystem is shown below,

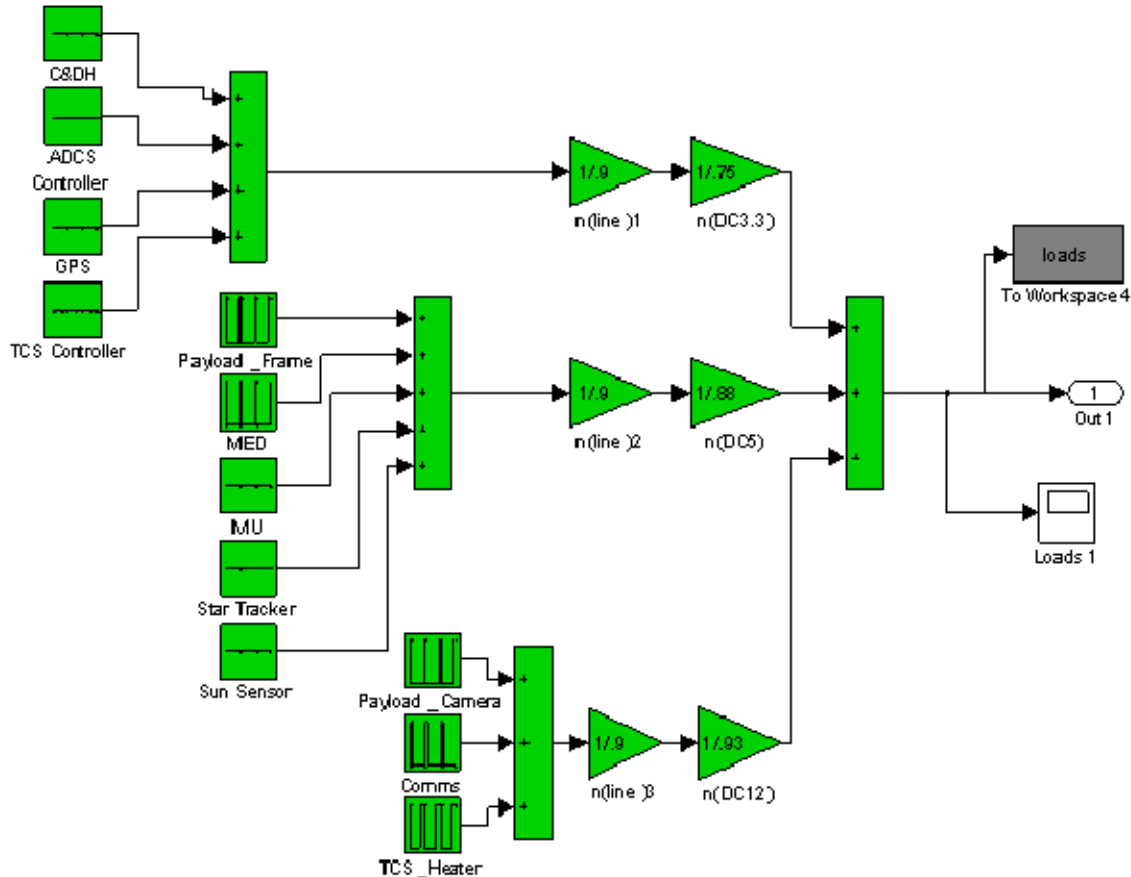


Figure 22. Contents of Load Subsystem Block

## F. POWER MANAGEMENT AND DISTRIBUTION, EFFICIENCIES, AND BATTERY

The control logic of the PMAD is represented by red blocks in the Simulink<sup>©</sup> model. This section of the model takes the loads and the power collected by the solar array as inputs and determines if the batteries are being charged or discharged. Several of the red blocks are designated as efficiencies of the Ocean Server IBPS BB-04 equipment. Figure 5 and Equation 6 were used

to determine the appropriate placement of these efficiencies in the Simulink<sup>©</sup> model. Some were placed in the green load block while some were associated with the red blocks and were subsequently used in the “logic” block. The exact values of all efficiencies will be dealt with in Chapter IV. It is very useful to refer to Figure 5 during the remaining discussion of this section.

The heart of the PMAD control logic are the “logic,” “Charge,” and “Discharge” blocks. The batteries will charge if the power from the solar arrays is greater than the power required by the load net of any applicable efficiencies. Conversely, the batteries will discharge if the product of the power from the solar arrays and any efficiencies is less than the power required by the load. Using the nomenclature of Figure 5 this can be stated mathematically as,

$$\begin{aligned} \text{Charge if } & \eta_s P_{sa} > \frac{P_L}{\eta_p} \\ \text{Discharge if } & \eta_s P_{sa} < \frac{P_L}{\eta_p} \end{aligned} \quad (19)$$

One important assumption here is that the voltage provided by the charge circuit is sufficiently higher than the battery voltage to allow charging. In an actual circuit, batteries cannot be charged unless the charge voltage is above the battery’s voltage. Because the dynamic model prescribes TINYSCOPE’s attitude as sun soaking, the system must be designed so that the charge voltage will be higher than the battery’s instantaneous voltage. This was done in the series calculation of Chapter II, Section D6.

The appropriate efficiencies depend on the reference point chosen in the equivalent circuit of Figure 5. Inspecting Figure 4 and Equation 5 (the general case) and comparing them to Figure 5 and Equation 6 (TINYSCOPE’s specific case), the point just before the power controller efficiency  $\eta_p$  in the BB-04 power controller was chosen as the reference point.

During charge, the power from the solar array will be split between power going to the load (net of efficiencies) and power going to the batteries (also net of efficiencies). This is expressed mathematically in Equation 20, below,

$$P_{sa} = \frac{P_L}{\eta_p \eta_s} + \frac{P_{bc}}{\eta_c \eta_l \eta_s} \quad (20)$$

Observe that the DC to DC converter and line losses are not shown in Equation 20. Again, this is because they are contained in the green “load” block and not the PMAD control logic blocks. Solving for the power going into the batteries produces the following equation,

$$P_{bc} = \left( P_{sa} \eta_s - \frac{P_L}{\eta_p} \right) \eta_l \eta_c \quad (21)$$

Equation 21 is contained in the red block labeled “Charge.”

During discharge, the power from the solar array is not sufficient to supply the required load power. Thus, the batteries must be used to partially or fully supply the load. In either case, no power is being delivered from the solar arrays to the batteries. The power required by the load may be expressed as,

$$P_L = P_{sa} \eta_s \eta_p + P_{bd} \eta_d \eta_2 \eta_p \quad (22)$$

Again, note that the specific DC to DC converter efficiencies for each voltage provided and the line losses are not included here because they are contained in the green “load” block. Solving Equation 22 for the power supplied by the battery results in,

$$P_{bd} = \frac{\frac{P_L}{\eta_p} - P_{sa} \eta_s}{\eta_d \eta_2} \quad (23)$$

Note that if no power is being supplied by the solar array, as during eclipse or extreme slewing during sunlight, the second term of the numerator goes to zero. Equation 23 is contained in the red block labeled “Discharge.”

The red block labeled “logic” contains the following test condition,

$$P_{sa} \eta_s - \left( \frac{P_L}{\eta_p} \right) \quad (24)$$

When Equation 24 leads to a positive number, the “Switch 1” block passes through the value from the “Charge” block. Conversely, when Equation 24 leads to a negative number, the “Switch 1” block passes through the value from the “Discharge” block.

The next block, “Convert to amp-sec,” divides the value with units of watts coming from the “Switch 1” block to ampere-seconds by dividing by the nominal battery voltage of 14.4 V. Ampere-seconds are then converted to Ah by dividing by 3,600 seconds/hour. The “Battery Capacity” block is a time integration block that starts out at a prescribed value and cannot rise above another prescribed value. The values entered are derived from the battery capacity used in the calculations of Equation 11. Two single string batteries that each have four 2.6 Ah cells in series produce a total capacity of 5.2 Ah.

## **G. PARAMETER FILE**

The contents of the parameter file are included in Appendix F for reference.

## **H. RESULTS**

Figure 23, below, depicts the output from the simulation run over three consecutive orbits using the initial conditions for Case 1. Figure 24, below, depicts the output from the simulation run over three consecutive orbits using the initial conditions for Case 2.

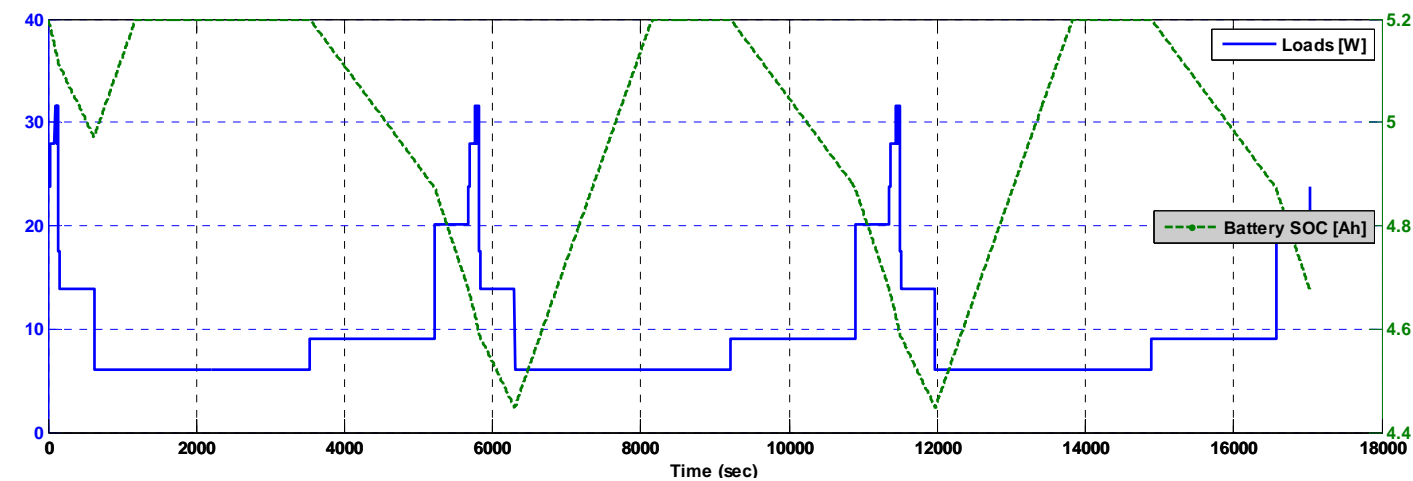
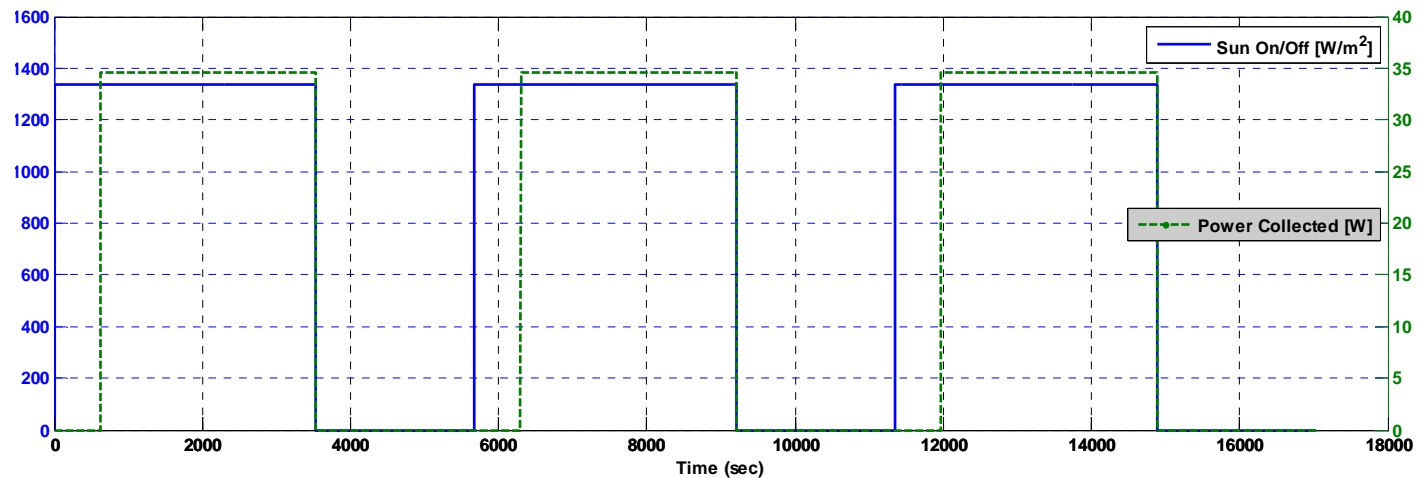


Figure 23. EPS Simulation Output, Case 1

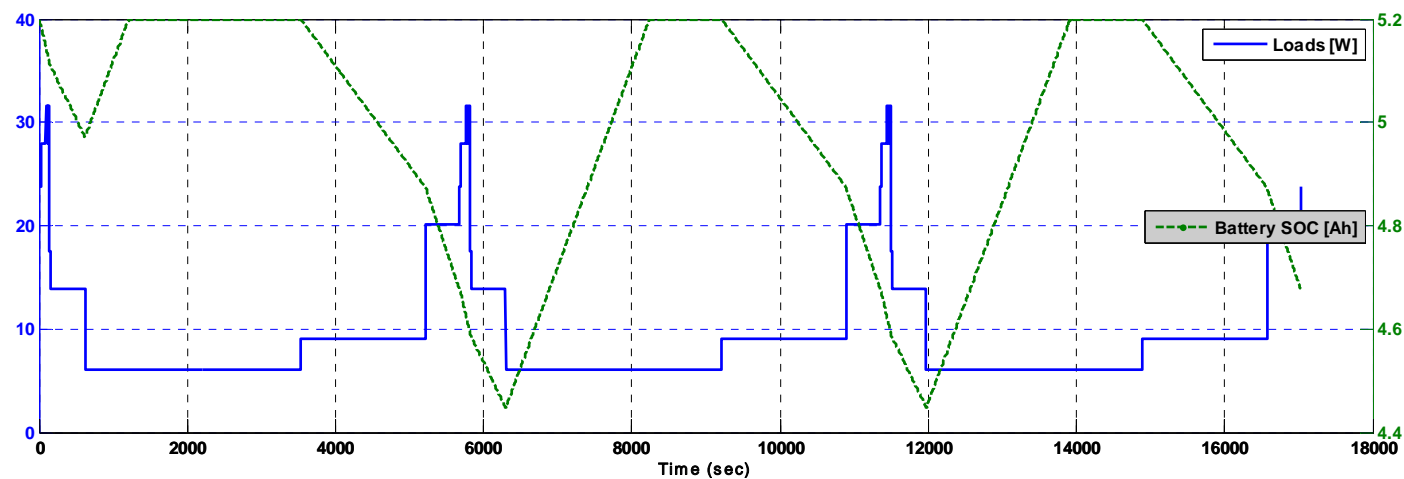
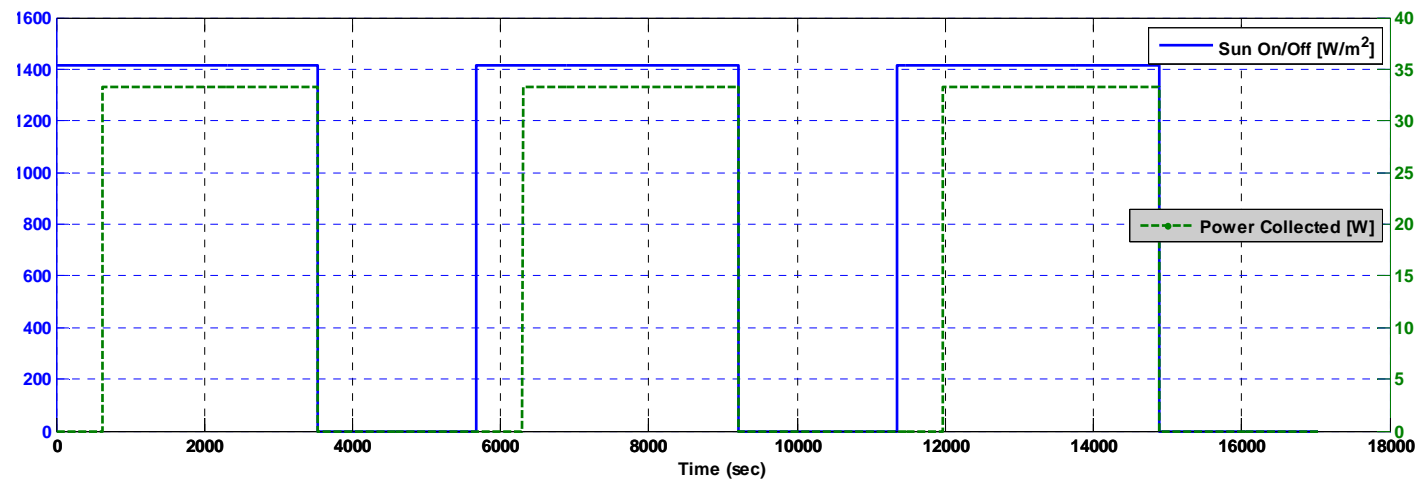


Figure 24. EPS Simulation Output, Case 2

The top panels of Figures 23 and 24 show data related to power collection. The solid blue line shows when TINYSCOPE is in or out of eclipse and the dashed green line shows how much power TINYSCOPE is collecting.<sup>f</sup> Case 1 collects about 35 W while Case 2 collects about 34 W. The difference in start times is caused by the “Power Factor” block being set to zero for the 620 second imaging period. Physically, this is when TINYSCOPE will be slewing; conservatively, TINYSCOPE will not be collecting any power. In reality, it is likely that TINYSCOPE will be collecting some power but this is not investigated here. The first 620 seconds were chosen because it would allow no battery charging before imaging loads would have to be supplied by the batteries.

The bottom panels of Figures 23 and 24 show the SOC of the battery and the load profile (adjusted for load line efficiencies and DC to DC converter efficiencies<sup>g</sup>) for the same period, of three orbits, as above. Overlaying the solid blue load profile on the dashed green SOC plot gives insight into the path of the SOC line. For example, the larger the jump in load power required, the more negative the slope of the SOC. One of the most critical aspects of the SOC line is whether it returns to the maximum level of 5.2 Ah by the end of the lighted portion of an orbit. If, as in this case, the SOC returns to 100% by the end of one orbit, single orbit energy balance has been achieved guaranteeing Equations 1 through 6 will hold.

Another important characteristic of the SOC line is the ratio of its minimum level to its maximum level. This is the battery depth of discharge (DOD). It can be seen that the battery SOC is initially at 5.2 Ah and drops to a minimum value of 4.45 Ah. The batteries maintain 85.5% of their charge resulting in a DOD of 14.5%. One can see that this DOD agrees with the value developed in Chapter II, Section F3. Thus, approximately 3,000 cycles or about 6 ½ months should be attainable.

---

<sup>f</sup> The green line is collected in the Simulink© model with the gray block labeled, “sun\_on\_off.” The blue line is collected with the gray block labeled, “power\_collected.”

<sup>g</sup> This load profile is higher than what is shown in Figures 6 through 8 because Figures 23 and 24 include the load line efficiencies and the DC to DC converter efficiencies. Reference Figure 22 to observe the placement of these efficiencies.

## I. SIMULATION CONCLUSION

One can see immediately that the results of the two cases are very close. This would not have been known without accomplishing the simulation, however. Based on both cases achieving single orbit energy balance and very reasonable battery DOD, the design of Chapter II using the 27% Emcore cells is recommended for TINYSCOPE. It should be noted that the simulation is based on many interdependent variables and care should be taken to update these parameters as required to ensure accurate results. With an established model for TINYSCOPE's EPS, it may now be run iteratively to establish sensitivities to solar array size, efficiencies, load level and timing, beta angle, orbit altitude, etc.

THIS PAGE INTENTIONALLY LEFT BLANK

## IV. HARDWARE TESTING

### A. INTRODUCTION

Whereas Chapters II and III focused on the design and simulation of the overall EPS of TINYSCOPE, Chapter IV examines the operating characteristics and possible limitations of the IBPS in the space environment. This task is required for any EPS design effort, but is even more critical when using the Ocean Server IBPS since it was designed for terrestrial use. Several questions arise immediately as to the ability of the IBPS to operate in space. Some of these questions are:

- Can the IBPS operate from a solar array?
- Can the IBPS operate using lower mass, and therefore lower capacity, batteries?
- What are the efficiencies of the components?
- Can the IBPS withstand the vibrations associated with a launch to low earth orbit?
- Can the IBPS survive TINYSCOPE's predicted thermal environment?
- Can the IBPS survive operating in a vacuum?

Most of these questions cannot be answered definitively in one chapter of a thesis—nor is that the intent. The purpose here is to conduct a preliminary investigation into the feasibility of successfully using the IBPS in a low-cost, moderate-risk space mission. This chapter will provide a reasonable amount of data and analysis upon which to base a sensible decision to either use or not use the Ocean Server IBPS. One question that is not addressed here is the susceptibility of the IBPS to a high energy radiation environment.

Before considering each of the above questions in turn, it is important to recall the motivation for looking into Ocean Server's IBPS. In particular, it stems from the guiding principles introduced in Chapter I, Section B2, i.e. use of COTS, short mission life, and low cost. It has been shown throughout Chapter II that the

IBPS meets all of these criteria. With that notion as a starting point, the hardware was tested and characterized as outlined in the subsequent sections.

## B. DETAILED HARDWARE DESCRIPTION

Before delving into the tests that were conducted, it is important to have a basic understanding of the system design and intended operation of the IBPS in general and the BB-04, DC-123 combination in particular. The information in this section is derived from Ocean Server documentation, namely [32], [33], and [34] except as noted.

An IBPS consists of one or more printed circuit boards, batteries, external power, and an external monitoring station. A typical setup for the boards is a base board, represented by “BB,” and a DC to DC converter board, represented by “DC.” Several different models of the IBPS provide various voltage, current, and power levels. The base board may be used alone but provides unregulated voltage. If a DC to DC converter board is used in conjunction with a base board, +/- 5% regulated voltage is provided but at an efficiency cost. In general, the DC board is more efficient when converting to a voltage that is close in magnitude and sign to the input voltage. This will be quantified in Section D, below. A representative IBPS is depicted in Figure 25.

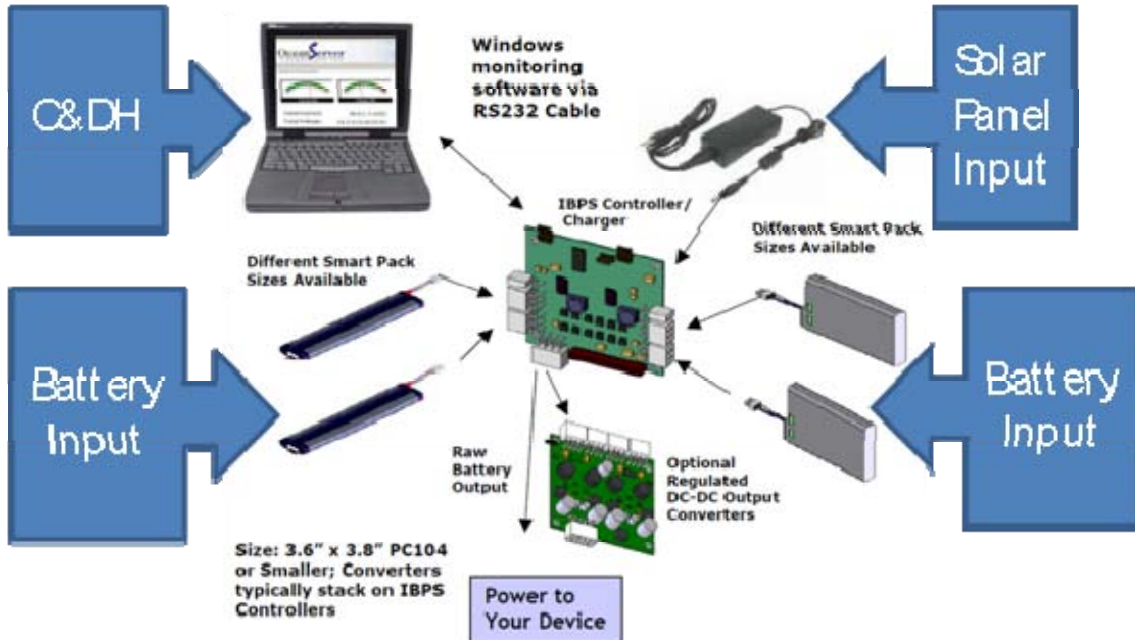


Figure 25. IBPS Components After [33]

The base board is designed to work with an AC adapter that provides 18 V at 5.56 A as an input. A serial communications connection may optionally be established to monitor system telemetry and command several system settings. Up to four OEM batteries may be connected to the BB-04.<sup>h</sup> Several different models of DC to DC converter may be connected to the base board, to which the load is then connected. Although 3.3 V, 5 V, +/- 12 V, 24 V, and 48 V are available on some models, the DC-123 provides only the first four voltage levels. The basic system specifications show that the BB/DC system is rated to work at up to 144 W from 0 °C to 50 °C. No rating is given with respect to vibration, radiation, or expected lifetime.

The telemetry available from the IBPS includes a dozen or so nonvolatile random access memory (NVRAM) data points along with detailed battery data including:

---

<sup>h</sup> Recall that the batteries are 14.4 V, 6.6 Ah, 95 Wh and are made up of 18650 lithium-ion cells. Ocean Server contracts with Inspired Energy to provide the 12 cell (three parallel strings of four series cells) batteries.

- A Smart Battery Data Specification Status code<sup>i</sup> (reported by battery)
- A code indicating charge power present, fully charged, fully discharged, or no good power (reported by battery)
- Voltage of battery (reported by battery)
- Current of battery—negative number implies discharge (reported by battery)
- Temperature of battery from thermocouple inside battery case (reported by battery)
- Charge percentage of battery (reported by battery)
- Capacity of battery in Ah (reported by battery)
- Total current of all batteries connected to the base board (calculated by base board)
- Average voltage of all batteries connected to the base board (calculated by base board)
- Average charge of all batteries connected to the base board (calculated by base board)
- Battery charge/discharge indicator (applied by base board, based on information reported by battery)
- Run time to empty in minutes and hours or time to fully charge in minutes and hours (calculated by base board based on information reported by battery and what the base board senses as the load)

Because much of the above data is collected by the batteries and then passed to BB, it can be monitored independently and subsequently compared to what BB reports via serial communications to check for proper operation of BB.

The following figures show close-ups of the base board (Figure 26) and the DC to DC converter board (Figure 28) as delivered, i.e. no modifications. Note the high number of passive and active components on the boards as well as the use of nylon connectors on each board.<sup>j</sup>

---

<sup>i</sup> See [50] for further information on this specification.

<sup>j</sup> The white connectors are Molex brand in the “Mini-fit Jr.” line of products. Reference [51] for additional details on representative Mini-fit Jr. Molex connectors.



Figure 26. Base board Power Controller, BB-04FR, Top Down View

Familiarity with the nomenclature of the connections will become very important in subsequent sections to maintain clarity during test setup and results discussions. Starting from the top left and moving in a counter-clockwise direction, connector nomenclature is listed below and is shown schematically in Figure 26:

- J1: Eight pin, Pins 2 and 4 are used as an On/Off switch
- J5: Two pin (positive voltage and ground), external power supply input. Charges batteries on J22 and J17
- J22: Five pin, battery connector input
- J17: Five pin, battery connector input
- J10: 10 pin, communications interconnect between BB-04 and DC-123
- J12: Five pin, battery connector input
- J21: Five pin, battery connector input
- J7: Two pin (positive voltage and ground), external power supply input. Charges batteries on J21 and J12

- J13: Four pin (two positive voltage, two ground), power interconnect between BB-04 and DC-123
- J8: 10 pin (converts to standard RS-232), serial communications input and output
- J9: 10 pin, factory use for programming onboard microprocessor only

Figure 27 shows a line drawing version of the picture in Figure 26. The connectors listed above are labeled with circular callout symbols in Figure 27. Comparing Figures 26 and 27 clearly identifies and shows the positions of the connectors.

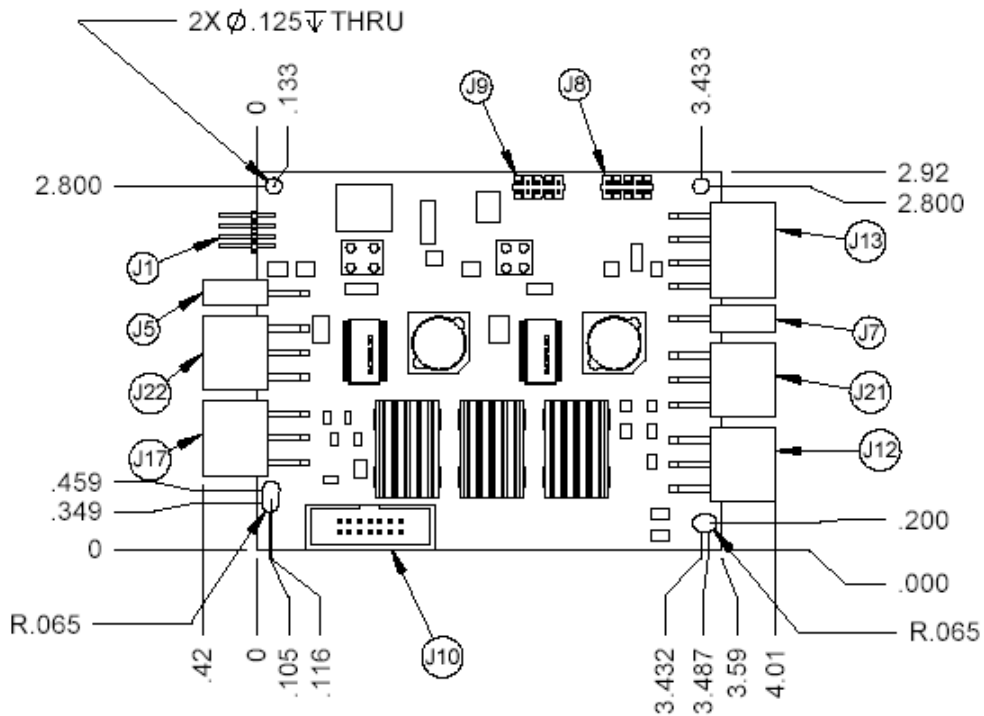


Figure 27. BB-04 Drawing From [33]

The DC-123 board rests on top of and on standoffs that are positioned through the corners of the BB-04. Again starting on the top left of Figures 28 and 29 and moving in a counter-clockwise direction, the connector nomenclature is:

- J6: Four pin (two 12 V power supply pins and two ground pins), load output
- J20: 20 pin (ATX pinout [35]), load output

- J10: 10 pin, communications interconnect between BB-04 and DC-123
- J2: Eight pin (four positive voltage, four ground), external power input
- J1: Eight pin (four positive voltage, four ground), external power input

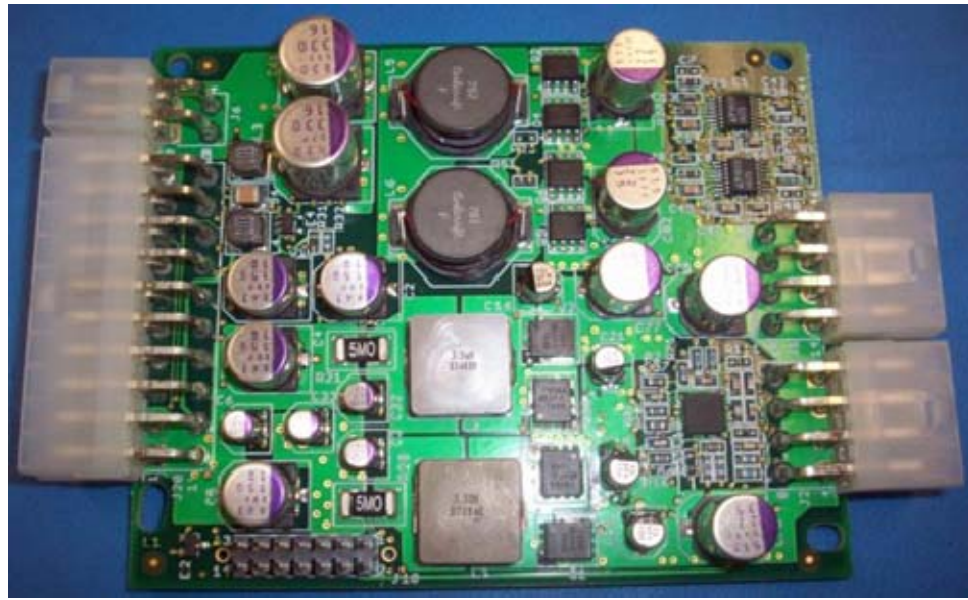


Figure 28. DC to DC Converter, DC-123SR, Top Down View

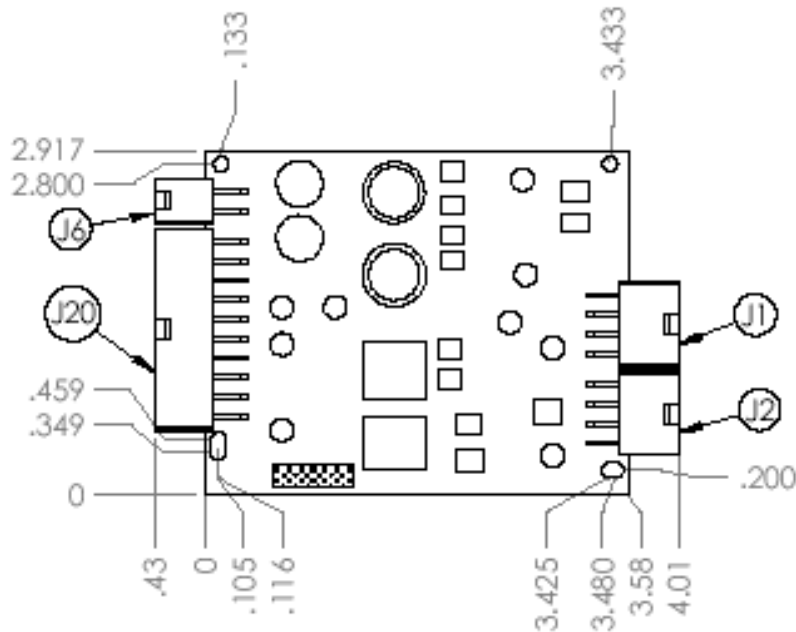


Figure 29. DC-123 Drawing From [33]

Passive components such as resistors, capacitors, and inductors maintain their electrical characteristics over relatively wide operating temperature ranges [36]. Although nylon, which makes up all of the white connectors in Figures 26 and 28, has a wide operating temperature range as well, it is also known to have a high outgassing rate in a vacuum relative to many other materials [37]. Additionally, certain types of electrolytic capacitors, the type used on the DC to DC converter board, are an outgassing risk in a vacuum. Outgassing is a critical issue for the electro-optical imaging payload of TINYSCOPE since any outgassed particles could render the optics useless.

Active components, such as integrated circuits, may be designed with various operating temperature ranges depending on manufacturer designs and processes. Since data for individual components was not supplied by Ocean Server for the IBPS, Table 10 was complied by close inspection of the BB-04 and DC-123 boards. Only components deemed critical from a temperature standpoint are included. Four categories of components are identified in yellow highlighting to identify them as potential limiting cases from a thermal standpoint.

In light of the potential mission limiting challenges raised above, several possible mitigating actions were identified and implemented on the test articles. These actions, along with several tests, are discussed in detail in the subsequent sections of this chapter.

D123SR									
Type / Component / Description	Board Nomenclature	Primary Case Marking	Add'l Marking	Mfg Part #	Manufacturer	Oper. Low Temp	Oper. High Temp	Qty	URL
Switching Regulator	E1, E3	LT832	1625	LTC1625	Linear Technologies	0*	70*	2	<a href="http://cds.linear.com/docs/Datasheet/1625f.pdf">http://cds.linear.com/docs/Datasheet/1625f.pdf</a>
Switching Regulator	E10	LT819	3728LE	LTC3728LE	Linear Technologies	-40	85	1	<a href="http://cds.linear.com/docs/Datasheet/3728lxfd.pdf">http://cds.linear.com/docs/Datasheet/3728lxfd.pdf</a>
Single N-Channel, Logic Level, PowerTrench® MOSFET	Q2, Q4, Q5, Q6	FAG3AP	FDS 6680A	FDS 6680A	Fairchild	-55	150	4	<a href="http://www.fairchildsemi.com/ds/FD%2FFDS6680A.pdf">http://www.fairchildsemi.com/ds/FD%2FFDS6680A.pdf</a>
N-Channel Reduced Qg, Fast Switching MOSFET	Q1, Q3	7860	AH T64B	Si7860DP	Vishay/Siliconix	-55	150	2	<a href="http://www.vishay.com/docs/71854/71854.pdf">http://www.vishay.com/docs/71854/71854.pdf</a>
N-Channel 30-V (D-S) MOSFET	Q30, Q32	7856A	AP T64B	Si7856ADP	Vishay/Siliconix	-55	150	2	<a href="http://www.vishay.com/docs/73157/73157.pdf">http://www.vishay.com/docs/73157/73157.pdf</a>
Schottky Rectifier	D2, D3, D5	FA506	B34	MBRS340	Fairchild	-65	125	3	<a href="http://www.fairchildsemi.com/ds/MB/MBRS340.pdf">http://www.fairchildsemi.com/ds/MB/MBRS340.pdf</a>
Total								14	* Same chip as 1625I but not tested to -40 - 85

BB-04SR									
Type / Component / Description	Board Nomenclature	Primary Case Marking	Add'l Marking	Mfg Part #	Manufacturer	Oper. Low Temp	Oper. High Temp	Qty	URL
Microchip PIC	E7	PIC18F458	-I/PT	PIC18F458-I/PT	Microchip	-40	85	1	<a href="http://ww1.microchip.com/downloads/en/DeviceDoc/41159d.pdf">http://ww1.microchip.com/downloads/en/DeviceDoc/41159d.pdf</a> <a href="http://www.linear.com/pc/downloadDocument.do?navId=H0,C1,C100,C1037,C1078,C1089,P2325,D1958">http://www.linear.com/pc/downloadDocument.do?navId=H0,C1,C100,C1037,C1078,C1089,P2325,D1958</a>
Dual Smart Battery System Mgr	E3, E4	LTC1760CFW		LTC1760CWF	Linear Technologies	0**	70**	2	
Dual 30V P-Channel PowerTrench MOSFET	Q18, Q19, Q20, Q21, Q22, Q23, Q30, Q31	PJ7AF	FDS 4935A	FDS4935A	Fairchild	-55	175	8	<a href="http://www.fairchildsemi.com/ds/FD/FDS4935A.pdf">http://www.fairchildsemi.com/ds/FD/FDS4935A.pdf</a>
N-Channel PowerTrench MOSFET	Q4, Q5, Q6, Q7, Q8, Q9	PJ9CS	FDS 8984	FDS8984	Fairchild	-55	150	6	<a href="http://www.fairchildsemi.com/ds/FD/FDS8984.pdf">http://www.fairchildsemi.com/ds/FD/FDS8984.pdf</a>
Dual 1-Of-4 FET Mux/Demux with -2 V Undershoot-Protection	E2	CU253C	76KG4 J6C3		Texas Instruments	-40	85	1	<a href="http://focus.ti.com/docs/prod/folders/print/sn74cbt3253c.html">http://focus.ti.com/docs/prod/folders/print/sn74cbt3253c.html</a>
Micropower low dropout regulators with shutdown	E9	LT80603	11295	LT1129	Linear Technologies	0	125	1	<a href="http://cds.linear.com/docs/Datasheet/112935ff.pdf">http://cds.linear.com/docs/Datasheet/112935ff.pdf</a>
RS-232-Compatible Transceivers	E8	3313	CUB	MAX3313	Maxim	0*	70*	1	<a href="http://datasheets.maxim-ic.com/en/ds/MAX3311-MAX3313.pdf">http://datasheets.maxim-ic.com/en/ds/MAX3311-MAX3313.pdf</a>
Total								20	* Same chip as EUB but not tested to -40 - 85 ** Spec sheet states that the chip is expected to work from -40 to 85 but isn't tested to these extremes

Table 10. IBPS Component Operating Temperature Limits

### C. SOLAR PANEL COMPATIBILITY TEST

To be used for TINYSCOPE's EPS, the IBPS must be easily configured for use with a solar panel. An Ocean Server technical note supplies guidance for implementing a solar panel with the BB-04 [38]. The application note was followed and battery charge/discharge data was collected. The system performed as expected. A PowerFilm Solar Model R15–300 Rollable Solar Charger with the following specifications was used [39].<sup>k</sup>

Specification	Value
Rated Power ( $P_{\max}$ )	5 W
Operating Voltage ( $V_{mp}$ )	15.4 V
Operating Current ( $I_{mp}$ )	0.3 A
Dimensions	292 mm x 531 mm
Weight	0.6 LBS

Table 11. Test Solar Panel Specifications

The load used during the test was a Microhard Systems, Inc. industrial wireless modem model number, MHX-2420. As a 2.4 GHz radio, it is representative of TINYSCOPE's communications subsystem. Although the current required is not specified, its rated voltage input is 9 V to 30 V [40]. The 12 V supply from DC-J20 was used to power the MHX-2420.

Figure 30 shows the overall field test setup while Figure 31 shows details of the power controller and load. The IBPS is on the left of Figure 31 while the load is mounted on the right.

Ocean Server provides software called FULLBATS that allows data logging of battery current, voltage, temperature, capacity, and a system status

---

<sup>k</sup> These specifications are given for an air mass value of 1.5.

code. This data is graphed in Figure 32 for the single battery that was attached to the BB-04 during the test period.



Figure 30. Solar Panel Test Setup

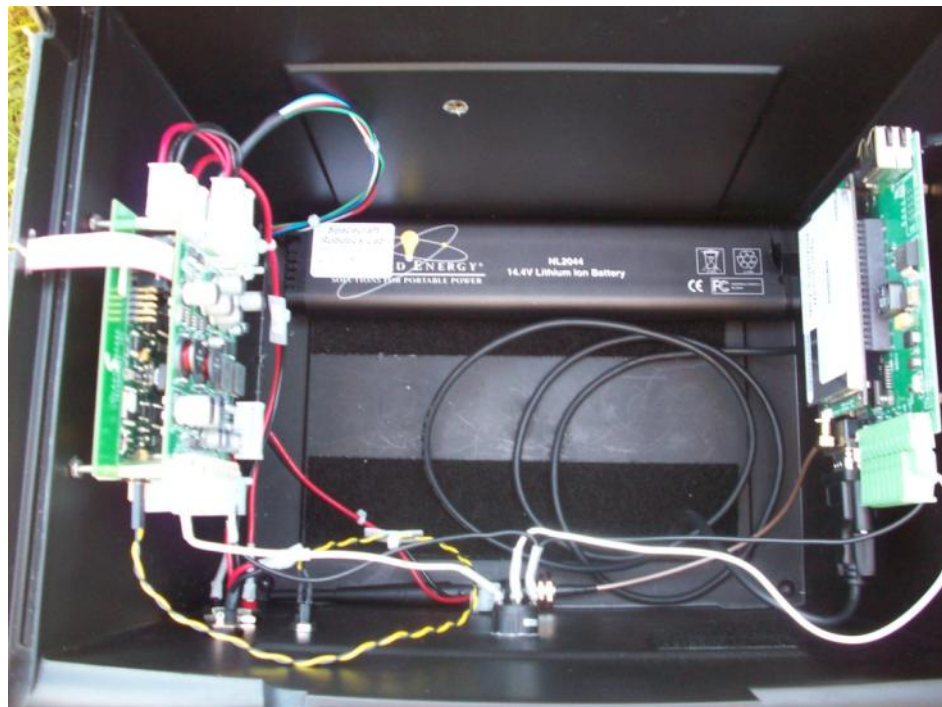


Figure 31. Detail View of Solar Panel Test Setup, IBPS on Left

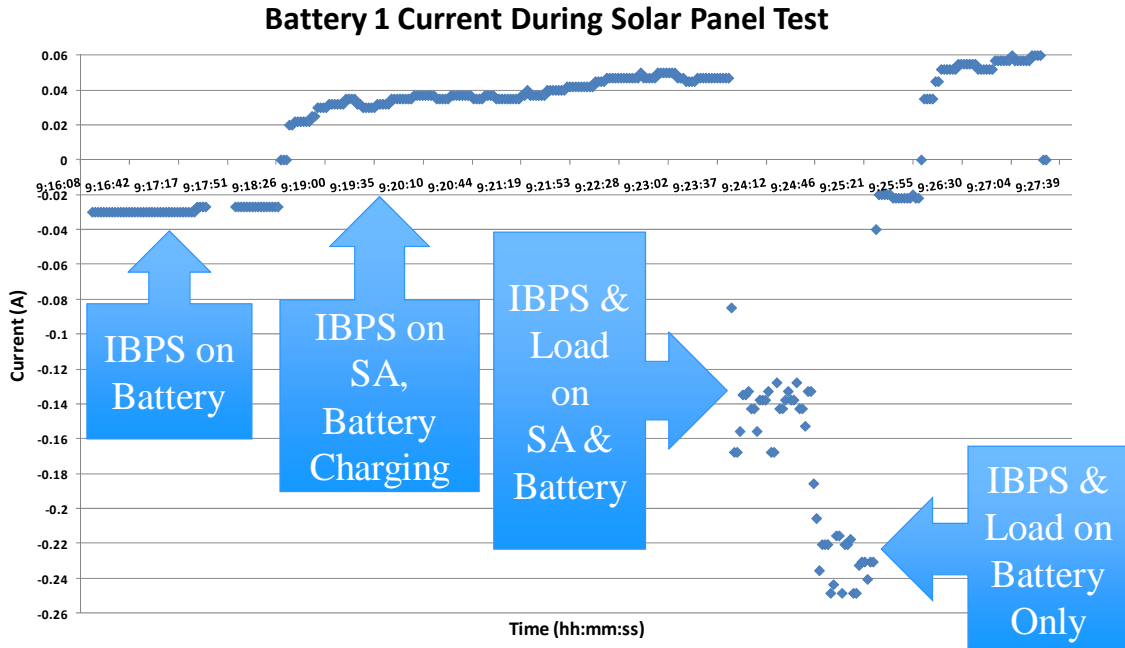


Figure 32. Battery Current During Solar Panel Test

Although the solar panel's operating voltage is 15.4 V, almost 18 V was seen during the test. This value is not recorded by FULLBATS and had to be measured directly with a multi-meter. The following test profile description follows the current levels from left to right in Figure 32. With the load off and only one battery connected to the BB-04/DC-123 system, the system drew about 30 mA from the battery. This is termed the quiescent power required by the BB/DC system. At about 09:18:25, the solar panel was plugged in. The BB uses externally supplied power to first supply the load with any remaining power going towards charging the battery [38]. Since there was no load other than the 30 mA quiescent power, most of the power collected by the solar panel went towards charging the battery. At 09:23:45, the MHX-2420 was turned on without putting it in a transmit or receive configuration. The data points near -0.14 A is with the MHX-2420 on and the solar panel plugged in. The data drops to -0.23 A due to the solar panel being unplugged during that time. At approximately 09:25:27, the MHX-2420 was turned off and the system returned to its initial state. At 09:26:00, the solar panel was again plugged in. Power collection increased to

about the levels seen from 09:18:29 to 09:23:45. It should be noted that although the panel is rated for 300 mA, a maximum of about 100 mA was recorded during the test. This is due variations in air mass the sunlight travels through, the temperature of the solar cells, and the incidence angle of sunlight on the solar panel. The air mass of the location of test is approximately 2.1 while the temperature and incidence angle are definitively known.

It bears repeating here that the IBPS is not a peak power tracking system. Ocean Server documentation states that the voltage from the solar panel must be in the 17.2 V to 24.2 V range [38]. However, during testing in the Small Satellite Laboratory voltages as low as 16 V were successful in powering the BB-04 and DC-123. Once the voltage of the external power supply was raised sufficiently above the battery voltage, the battery also began charging (this was 16.3V during this particular test). Although there are many different strategies to avoid overcharge in a direct energy transfer system, it is believed that the IBPS opens the incoming current circuit once the load and battery charge currents have been satisfied. Additional testing is needed to verify this, however.

During the solar panel test, the system behaved precisely as documented and expected. These results suggest that the BB-04 and DC-123 can successfully be used with a solar panel for TINYSCOPE's EPS. However, the design must take into account the direct energy transfer approach of the IBPS. This was accounted for in Chapter II, Section D6 by ensuring there are ample solar cells in series to provide adequate voltage.<sup>1</sup>

#### D. BATTERY COMPATIBILITY TEST

As mentioned in Chapter II, Section F, the standard OEM batteries have mass and volume levels that are too high to be practical for TINYSCOPE's EPS. Because of this, two alternative batteries were investigated and tested with the BB-04 and DC-123 IBPS. These alternatives were chosen because their

---

<sup>1</sup> This method is tantamount to a "brute force" approach. Essentially, more than enough solar cells are provided for in series and parallel to account for inefficient collection.

nominal voltage is identical to the OEM battery, i.e. 14.4 V, and they adhere to the Smart Battery Standard specification. It was believed that these features would increase the likelihood that the batteries would work correctly with the IBPS. Similar to the OEM battery, both alternatives are manufactured by Inspired Energy. Table 12 summarizes the pertinent specifications of the standard OEM battery and the two alternatives considered. Figure 33 shows a picture of the batteries in Table 12.

Model #	Series Cells	Parallel Strings	Total Cells	Nominal Voltage (V)	Capacity (Ah)	Length (mm)	Width (mm)	Height (mm)
NL2044HD22	4	3	12	14.4	6.6	285	58.9	22.3
NH2054HD26	4	2	8	14.4	5.2	152.4	78.7	22.9
ND2054HD26	4	1	4	14.4	2.6	86.4	78.7	22.9

Table 12. Battery Data Comparison



Figure 33. Graphical Battery Comparison

To ensure realistic results, the batteries were tested under load and charging conditions. The baseline functional test procedure is detailed in Section E, below. A load bank using representative TINYSCOPE loads for each

voltage was implemented using variable resistors and a DB-15 connector to interface with DC, J20. The resistance values were derived using the load detail in Appendix B and are close to TINYSCOPE's average values during payload operations. Although TINYSCOPE has no -12 V loads, it was decided to include a load for this value during the testing for completeness. Approximately half of the resistance value for the +12 V load was applied to the +12 V load while the other half was applied to the -12 V load. A picture of the load bank is shown in Figure 34, below. Moving from back to front in Figure 34, the resistances of the loads are as follows: the -12 V load is  $21.04\ \Omega$ , the 5 V load is  $7.204\ \Omega$ , the 12 V load is  $33.78\ \Omega$ , and the 3.3 V load is  $11.61\ \Omega$ .

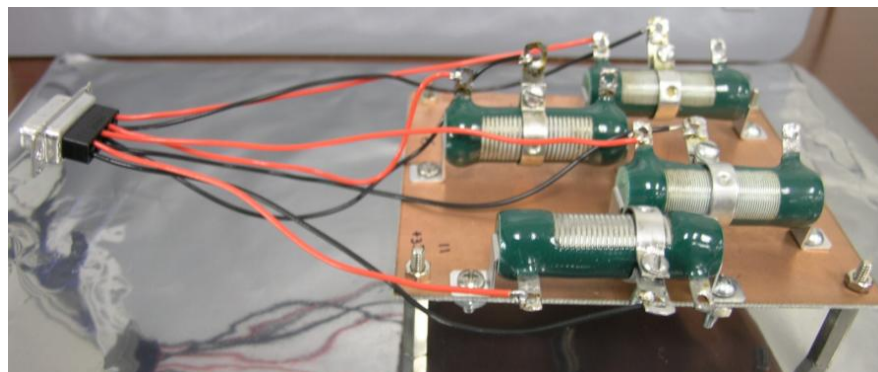


Figure 34. Representative Load Bank

The battery alternatives do not come equipped with the standard 6-pin Molex Mini-fit Jr. connector as the OEM batteries do. Thus, they cannot be immediately interfaced with the BB-04 (at connectors J22, J17, J21, and J12). The custom battery connector shown in Figure 35 was built using parts sold by Inspired Energy.<sup>m</sup>

---

<sup>m</sup> The 5-pin black connector is a right angle battery mating connector, left-hand key. Inspired Energy model # 610018, AMP model # 5787428-1. The green PCB is heavy-duty circuit board for standard battery connectors (1.6 mm thick). Inspired Energy model # BL237A.

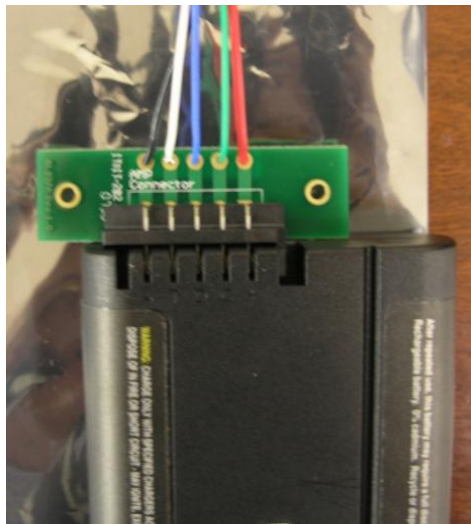


Figure 35. Custom Battery Harness

An external DC power supply with a 20 V and 2 A limit was input to BB-04, J5 and J7. The load bank was hooked up to DC-123, J20. A set of four each of the 5.2 Ah and 2.6 Ah batteries were connected, in turn, to BB-04 J22, J17, J21, and J12. Figure 36 shows a top-level setup.

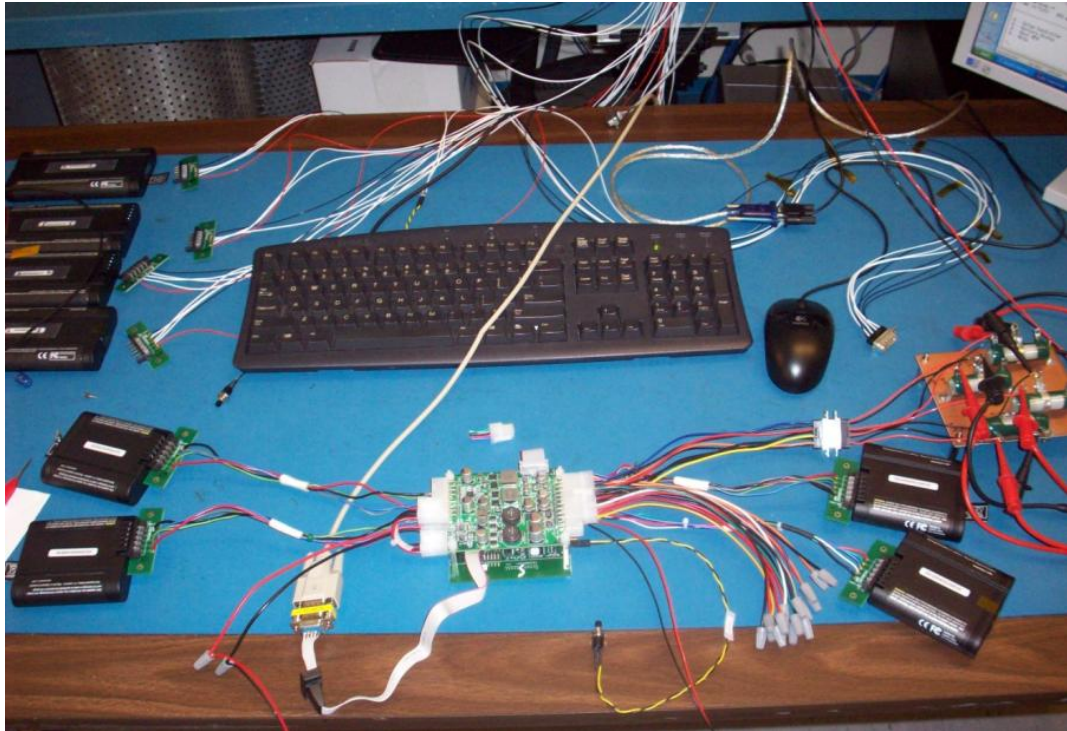


Figure 36. Battery Compatibility Test, Top-Level Setup

The following test description is easiest to understand while referring to the graphs in Figure 37. For about the first 550 seconds, the batteries were plugged in with no load and no external power supply. This means the batteries supported only the quiescent loads of the IBPS. Just before 300 seconds into the test, all loads were turned on simultaneously (via pins two and four of J1 on BB-04). Panels C and D of Figure 37 show the loads activating while panels E and F show the batteries being used. From 300 seconds to about 550 seconds, the loads were left on to ensure the batteries could support the loads. From about 550 seconds to about 850 seconds the external power supply was allowed to supply up to 2 A of current. This was done to ensure the IBPS could charge the non-OEM batteries. Panels A and B show the increase in power supply voltage and current. Since the loads were still being supported, panels C and D remain unchanged. However, battery voltages begin to increase (panel E) and battery current becomes positive (panel F). Positive current values imply charging whereas negative values imply discharging, i.e. outgoing current. Because there is only about 1 A going to charge the batteries and this is divided among four batteries, panel G does not show much of a change in percent increase until just before the test ends. The results of the test for ND2054HD26 “small battery” are shown in Figure 38.

Both sets of batteries were successfully controlled by the BB-04, DC-123 IBPS. The batteries supported the quiescent loads of the IBPS, representative on-orbit loads, and were also able to be charged by the IBPS. The positive results shown in Figures 37 and 38 give high confidence that the IBPS can be operated with either of the smaller mass, lower capacity batteries that were tested. It should be noted that any alternative batteries must have a nominal voltage of 14.4 V and must be Smart Battery Standard specification compliant. The Linear Technologies Dual Smart Battery System Manager IC’s (reference Table 10) must interface to batteries that have this capability. Non-compliance with this requirement could lead to over or under charging of the lithium ion cells resulting in damage or injury.

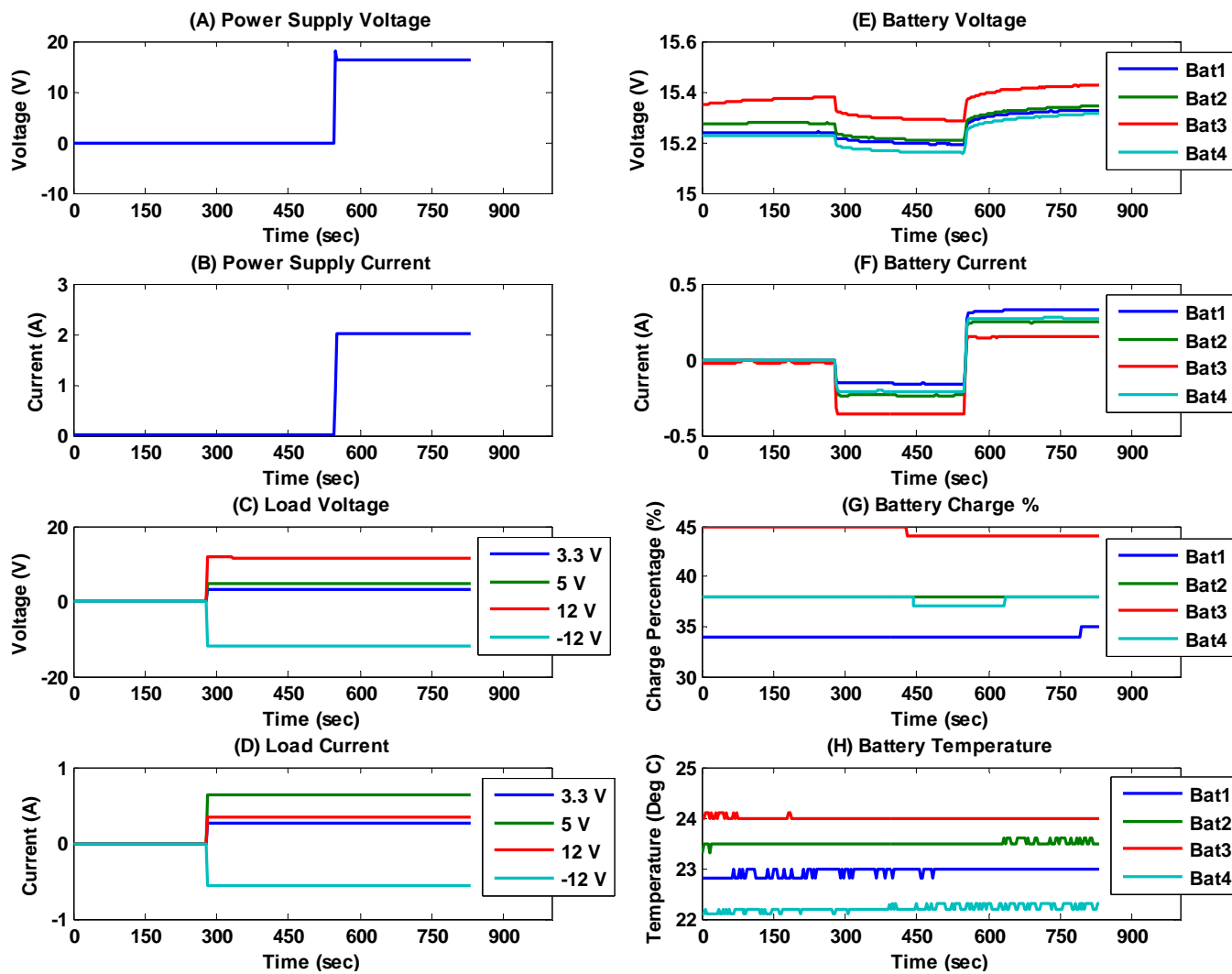


Figure 37. Battery Compatibility Test, NH2054HD26 “Medium Battery”

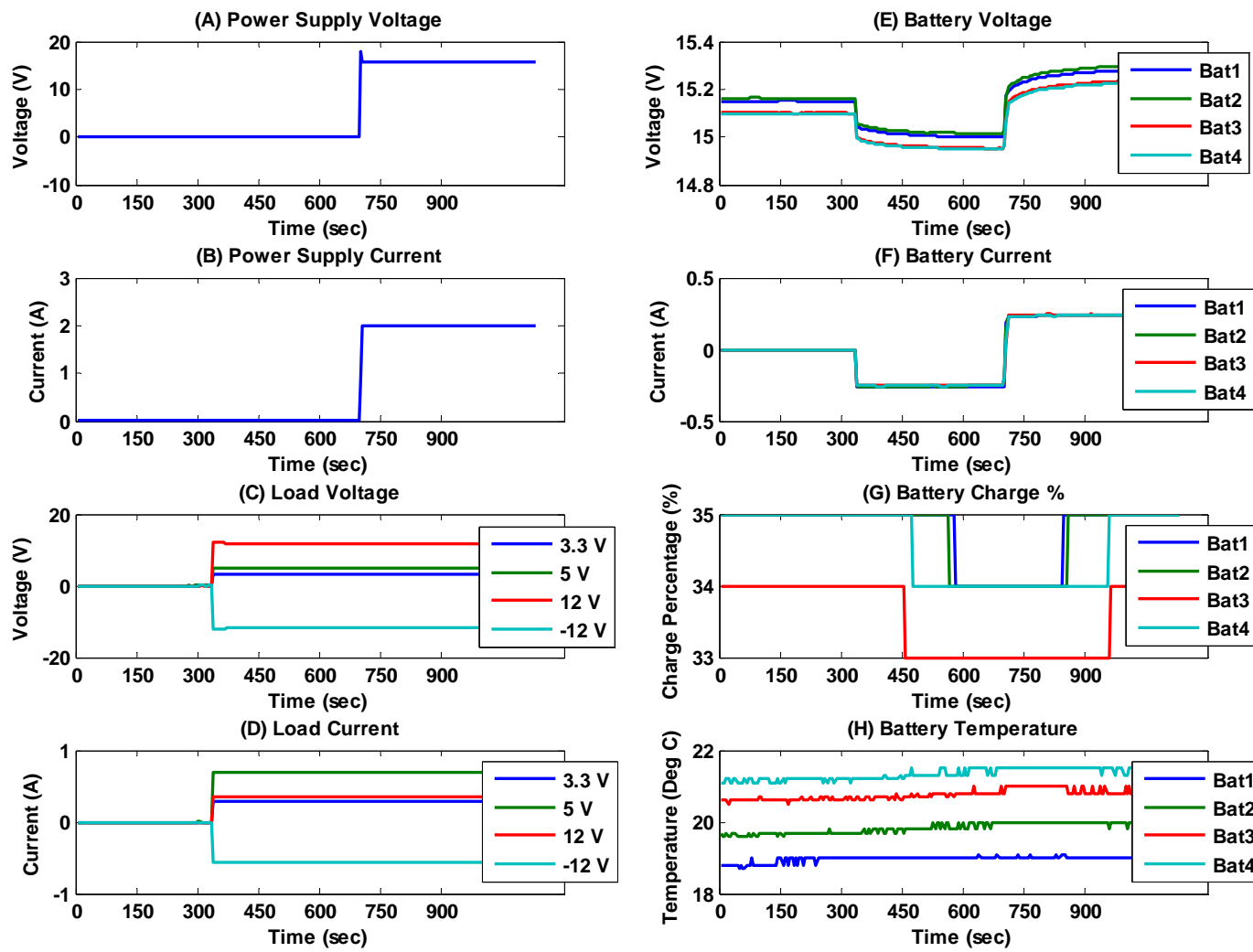


Figure 38. Battery Compatibility Test, ND2054HD26 "Small Battery"

## E. IBPS EFFICIENCIES

To more accurately predict the amount of power that must be collected by the solar panels to support the loads and battery charging, system efficiencies must be identified, measured and accounted for (especially for use in the EPS simulations of Chapter III). The IBPS equivalent circuit was thoroughly developed in Chapter II, Section A and Appendix A. The present section documents how the measurements were taken and the process used to calculate the following efficiencies:

- $\eta_s$  - Line efficiency from the solar panel to the power controller.
- $\eta_c$  - Charge efficiency of the batteries.
- $\eta_d$  - Discharge efficiency of the batteries.
- $\eta_1$  - Efficiency of the power controller during charging
- $\eta_2$  - Efficiency of the power controller during discharging
- $\eta_p$  - Nominal efficiency of the power controller
- $\eta_3$  - DC to DC converter efficiency for the 3.3 V load.
- $\eta_4$  - DC to DC converter efficiency for the 5 V load.
- $\eta_5$  - DC to DC converter efficiency for the 12 V load.
- $\eta_6$  - DC to DC converter efficiency for the -12 V load.
- $\eta_{Line}$  - Line efficiency from the output of each of the DC to DC converter load voltages to the physical load.

Both the solar array to power controller efficiency  $\eta_s$  and the load line efficiency  $\eta_{Line}$  are based on resistance values in power transmission lines. These values cannot be known at this phase of TINYSCOPE's EPS design since the physical configuration of the spacecraft is still evolving. However, a 90% efficiency is considered conservative and is used for both parameters. Therefore,  $\eta_s$  and  $\eta_{Line}$  are set to 0.90.

Although the manufacturer gave general case battery charge and discharge efficiencies, efficiency can vary widely based on how much current is

going into or out of the batteries and what the ambient temperature is. The faster the batteries are charged or discharged, i.e. the higher the “C”, the less efficient they are. Ambient temperatures beyond the battery’s optimum operating range can also cause efficiency to drop. Because the design in Chapter II calls for very low “C” values, i.e. small charge and discharge currents, no adjustment was made for this variable. As discussed previously, thermal modeling suggests the average internal temperature of the satellite will vary from about -20 °C to 20 °C. The batteries are rated for discharge from -10 °C to 50 °C and charge from 0 °C to 45 °C. During discussions with manufacturer technical personnel, it was confirmed that the charge and discharge efficiencies of the batteries can be safely assumed to be 95%. Thus  $\eta_c$  and  $\eta_d$  will be assumed to be 0.95.

The remaining efficiencies were measured in representative system configurations as power out of a given component divided by power in to that same component. All power values were calculated as the product of a measured voltage and a measured current. Figure 5 is repeated below, as Figure 39, for convenience with the addition of numbered locations on the equivalent circuit showing measurement points. All measurements are contained in Appendix H.

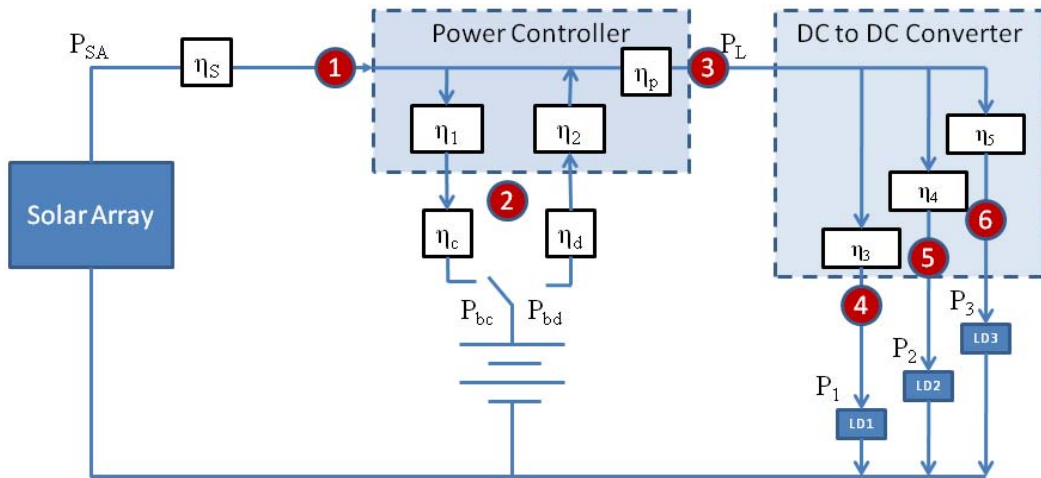


Figure 39. TINYSCOPE EPS Equivalent Circuit With Efficiency Measurements

The basic setup of the system was one NH2054HD26 “Medium Battery” and an external power supply connected to the base board. The battery was not connected during discharge only measurements to isolate the load voltage and current measurements. The DC to DC converter was connected to the base board and the load was connected to the DC to DC converter. The load measurements were made with only one load attached at a time to isolate the DC to DC converter’s efficiency for each voltage that it supplies. The power controller efficiency was measured during discharge for all loads connected and then each load connected individually. The power controller efficiency was also measured during charge when no loads were connected and then with all loads and a battery connected. A summary of the findings is given in Table 13, below.

Name	Efficiency	Measured As
$\eta_2 \eta_p$	0.95	Point 3 / Point 2 (NOTE: No battery attached during measurement.) This is the discharge efficiency of the power controller. Each individual efficiency is assumed to be the square root of 0.95.
$\eta_1$	0.89	Point 2 / Point 1 and (Point 2 + Point 3) / (Point 1). This is the power controller efficiency in charge.
$\eta_3$	0.75	Point 4 / Point 3
$\eta_4$	0.88	Point 5 / Point 3
$\eta_5$	0.93	Point 6 / Point 3
$\eta_6$	0.73	Not Shown. This is the efficiency of the DC to DC converter for the -12 V load.

Table 13. EPS Efficiencies

It should be noted that the values obtained for efficiencies are reasonable approximations at best. This is because circuit efficiencies vary based on

dynamic conditions like load impedance, temperature, etc. This is clearly evidenced by the differing values for power controller charge and discharge efficiencies. Despite these limitations, the values obtained are adequate first order approximations. Inspection of Figures 16 and 22 in Chapter III show that the efficiency values in the EPS model are taken from Table 13. If significant changes are made in TINYSCOPE's loads, it is recommended that efficiency testing be re-accomplished with the values input back into dynamic simulation of Chapter III.

## F. BASELINE FUNCTIONAL TEST AND CONTROL SOFTWARE DESCRIPTION

### 1. Overview

Because IBPS operation is undocumented for vibration and extreme thermal-vacuum environments, a baseline functionality test was developed to monitor and document any changes in operational capability from one test to another. Although the test was not exhaustive, most of the important features of the IBPS were monitored. Below, Figure 40 shows a graphical overview of the test setup.

The blue shaded boxes are associated with the normal operation of the IBPS and the black shaded boxes are related to test data monitoring and control. The arrows represent the direction of travel of either power or data. The DC to DC converter is connected to the base board for power and data. Four batteries of one capacity size are connected to the base board and the load bank of Figure 34 is connected to the DC to DC converter. A base board connection to a control computer is part of the standard operation of the IBPS. Data is passed from the base board to the computer while commands may also be sent from the computer to the base board. A power supply limited to 20 V and 2 A is connected to the base board to provide power and battery charging when required. Two connections are required to be able to charge all four batteries

simultaneously. A normally open pushbutton switch is connected to the base board to control power to the loads through the DC to DC converter.

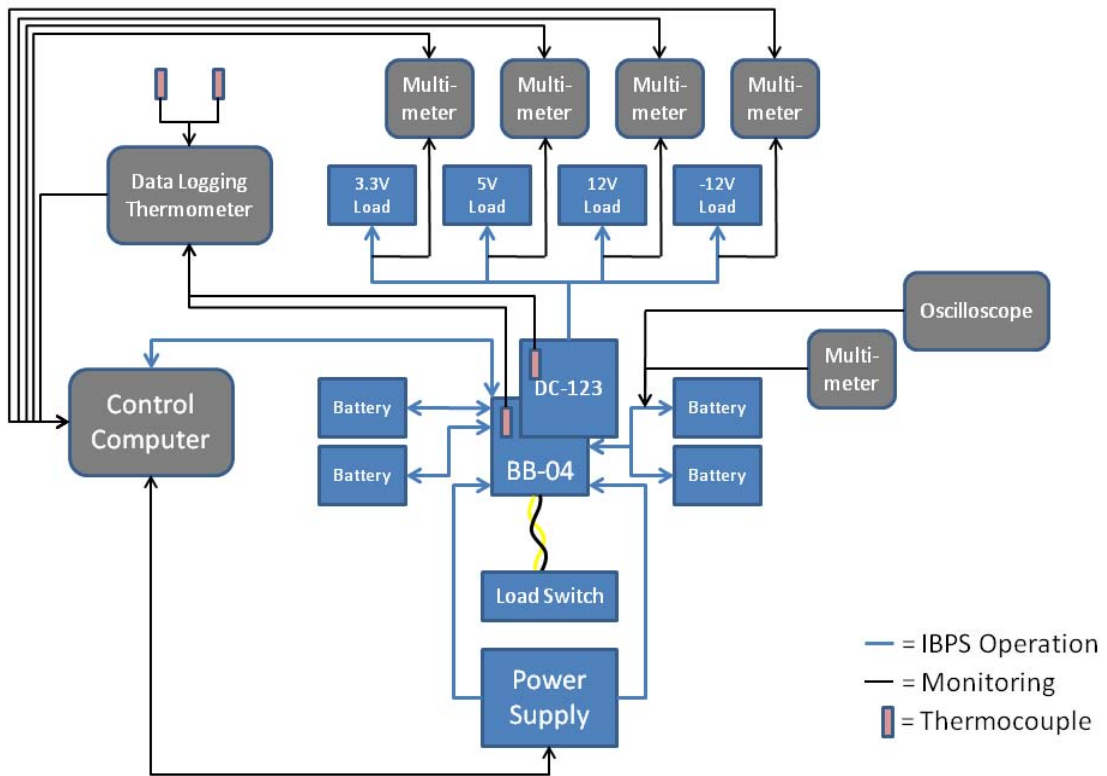


Figure 40. Baseline Functional Test Overview Diagram

The remaining items depicted in Figure 40 are not needed for the normal operation of the IBPS. Four programmable multimeters are used to sense the voltage at the loads. This data is collected and graphed by custom designed control software written by Mr. Jim Horning of NPS' Space Systems Academic Group Small Satellite Laboratory. The software also plots power supply, battery voltage, and battery current levels as well as setting the output of the power supply. A handheld multimeter and a bench top oscilloscope are used to periodically record battery voltage and current levels independently of the IBPS. A Hall Effect sensor on the oscilloscope is used for the current measurement. Finally, up to four thermocouples are positioned on the IBPS or the thermal-vacuum chamber and connected to a data logging thermometer. This data is sent to data logging software also residing on the control computer. A full listing

of software and hardware required for baseline functional testing is listed in Appendix I. A picture showing the actual setup of Figure 40 is shown in Figure 41.

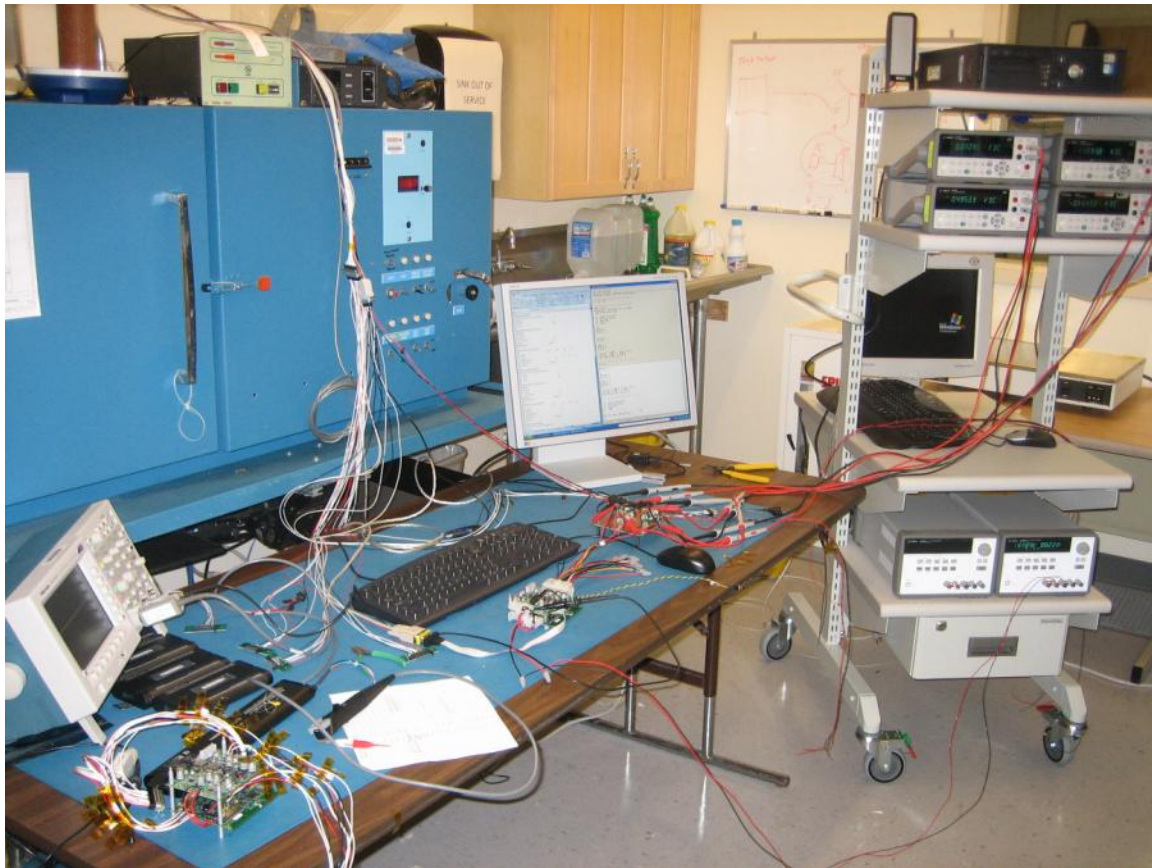


Figure 41. Baseline Functional Test Physical Setup

## 2. Procedure and Timeline

A standard procedure was followed during each baseline functional test for ease of comparison with subsequent tests. In this way, one can see at a glance if the IBPS operation was consistent from one test to another. The procedure was as follows:

- With batteries connected and the power supply and load disconnected, the IBPS was run for approximately five minutes. At the end of five minutes, independent battery and voltage measurements were taken at the batteries.

- The loads were then turned on for approximately five minutes after which time independent battery measurements were taken and recorded again.
- Finally, the power supply was turned on for five minutes with another set of battery measurements taken again.

This timeline is depicted in Figure 42 that shows a screen shot of the “OS\_Tester1.py” control software.

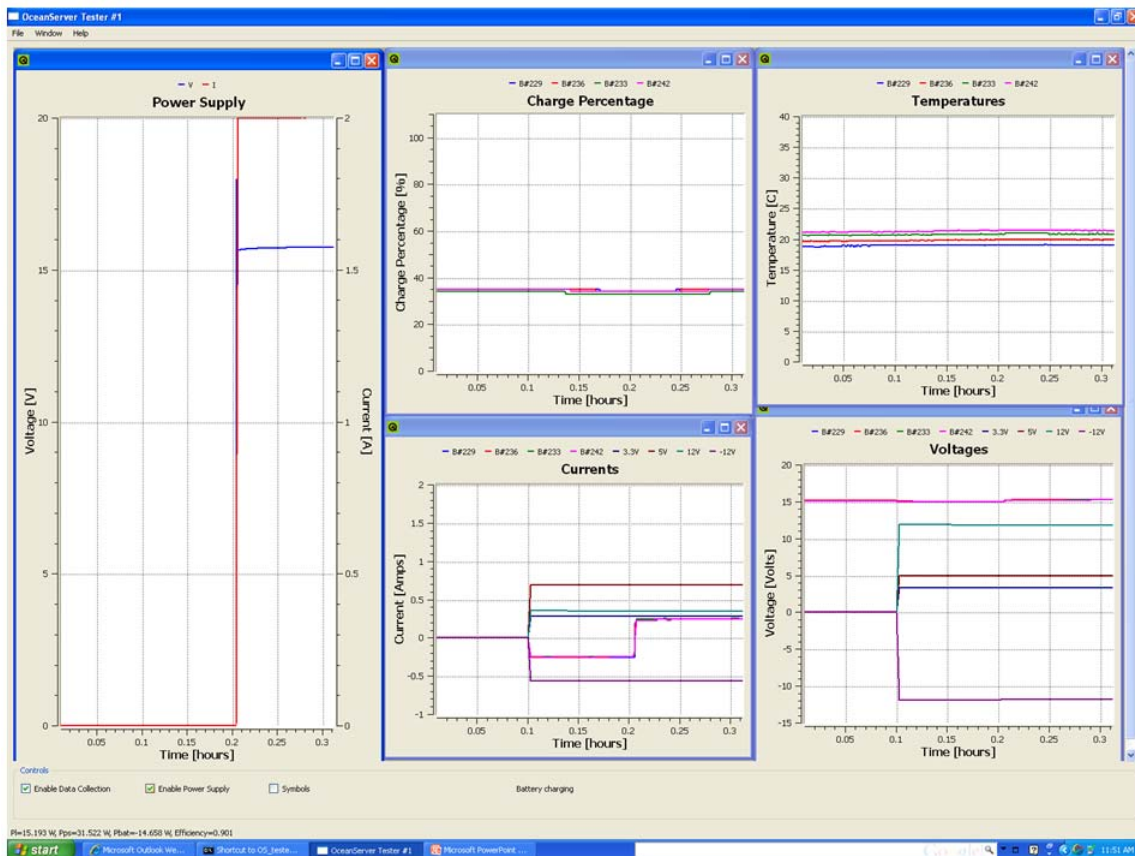


Figure 42. OS\_Tester1.py Control Software Screen Shot

Among the IBPS reported data, the control software monitors battery voltage, battery current, battery temperature, and battery charge percentage. The software additionally monitors the voltage and current of the power supply and the voltage of the loads. While load current is also graphed, it is not monitored directly—it is calculated from the application of Ohm's Law since the voltage is measured and the resistance is set by the test conductor. In addition

to monitoring the above data, the control software also allows the operator to select whether or not the power supply is active.

When the test begins, the batteries are connected with no load and no power supply. Therefore, the power supply plot should be zero for voltage and current. Charge percentages should reflect values close to what was recorded at the end of the last test. The battery temperatures should be room temperature, i.e. about 20 °C. All currents as well as all load voltages should be at zero. Battery voltages will not actually be zero but very close to it.<sup>n</sup> Battery voltages should be about 14.4 V but can be anywhere between 11 V to 16 V.

At five minutes into the test, the loads turning on cause an immediate change in the load voltage and load current plots. The load voltages measured by the multimeters move to their appropriate level (as defined by which pin on DC-123, J20 they are connected to). Since the load currents are calculated from the load voltages, these lines should move to their respective values as well. For the given load bank, battery currents should sum to approximately -1 A. For four batteries, this is -250 mA each. The negative sign represents current leaving the batteries. As time progresses with the loads on, there should be a slight downward trend in charge percentage and battery voltage. There may be a corresponding slight increase in battery temperature as the inefficiency of converting chemical energy to electrical energy introduces heat.

At the ten-minute point, the power supply is turned on with an immediate change in the power supply voltage and current plot. The power supply voltage increases to 20 V while the power supply current increases to 2 A. Another immediate change occurs in the battery current plot. Because the base board first uses the external power supply to source the load, the battery current stops being negative. Approximately 1 A of the external power supply's current is used to source the load with the remaining 1 A used to charge the batteries. After several minutes with the external power supply activated, there should be a slight

---

<sup>n</sup> Recall that the quiescent power of the BB-04/DC-123 IBPS is about 20 to 30 mA. Although the 5 to 7 mA per battery is not discernable on the plot, it is recorded in the database.

upward trend in the battery charge percentages as well as the battery voltages. Battery temperature may be observed to continue to slightly increase as the batteries are charged.

### **3. Proper Operation**

Proper operation of the IBPS can be distinguished by several facts. First, the trend of the plots should be smooth. If the plots are discontinuous or data points begin dropping out, there may be a problem with the IBPS. Secondly, if the plots do not follow the timeline discussed above this could also indicate a problem. One indication may be that when the loads are turned on at the five-minute point the voltage and/or current plots do not change. Another example of a possible problem would be at the ten minute point where the external power supply is turned on. The batteries should immediately begin charging causing their current plots to go positive. A final way to discover a problem is by comparing the independent battery voltage and battery current measurements of the IBPS and the handheld multimeter/benchtop oscilloscope. Further investigation would be needed if these values differ more than about 10%.

The baseline functional test was used during battery compatibility testing; before and after vibration testing; and before, during, and after thermal-vacuum testing. One can observe the similarity of the battery compatibility plots in Figures 37 and 38 with baseline functional test in Figure 42. The only difference between the plots is in the presentation of the data. In Figures 37 and 38 the data reported by the IBPS is in the right column of plots while the data reported by the power supply and multimeters is shown in the left column of plots. The specifics of how the baseline functional test was used is further elaborated below for vibration and thermal-vacuum testing.

## G. ENVIRONMENTAL TESTING

### 1. Overview

Environmental testing for space missions is a function of many variables. Numerous test standards exist to which individual programs apply a custom set of specialized criteria. Some of the criteria are strictly adhered to such as those required by launch providers to minimize the risk of catastrophic launch failure. Other criteria are less stringent and may be tailored based on the level of risk the program is willing to accept. Despite these variations, a broad model of a qualification program is outlined in section 12.4 of [15]. Figure 43 summarizes the qualification testing flow.

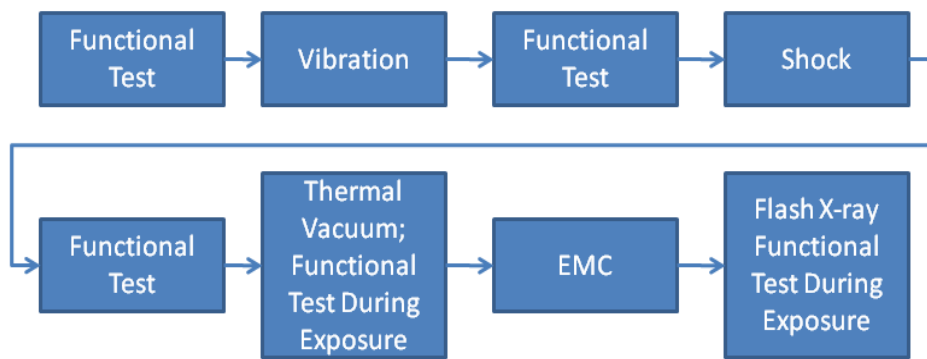


Figure 43. Flow of Qualification Testing for Components After [15]

The above testing flow applies to all “flight-type” hardware and software to ensure that the spacecraft will operate as intended [15]. The tests are arranged in the general order in which the satellite will see the respective environments. The functional test checks proper operation of the component before and after each environmental test. Vibration testing assesses if the component can withstand the vibration loads produced during launch vehicle takeoff and ascent. Shock testing simulates explosive release of launch vehicle components such as the payload fairing and solid rocket boosters. A thermal vacuum chamber tests spacecraft components in the pressure and thermal environment they will see in orbit. Electromagnetic compatibility (EMC) and flash x-ray testing are typically only used when a component or satellite must be able to withstand the effects of

nuclear weapons in space. Because this does not apply to TINYSCOPE, the last two tests will not be discussed further. Shock testing was also not investigated due to time constraints and the lack of test equipment availability.

Vibration and shock testing are typically highly dependent upon the launch vehicle that will deliver the satellite into orbit while thermal vacuum testing is dependent upon factors like the orbit of the satellite, the components used, and the overall physical configuration. Thus, a program has more freedom to tailor thermal vacuum requirements than vibration and shock requirements. An additional challenge is the fact that it is very difficult to test a satellite or component to appropriate vibration or shock levels before the launch vehicle is known (as is the current situation with TINYSCOPE). One approach to this issue is to test to very high levels to ensure that the component or satellite may be launched on any launch vehicle. This method must be balanced with program cost, schedule, and the level of risk accepted.

To establish appropriate levels of testing for the IBPS, one must look beyond the basic outline in [15]. Two much more detailed standards commonly used in establishing the types and levels of testing required are the General Environmental Verification Standard (GEVS) [41] and the Test Requirements for Launch, Upper-Stage, and Space Vehicles Report (TR 06–11) [42]. GEVS is produced by the National Aeronautics and Space Administration’s Goddard Space Flight Center while TR 06–11 is written by The Aerospace Corporation under the auspices of the United States Air Force’s Space and Missile Systems Center. The two references cover much of the information but from two different perspectives—GEVS is from a civil space standpoint while TR 06–11 is from a National Security Space point of view. Although TINYSCOPE does not fall neatly into either category, the two documents were used to create a tailored set of test levels in the context of the test flow of Figure 43.

Two definitions that are critical to determining which tests should be conducted and to what levels are the level of assembly and the test category. Test category generally falls into “development,” “qualification,” or “acceptance.”

Development testing, as defined in [42], is used to: “a. Validate new design concepts or the application of proven concepts and techniques to a new configuration. b. Assist in the evolution of designs from the conceptual phase to the operational phase. c. Validate design changes. d. Reduce the risk involved in committing designs to the fabrication of qualification and flight hardware. e. Develop and validate qualification and acceptance test procedures. f. Investigate problems or concerns that arise after successful qualification.” Qualification testing is “conducted to demonstrate that the design, manufacturing process, and acceptance program produce hardware/software that meet specification requirements with adequate margin to accommodate multiple rework and test cycles” [42]. Finally, acceptance testing is conducted “to demonstrate the acceptability of each deliverable item to meet performance specification and demonstrate error-free workmanship in manufacturing. Acceptance testing is intended to stress screen items to precipitate incipient failures due to latent defects in parts, processes, materials, and workmanship.” Essentially, development testing is used early on in the development while qualification testing is used to validate a given design to ensure it can operate in its intended environment. Finally, once a design is settled on, acceptance testing tests to lower levels than qualification (to save time and money) but still high enough levels to screen out items that may have poor workmanship.

A strong case can be made for testing the IBPS to qualification levels to verify that the design will operate correctly. However, the test categories usually apply to components and systems that were designed from the beginning for use in space. Because that is not the case for the IBPS, an argument can be made that an iterative approach should be used to discover at what level the component will fail. For this reason, the test category definitions were not applied strictly to the IBPS testing. Where practical, qualification levels were used.

Level of assembly refers to the parts under test and can be defined at many levels. The most pertinent levels of assembly for this discussion are quoted from [41]:

- Component – A functional subdivision of a subsystem and generally a self-contained combination of items performing a function necessary for the subsystem's operation. Examples are electronic box, transmitter, gyro package, actuator, motor, battery. [The terms "component" and "unit" are often used interchangeably.]
- Assembly – A functional subdivision of a component consisting of parts or subassemblies that perform functions necessary for the operation of the component as a whole. Examples are a power amplifier and gyroscope.
- Subsystem - A functional subdivision of a payload consisting of two or more components. Examples are structural, attitude control, electrical power, and communication subsystems. Also included as subsystems of the payload are the science instruments or experiments.
- Payload - An integrated assemblage of modules, subsystems, etc., designed to perform a specified mission in space. For the purposes of this document, "payload" and "spacecraft" are used interchangeably. Other terms used to designate this level of assembly are Laboratory, Observatory, Satellite and System Segment.

Given that the IBPS represents a significant portion of the EPS, the most appropriate level of assembly definition for the IBPS is "subsystem". The exact levels to which the IBPS was tested is discussed further in the following sections.

## **2. Vibration Testing**

Qualification levels for subsystems are given in TR 06–11 as the same levels for payloads. These are defined as 6 dB above acceptance levels at three minutes per axis. Acceptance levels are depicted in Figure 44.

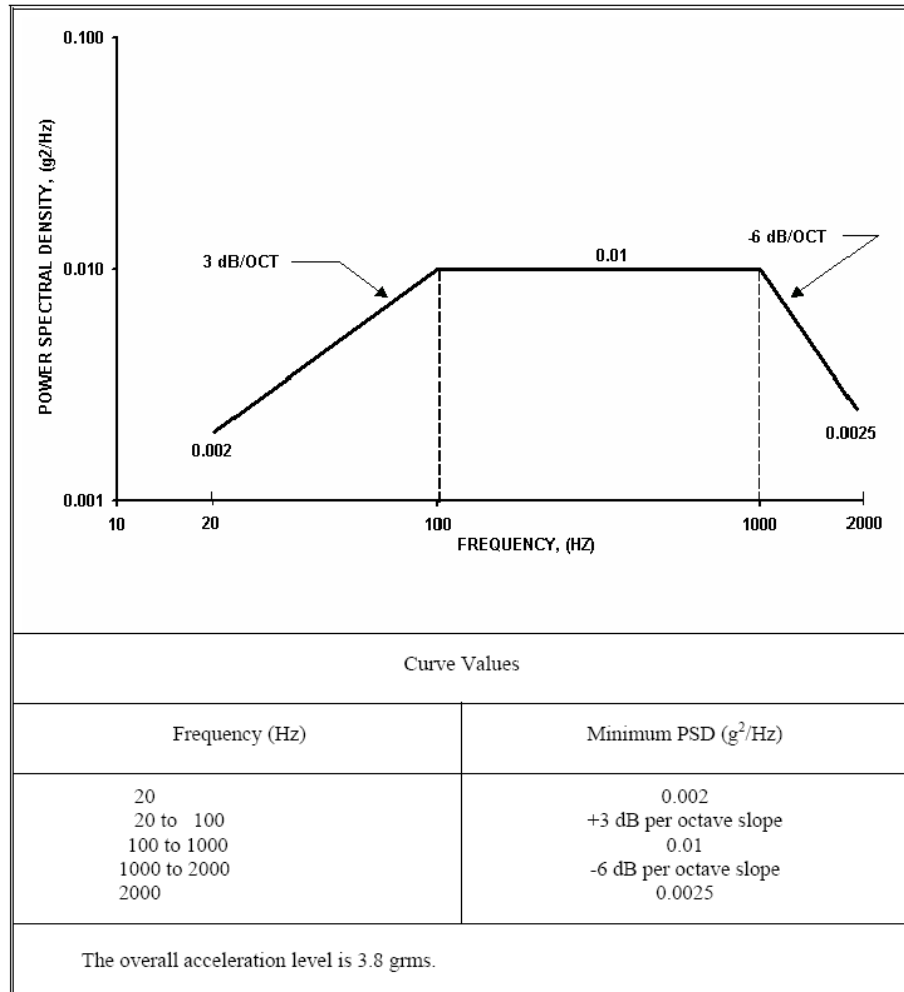


Figure 44. Minimum Random Vibration Spectrum, Vehicle Acceptance Tests From [42]

The GEVS states in section 2.4.2.4 that subsystem vibroacoustic tests are recommended when “the subsystem is expected to be significantly excited by structureborne [sic] random vibration.” It goes on to state that “specific test levels are determined on a case by case basis.” However, GEVS also specifies component minimum test levels as follows:

Frequency (Hz)	ASD Level ( $\text{g}^2/\text{Hz}$ )
20	0.01
20-80	+3 dB/oct
80-500	0.04
500-2000	-3 dB/oct
2000	0.01
Overall	6.8 g <sub>rms</sub>

The plateau acceleration spectral density level (ASD) may be reduced for components weighing between 45.4 and 182 kg, or 100 and 400 pounds according to the component weight (W) up to a maximum of 6 dB as follows:

$$\begin{array}{lll} \text{dB reduction} & \frac{\text{Weight in kg}}{= 10 \log(W/45.4)} & \frac{\text{Weight in lb}}{10 \log(W/100)} \\ \text{ASD(plateau) level} & = 0.04 \cdot (45.4/W) & = 0.04 \cdot (100/W) \end{array}$$

The sloped portions of the spectrum shall be maintained at plus and minus 3 dB/oct. Therefore, the lower and upper break points, or frequencies at the ends of the plateau become:

$$F_L = 80 (45.4/W) [\text{kg}] \quad F_L = \text{frequency break point low end of plateau} \\ = 80 (100/W) [\text{lb}]$$

$$F_H = 500 (W/45.4) [\text{kg}] \quad F_H = \text{frequency break point high end of plateau} \\ = 500 (W/100) [\text{lb}]$$

The test spectrum shall not go below 0.01  $\text{g}^2/\text{Hz}$ . For components whose weight is greater than 182-kg or 400 pounds, the workmanship test spectrum is 0.01  $\text{g}^2/\text{Hz}$  from 20 to 2000 Hz with an overall level of 4.4 g<sub>rms</sub>.

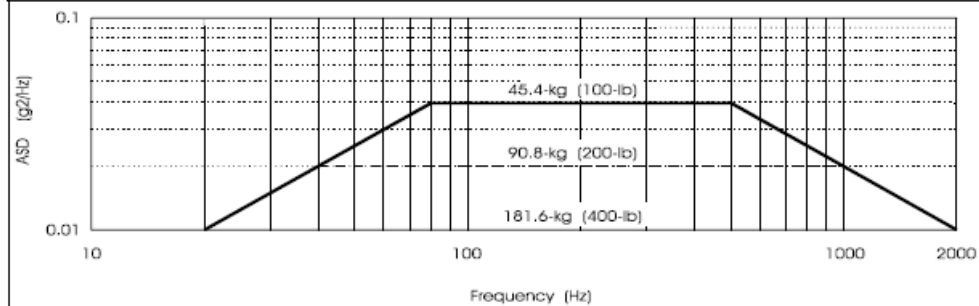


Figure 45. Component Minimum Workmanship Random Vibration Test Levels From [41]

By the following equation [43], qualification levels defined in TR 06-11 offset the graph in Figure 44 to be four times higher than shown.

$$dB = 10 \log_{10} \left( \frac{g^2 / Hz}{g^2 / Hz-Ref} \right)$$

$$6dB = \text{Ratio of 4 on } g^2 / Hz$$
(25)

This essentially brings the TR 06–11 levels up to the levels defined in GEVS for minimum workmanship. Although GEVS begins to fall off at a lower frequency, i.e. 500 Hz, the slope is not as steep as that of TR 06–11. The levels in Figure 45 were used for the IBPS.

Figures 46 and 47 show the IBPS on the vibration test stand. Two custom harnesses are visibly secured to static test mounts in the 11 o'clock position. The data collected during the test is in Appendix J. The vertical axis, defined as in and out of the page in Figure 46, was the only axis tested. The main justification for this was to balance the risk of breaking the IBPS at high or extended vibration levels before being able to test it in the thermal-vacuum chamber. Although time constraints precluded completion, the original intent was to perform a second vibe test on all three axes after thermal-vacuum testing.

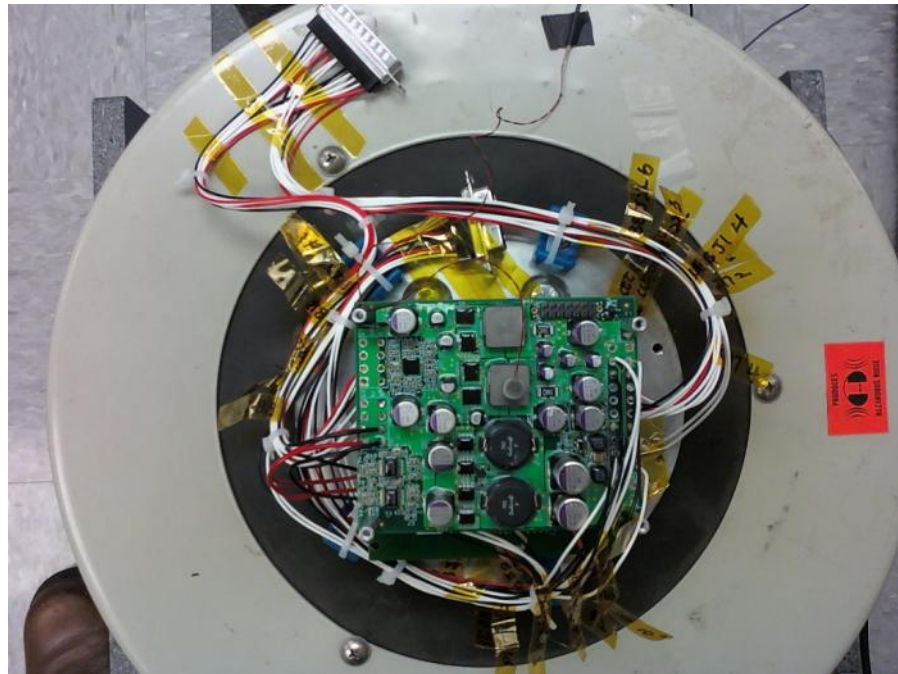


Figure 46. IBPS on Vibration Test Stand, Top Down View

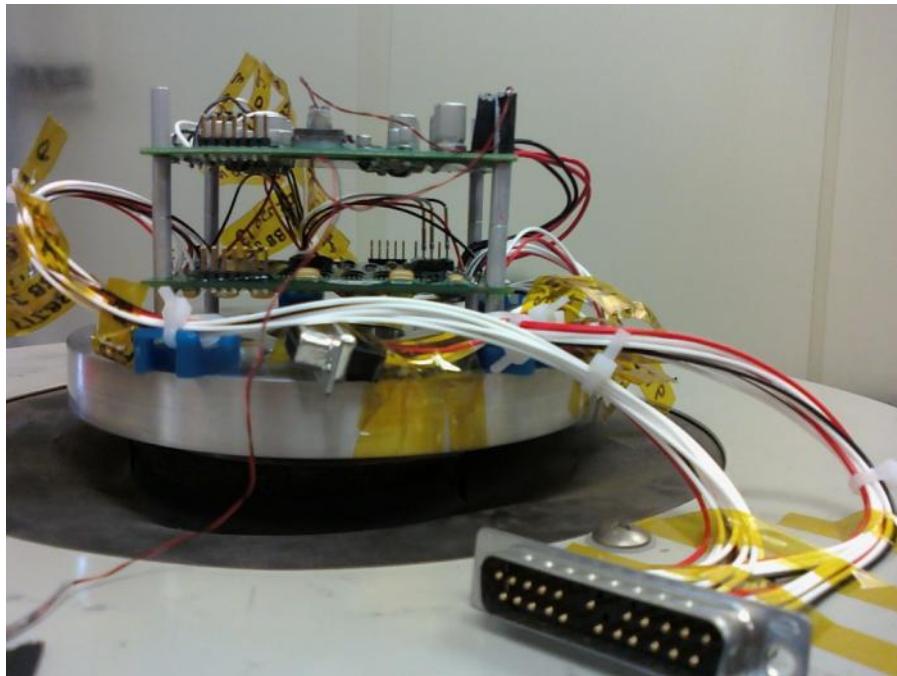


Figure 47. IBPS on Vibration Test Stand, Side View

In addition to the baseline functional test, a visual inspection of the IBPS was conducted before and after vibration testing. No cracks, nicks, scratches, breaks, etc. were found in any of the solder joints or circuit boards. Figure 48 illustrates the results of the functional test of the IBPS after the vibration test (data collected on 23 Oct 09).

The plots in Figure 48 follow closely the functional test timeline detailed in Section E2, above. Additionally, all the plots meet the necessary conditions outlined in Section E3 to conclude that the IBPS operated as expected after the vibration test. Thus, the IBPS is sufficiently designed to survive a representative launch environment.

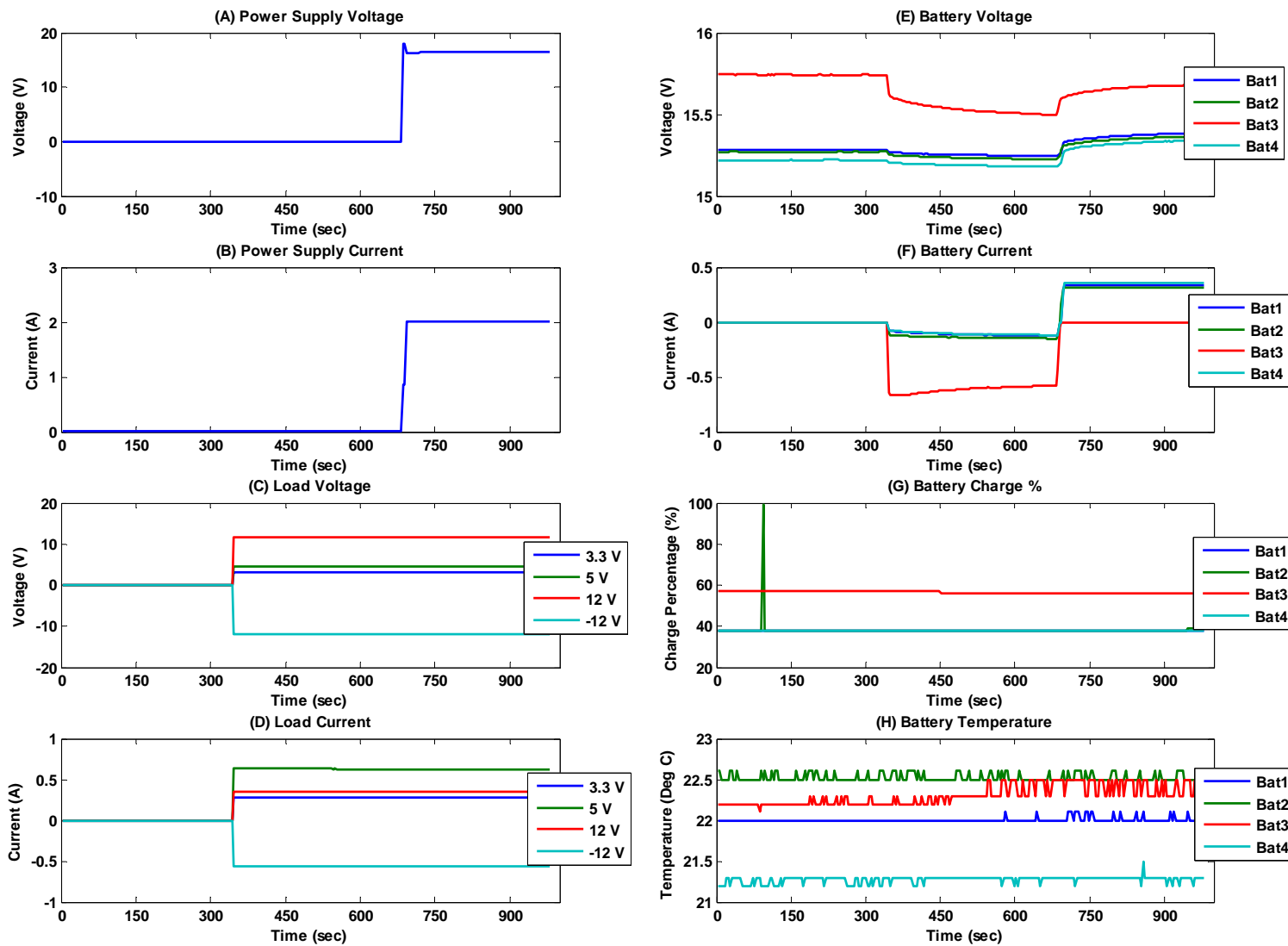


Figure 48. Post Vibration Functional Test, 23 October 2009

### 3. Thermal-Vacuum Testing

Thermal-vacuum qualification criteria for subsystems is given in TR 06–11. Section 7.3.7 of [42] implies that all equipment that can be tested at the unit level should be even if the equipment is classified at the higher subsystem level. The unit level criteria, shown in Figure 49, are much more stringent than the subsystem level criteria. Subsystem levels are defined as the same as the system or payload levels.

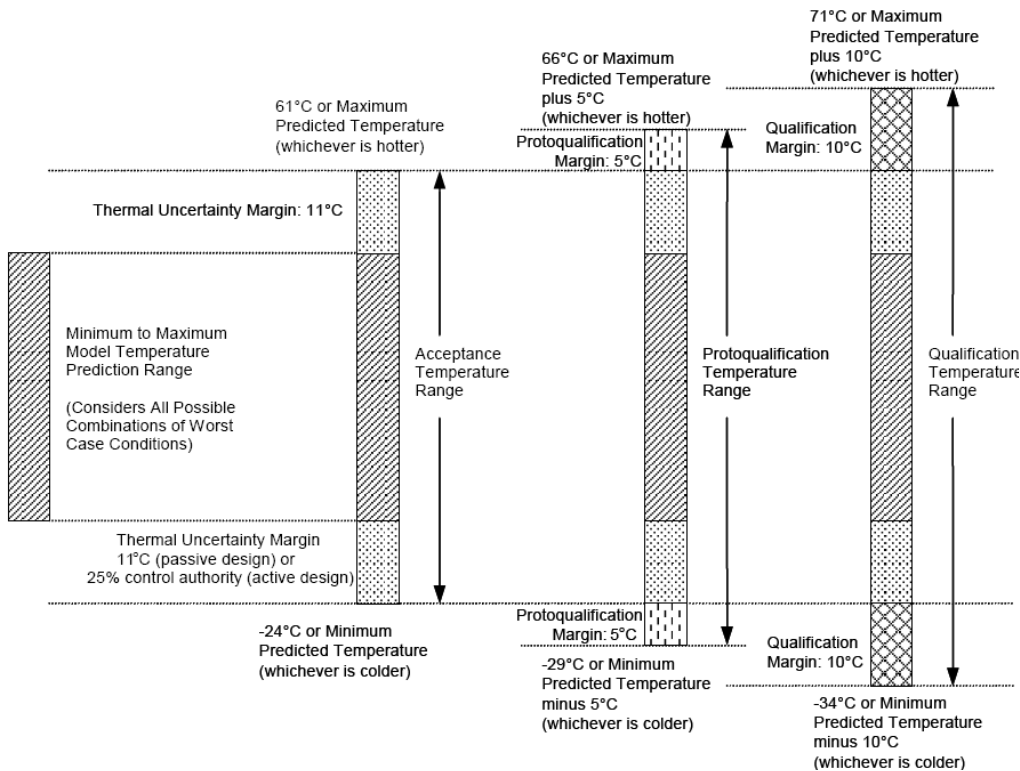


Figure 49. Unit Test Temperature Ranges and Margins From [42]

The temperatures listed in Figure 49 are required to be repeated a particular number of times. The minimum number of cycles for electronic equipment is prescribed as four cycles for all testing categories, e.g. qualification and acceptance.

As can be seen on the left side of Figure 49, all thermal vacuum testing is indexed to minimum and maximum model temperature predictions. These are defined as, “the hottest and coldest temperatures predicted from thermal models

using applicable effects of worst-case combinations of equipment operation, internal heating, vehicle orientation, solar radiation, eclipse conditions, ascent heating, descent heating, and degradation of thermal surfaces during the service life [42].” The minimum and maximum predicted temperatures (MPT) are then found by adding an uncertainty margin to the minimum and maximum model temperatures. The MPT is defined as, “The highest and lowest temperatures that an item can experience during its service life, including all test and operational modes [42].” One can see the minimum and maximum model predictions on the left of Figure 49 while the MPTs are shown on the right. Subsystem and payload level criteria are shown in Figure 50.

Qualification:	10°C beyond acceptance temperatures for 8 cycles.
Protoqualification:	5°C beyond acceptance temperatures for 4 cycles.
Acceptance:	Minimum and maximum predicted temperatures for 4 cycles.

Figure 50. Payload Test Temperature Ranges From [42]

All levels of testing require a pressure no higher than  $10^{-4}$  Torr or the pressure at the service altitude, whichever is lower. Because the IBPS has not been previously tested at the unit level, a strict interpretation of TR 06–11 would require the application of the requirements in Figure 49. This would mean four temperature cycles between -34 °C and 71 °C.

NASA’s GEVS temperature criteria for all levels of assembly are shown in Figure 51. A pressure of no more than  $10^{-5}$  Torr is required. The main difference in requirements between the levels of assembly in GEVS is the number of thermal cycles. The subsystem level is required to successfully complete four hot/cold cycles.

Both the GEVS standard in Figure 51 and the TR 06–11 standard in Figure 49 are indexed to minimum and maximum expected temperatures. However, the margins required in GEVS are 5 °C and 10 °C for acceptance and qualification, respectively while the range expands to 11 °C and 21 °C for the same test categories in TR 06–11.

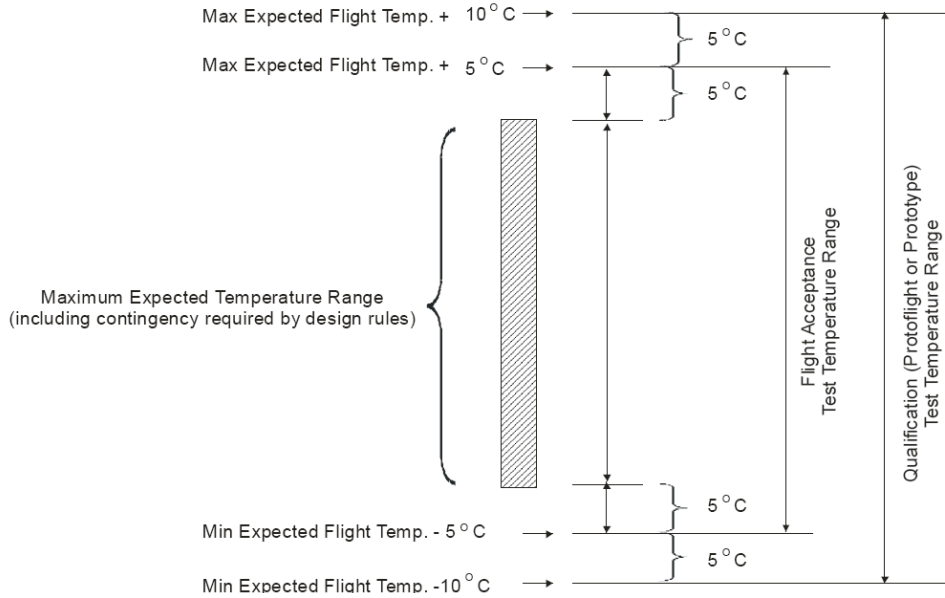


Figure 51. Thermal-Vacuum Temperatures From [41]

The thermal vacuum levels required of the IBPS from GEVS are  $\pm 10^{\circ}\text{C}$  from the minimum and maximum expected temperatures.

Because both TR 06–11 and the GEVS are indexed to a set of predicted temperatures, a reasonable estimate for expected IBPS temperatures had to be obtained. As a proxy for the IBPS temperature, the following three distinct models were used to approximate TINYSCOPE’s average internal temperature: a TINYSCOPE single node analysis developed from the material in Chapter 11 of [15], a Matlab/Simulink dynamic EPS and thermal control model developed from [16], and the NX modeling accomplished in Chapter V, Section B of [5]. The results of these models are presented without development.

The Microsoft Excel based single node analysis treats the entire TINYSCOPE spacecraft as one lumped thermal node. This model predicts a temperature range from  $-10.7^{\circ}\text{C}$  to  $23.3^{\circ}\text{C}$ . The Matlab/Simulink<sup>©</sup> model has 52 nodes and is documented in [44]. The model is simplified in that it assumes body mounted solar panels and a continuously nadir pointing spacecraft but it allows for the temperature of the IBPS node to be read individually. This model

predicts a temperature range of 2.9 °C to 14 °C for the IBPS.<sup>o</sup> Lastly, the NX model shows an average satellite internal temperature of -20.6 °C to 24.4 °C. Notice that the single node model and the NX model give a composite for the average internal temperature of the entire spacecraft whereas the Matlab/Simulink© model gives the temperature for one component, i.e. one node. Given these estimates of the minimum and maximum model temperatures, a range for thermal-vacuum testing can now be selected.

Recalling that the satellite program has a reasonable level of flexibility in choosing the required thermal-vacuum limits, the final levels chosen for the IBPS were -30 °C to 70 °C for four cycles. These levels were primarily selected because they almost reach the more strict TR 06–11 (Figure 49) and encompassed the GEVS limits (Figure 51). Additionally, the limits seemed reasonable given the temperature limits of the devices given in Table 10. Several of the components on the IBPS are rated from 0 °C to 70 °C. Therefore, it was initially believed that the upper temperature limit would not force the IBPS out of expected operation but that the lower limit would be problematic.

Appendix K lists the test procedures developed for and used during the conduct of two thermal vacuum tests. Notes taken during the tests are contained in Appendix L. Although originally one thermal-vacuum test of four complete cycles was planned, this turned out to be impossible for two main reasons. First, to create as similar an environment as possible for the IBPS in space, heat conduction was avoided—no heating or cooling plate was used in the TVAC chamber. Figure 52 shows the IBPS situated on a test stand made of the material Delrin along with four long screws. Delrin has a very low thermal conductivity ensuring no heat would be transferred from the walls of the thermal-vacuum chamber to the IBPS through conduction. Because only radiative heating was used, it took a very long time to achieve required temperatures. The thermal profile in Figure 53 shows that it took more than 1.5 hours from the time

---

<sup>o</sup> The average internal temperature of the satellite with this model is -8 °C to 12 °C.

the test started at 1006 to achieve 70 °C on the IBPS boards. The test procedures then called for a one hour soak time. The same issue occurred when attempting to achieve the low temperature, i.e. it took two hours to go from 67 °C to -12 °C on the base board. Reaching the targeted -30 °C would have taken an extremely long time. Additionally, the requirement for the one hour cold soak was not modified so that the test could be concluded. At this point in the test, it was decided that a second thermal-vacuum test would be required that would focus exclusively on the cold environment. The results of this second thermal-vacuum test are reported after the present discussion of the first thermal-vacuum test.



Figure 52. IBPS in Thermal-Vacuum Chamber

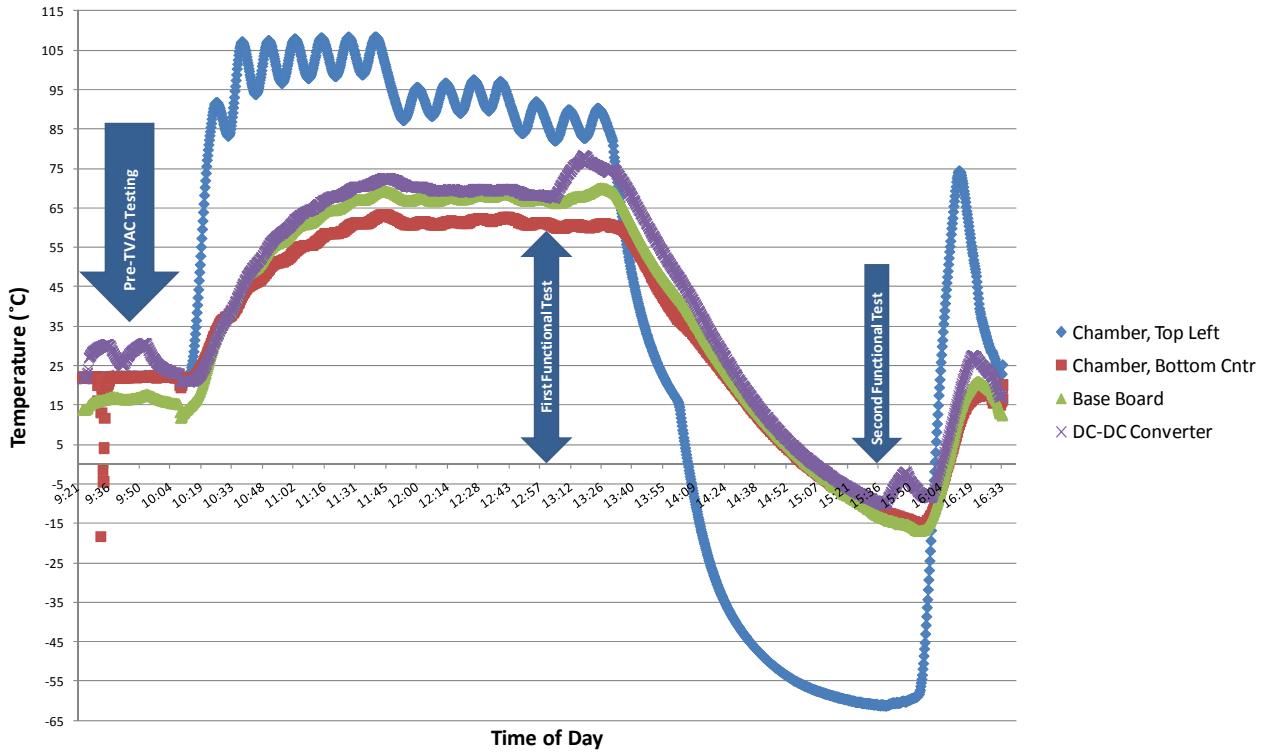


Figure 53. Temperature Profile, 28 October 2009 TVAC Test

The second reason four cycles could not be achieved is because there was a malfunction on one of the IBPS boards that necessitated real-time troubleshooting to salvage the test. At approximately 1314, when the base board was about 68 °C and the DC converter board was about 77 °C, batteries three and four attached to the base board were no longer being used by the IBPS. The control program, OS\_Tester1.py, seemed to stop providing output and no longer responded to operator inputs. All loads were still being supported but only through batteries one and two or the external power supply. After the problem was more fully characterized, it was decided to continue testing with the remaining batteries. Although a definitive reason for the malfunction has not been found, it is hypothesized that one or more of the chips on the IBPS stopped operating due to being so far outside of its normal operating temperature range.

Figure 53 shows data collected by thermocouples that were placed on the IBPS (one each on the base board and the DC to DC converter) and the thermal-

vacuum chamber walls (one each at top center and bottom left). In addition to this plotted data, the thermal-vacuum chamber had a temperature reading on the front panel that is not automatically recorded by a computer. Periodic readings were documented in the test notes of Appendix L.

The functional testing during the first thermal-vacuum test is shown in Figure 54 on the following page. The zero on the abscissa corresponds to approximately 1258 in Figure 53. Therefore, the left side of Figure 54 depicts the functional test during the high temperature. The long period from about 1,900 seconds to about 9,000 seconds is the time it took to go from the high temperature of 70 °C to the low temperature of about -15 °C. Again, there was no one-hour cold soak. The right side of Figure 54 shows the functional test at the cold temperature from about 9,000 seconds to 10,000 seconds and then one final functional test after the thermal-vacuum chamber was returned to ambient temperature and pressure (from about 11,000 seconds to 12,000 seconds). These three areas are shown in exploded views in Figures 55 and 56.

Upon close inspection of Figure 55, it can be observed that up until the time of the partial failure described above (approximately 850 seconds), the functional tests gave results that are consistent with proper IBPS operation (detailed in Sections E2 and E3, above). For example, the batteries were at very low current (Panel F) and normal voltage (Panel E) while supporting the quiescent load of the IBPS (through almost 200 seconds). Then, when the loads were activated at about 200 seconds, Panels C and D show the expected results e.g. the load voltages rise to their nominal levels of 3.3 V, 5 V, 12 V, and -12 V. The fault appears at approximately 850 seconds where OS\_Tester1.py stops collecting data in all eight panels. The remaining points collected from about 1,600 to 2,000 seconds evidence the troubleshooting steps but also show that the remaining two batteries were able to support the loads without a problem. For example, at 1,700 seconds, Panels F and G show expected results when the load is activated (as shown in Panels C and D). Panel H in Figures 54 to 56 has been zoomed in to exclude a momentary data dropout to 0 K at 3,515 seconds.

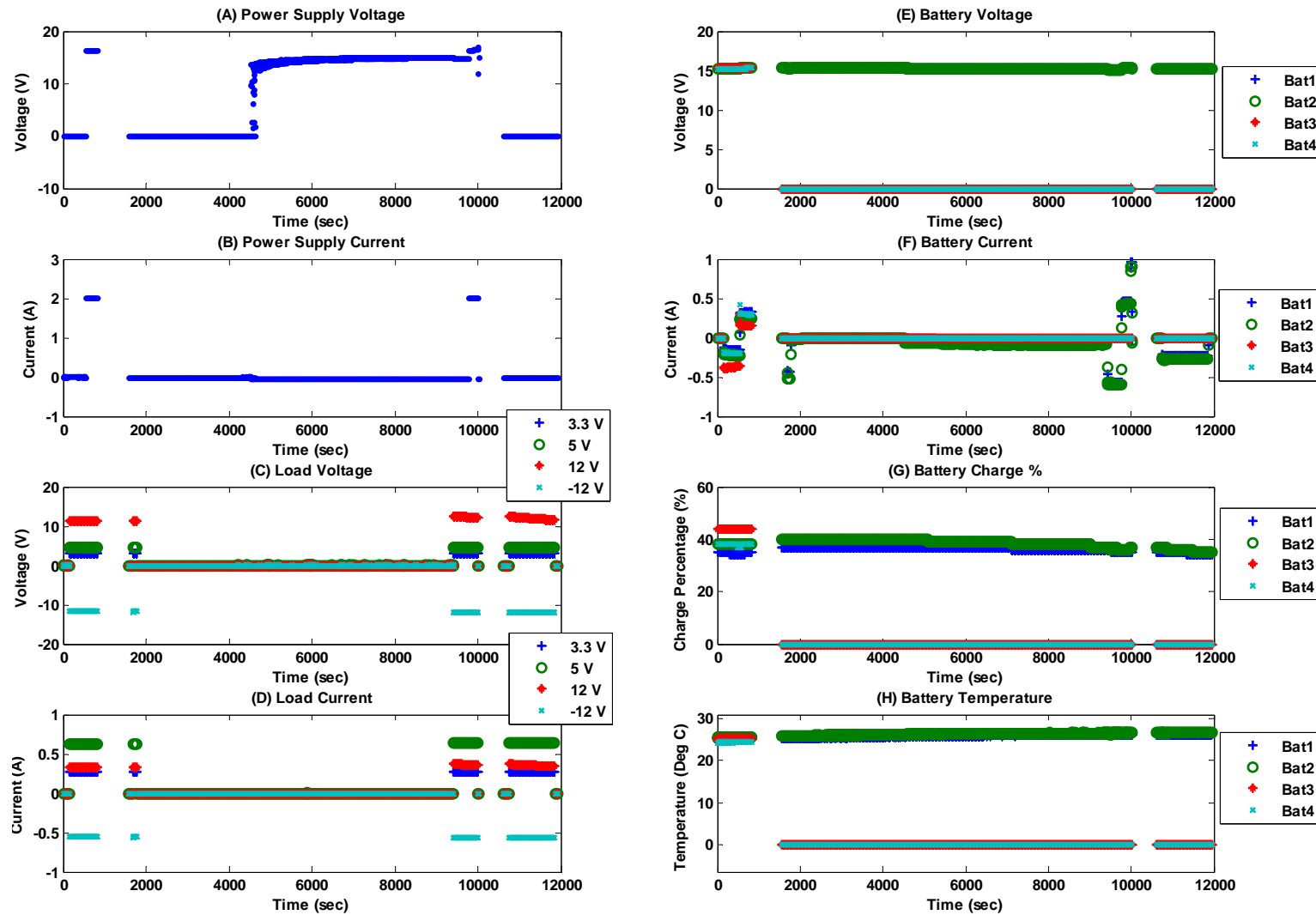


Figure 54. Functional Test Results, First Thermal-Vacuum Test

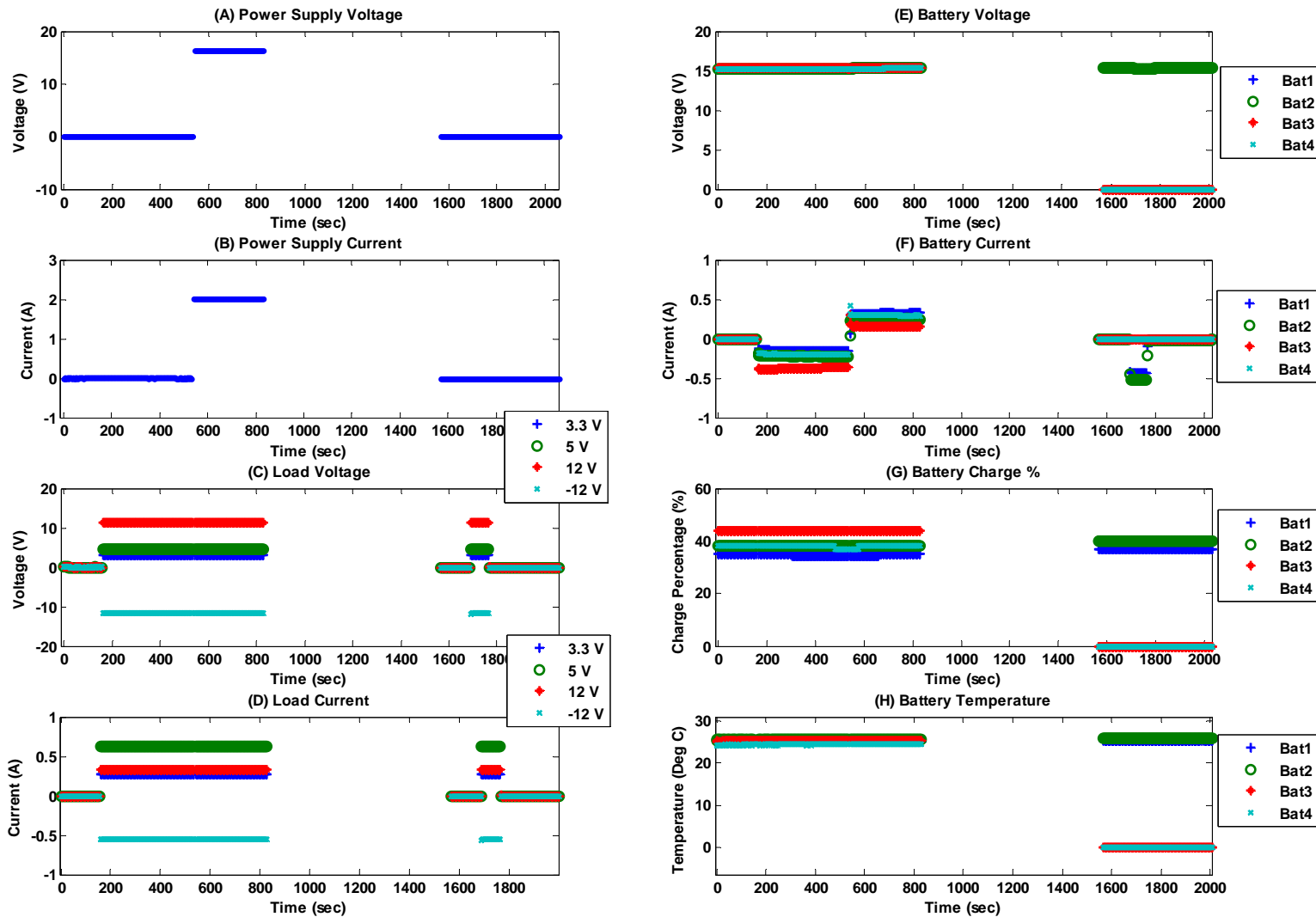


Figure 55. Functional Test Results, First Thermal-Vacuum Test, 0 to 2,000 Seconds

Although the cold soak objective was not achieved and the IBPS had already partially failed, the functional test results at the cold temperature are nonetheless presented for completeness in Figure 56 on the following page. On the left side of the graph, at about 9,250 seconds, one can see that batteries one and two supported IBPS quiescent loads as expected (Panels C and D). When the loads were turned on at about 9,400 seconds, the battery currents went negative (Panel F) and the load voltages (Panel C) and currents (Panel D) moved to their expected values. Additionally, battery voltage (Panel E) and battery charge (Panel G) show the gentle negative slope during discharge and then moderate positive slope as the power supply was used to source the load and charge the batteries. At 10,000 seconds, the batteries were disconnected from the IBPS and OS\_Tester1.py was exited to return the thermal-vacuum chamber up to ambient pressure and temperature.

Upon ambient conditions being achieved, the IBPS was again connected and a functional test run from about 10,600 to 12,000 seconds. The results here are the same as before—all data is as expected. Battery currents are low during quiescent loading and then increase as required to support the TINYSCOPE representative load. One step in the final functional test that was erroneously left out was turning on the power supply to check the batteries for charge capability. Even though this was not done here, it was accomplished later on. This data will be presented as part of the second thermal-vacuum test.

Although the cold soak was not achieved, the final test was run after returning the board to ambient condition in just 10 minutes. This gives a good indication that the IBPS is fairly robust.

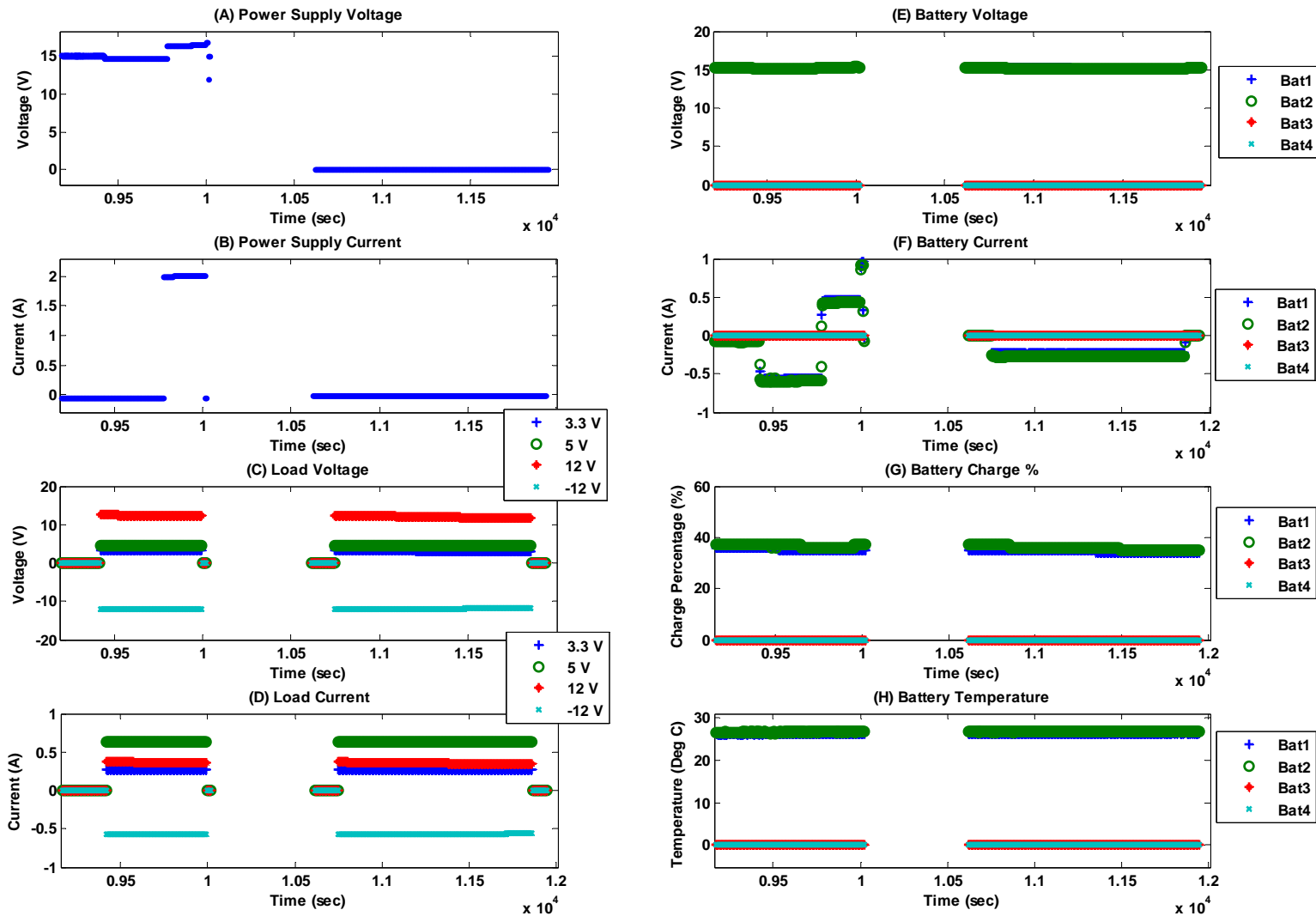


Figure 56. Functional Test Results, First Thermal-Vacuum Test, 9,500 to 12,000 Seconds

The temperature profile for the second thermal-vacuum test is presented in Figure 57. The IBPS was turned on after achieving a vacuum. Three of the thermocouples appeared to malfunction, i.e. go to an overload condition, shortly after closing the chamber door. However, one temperature data point, the DC to DC converter, was still successfully collected.<sup>p</sup> Additionally, manually recorded temperatures from the thermal-vacuum front panel are noted in Appendix L. The temperature can be seen to plateau at about 13:30 and then begin to slowly rise. At this point it was determined that the functional test should commence despite the fact that the target temperature of -30 °C and the associated cold soak was not attained.

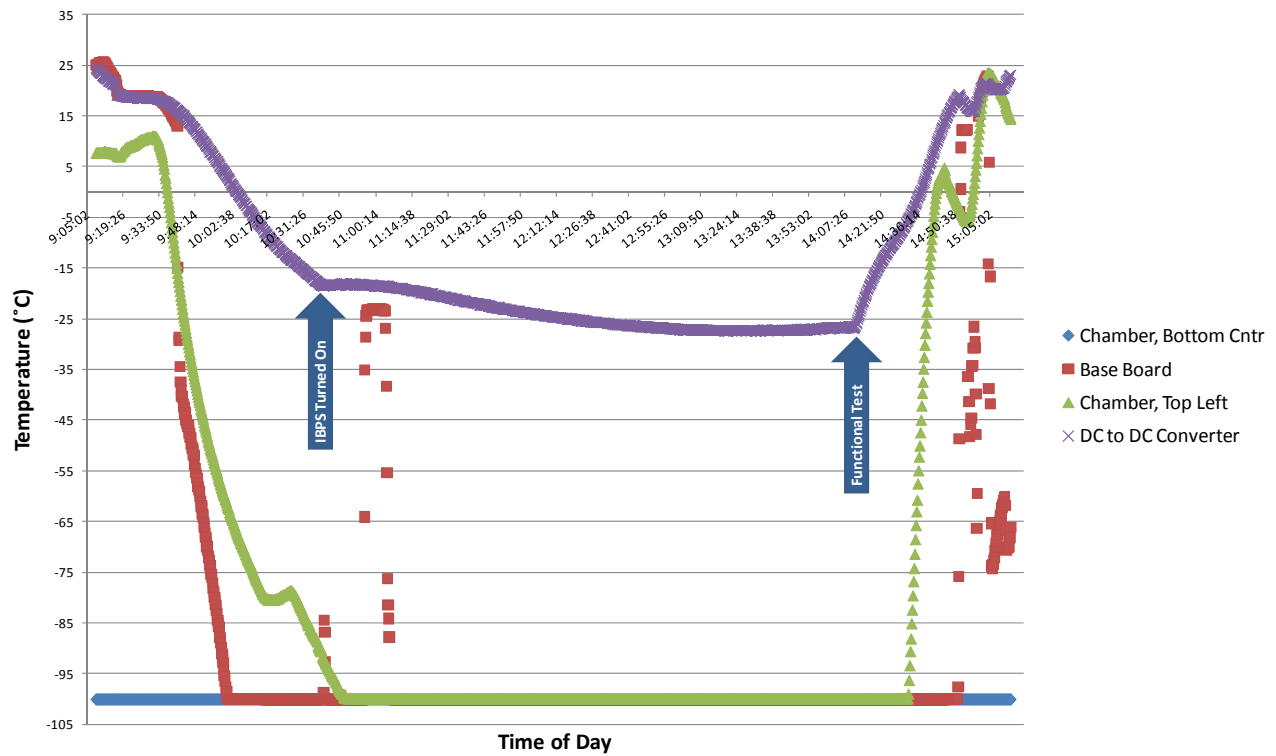


Figure 57. Temperature Profile, 17 November 2009 TVAC Test

<sup>p</sup> One may notice that the temperature of the DC to DC converter was consistently warmer than that of the base board in Figure 51. This makes sense given that the efficiency of the DC to DC converter is lower than the base board, i.e. more heat is produced by the DC to DC converter. Because of this, it can be inferred that the base board was cooler than what is shown in Figure 55 for the DC to DC converter.

Since the same IBPS unit was used for both tests, only functional test data for batteries one and two could be collected. A detailed view of the IBPS just before the second thermal-vacuum test began is shown in Figure 58 while the results of the functional test are presented in Figure 59. The functional test was modified slightly to keep the IBPS on through the period when the thermal-vacuum chamber was returning to ambient temperature and pressure. With this modification in mind, the data are as exactly as expected. Batteries one and two support quiescent loads from 0 to 12,500 seconds until the loads are initiated. At that time the battery currents go negative and the load voltages and currents go to their expected values. Although there are a couple of data dropouts in Panel E, Panel G shows data consistent with a long period of discharge followed by a shorter period of high rate charge. Additionally, the battery temperatures rise throughout the test period. In short, the IBPS performed flawlessly.

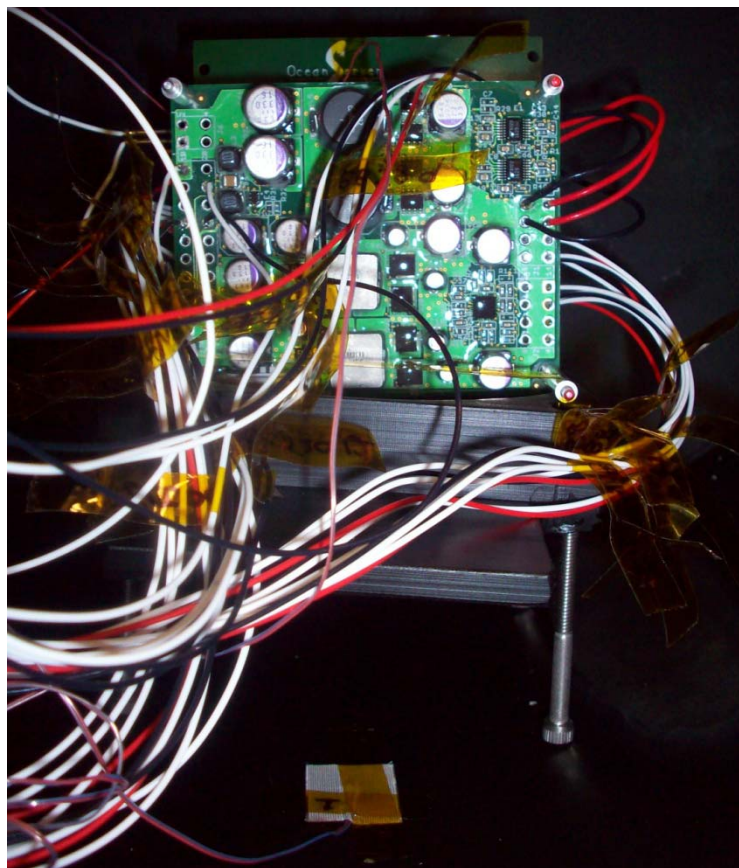


Figure 58. IBPS in Thermal-Vacuum Chamber, Second Test

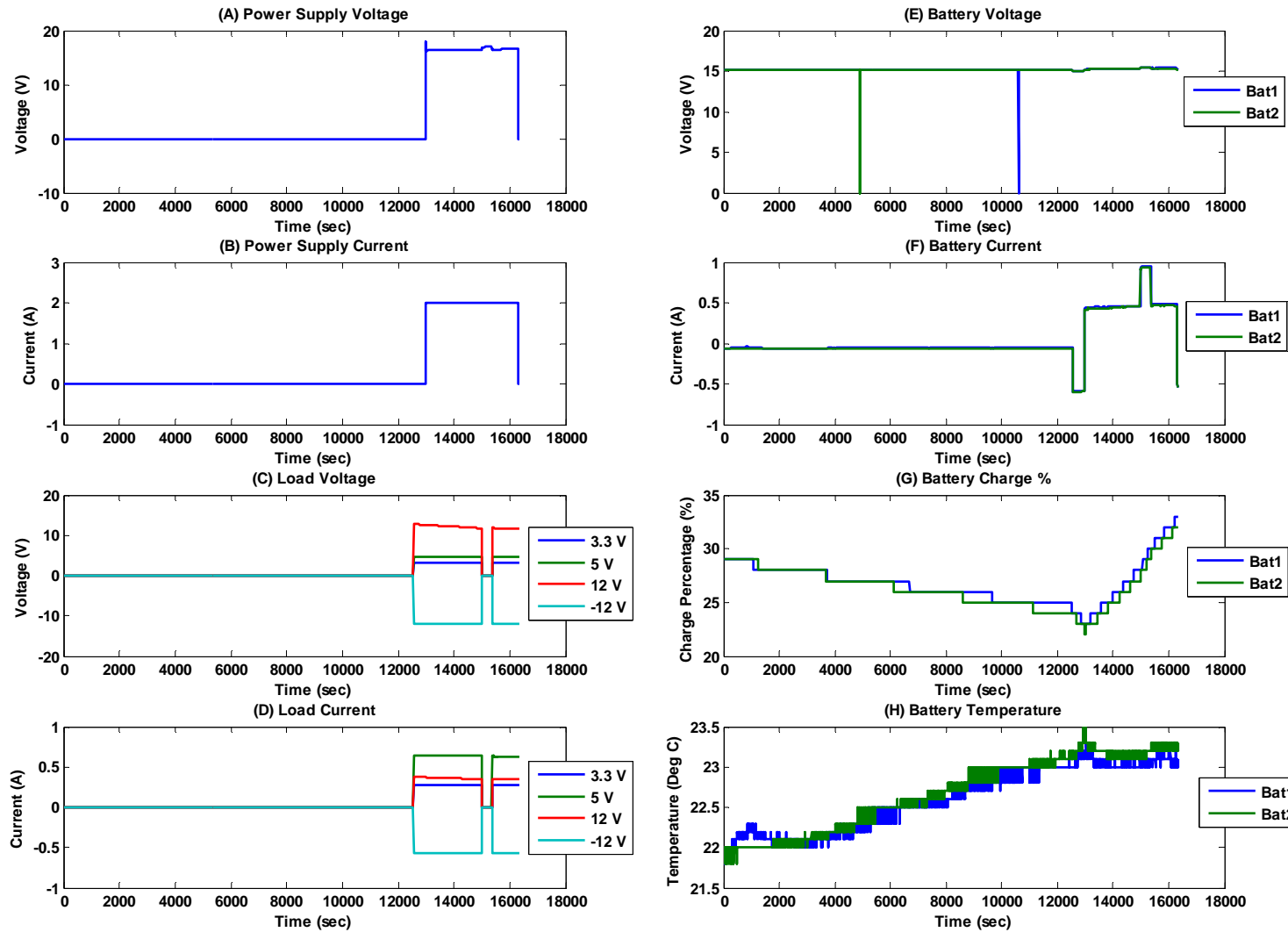


Figure 59. Functional Test, Second Thermal Vacuum Test

## H. HARDWARE TESTING SUMMARY

Building on the design and simulation work in Chapters II and III, Chapter IV endeavored to characterize the Ocean Server IBPS hardware. The main questions that were explored were:

- Can the IBPS operate from a solar array?
- Can the IBPS operate using lower mass, and therefore lower capacity, batteries?
- What are the efficiencies of the components?
- Can the IBPS withstand the vibrations associated with a launch to low earth orbit?
- Can the IBPS survive TINYSCOPE's predicted thermal environment?
- Can the IBPS survive operating in a vacuum?

Although exhaustive inquiries could not be accomplished in all cases, the results clearly show that the IBPS is very robust. Its functions were successfully exercised during solar panel testing, battery testing, efficiency testing, vibration testing, and thermal-vacuum testing.

Solar panel testing showed that the IBPS can be supplied from a very low current level source. The solar panel used supplied a maximum of 100 mA whereas TINYSCOPE will provide approximately 1.5 A (reference Table 8). More importantly, although the test solar panel was rated at only 15.4 V, it was still able to supply a voltage closer to 18 V. This bodes well for the solar panel design which calls for 17.3 V (reference Table 8).

Battery compatibility testing showed that the IBPS can operate off of smaller, lower capacity batteries. This is critical to optimizing the volume and mass of TINYSCOPE's EPS. This is especially true considering the fact that the final list of subsystem components to be used on TINYSCOPE is yet to be determined. It bears restating that the capacity of battery used will affect the expected number of cycles. Additionally, the use of two smaller capacity batteries will provide some defense against IBPS malfunction as was discovered during thermal-vacuum testing.

Finding the efficiencies of the IBPS was critical to fully modeling the EPS design in Matlab/Simulink. Without complete knowledge of how much power is available to the loads and for battery charging, it is impossible to correctly size the solar panels or battery capacity. Thus, as TINYSCOPE's design evolves, efficiency testing must be re-accomplished to ensure accurate efficiencies are used during dynamic EPS modeling.

Although standards call for many different types of space vehicle testing, vibration and thermal-vacuum testing were considered to be of primary importance since they are somewhat representative of the types of testing. The overall approach was initially to vibration test to a medium level in one axis and then thermal-vacuum the same unit to a reasonable level. After that, the same unit would then go back through a more thorough vibration test in all three axes with another more rigorous thermal vacuum test. Because of unforeseen hardware problems and unaccounted setup effort, only the first half of the approach was executed. Despite this, much data was gathered and analyzed. Not only did these tests provide unexpected information regarding the use of multiple batteries, they also provided a reasonable basis of confidence for successfully using the IBPS in space.

The purpose of the work documented in this chapter was to conduct a preliminary investigation into the feasibility of successfully using the IBPS in a low-cost, moderate-risk space mission. This chapter provided a reasonable amount of data and analysis upon which to base a sensible decision to pursue further the use of the Ocean Server IBPS within the context of the guiding principles of Project TINYSCOPE: use of COTS, short mission life, and low cost.

THIS PAGE INTENTIONALLY LEFT BLANK

## V. RECOMMENDATIONS AND CONCLUSIONS

Given the guiding principles of Project TINYSCOPE, a nanosatellite EPS was designed, simulated, and potential hardware was tested. One of the most challenging parts of this thesis was to keep the EPS design up to date in the face of continuously changing power requirements. The power requirements changed because of two main reasons. First, the set of components required for a mission such as TINYSCOPE is not yet well characterized<sup>q</sup> and no one on the present TINYSCOPE student-officer team has actual experience designing and building operational satellites. This meant that a static set of subsystem components and their associated electrical requirements was not available. Without this knowledge, it is extremely difficult to correctly size the capacity of the batteries and the solar array. Additionally, specific voltage and current requirements cannot be known until the set of components are known. This means that the EPS could be potentially overdesigned if unneeded voltages are included. Overdesigning means eating into mass and volume margin causing potential difficulties in satellite configuration.

The second reason power requirements were persistently altered is because a standardized imaging period profile was not developed before EPS design and simulation commenced. Which pieces of equipment are powered on and the timing of power up makes a significant difference in what is required of the EPS. Questions such as, “Will the communications equipment be on during imaging?” have huge implications when the communications load could be as high or higher than the imaging load. The number of images TINYSCOPE will take and what actions have to be taken before and after imaging can also drastically modify the level of power needed. One example of this difficulty came in the form of how many images TINYSCOPE can take in an imaging period. Originally proposed as four images in one 10 minute imaging period, this

---

<sup>q</sup> Although there have been many electro-optical imaging satellites launched and operated, none of these was of the size or imaging capability of TINYSCOPE.

assumption came under pressure when it became obvious that the amount of time needed to download the data in four images could be extensive. Time over one spot on the earth is a luxury a LEO satellite does not have.<sup>r</sup> Thus, a high data rate implies a high communications transmit power. Higher communications power could lead to a larger solar panel and batteries. Therefore, the author took a fixed baseline of TINYSCOPE and designed to it. Thus, as that baseline changes, the work accomplished in this thesis must be updated, revised, and expanded.

Despite the challenges associated with the overall design of the EPS, the progress made with regard to the dynamic EPS model and hardware testing is important. The dynamic EPS model shows that the design is feasible with enough margin to accommodate relatively large changes in power requirements. It is very conservative to assume, as the EPS model does, that no power will be collected during imaging. This approach extends the amount of time the batteries must support the load and reduces the amount of time available for charging the batteries. This means that any power provided at an adequate voltage during imaging operations will reduce the battery depth of discharge. This has the effect of increasing the predicted battery life. Despite this robustness, the dynamic EPS model should be updated as loads and therefore efficiencies evolve.

Although the hardware testing was not exhaustive, a relatively large amount of data was collected that, after analysis, showed that the IBPS has a high likelihood of operating successfully in space. To be prudent, the author makes two recommendations. First, it would be wise to accomplish a full suite of three axis vibration testing to GEVS generalized random vibration levels. Once that is done, the IBPS should be thermal-vacuum tested, with soak periods, for at least one uninterrupted hot/cold cycle to GEVS qualification levels. Second,

---

<sup>r</sup> Typically less than 10 minutes for LEO spacecraft with a reduction of one to two minutes for establishing communications for rising above the horizon and breaking communications when the satellite is setting below the horizon.

additional troubleshooting of the IBPS malfunction experienced during the first thermal-vacuum test should be completed. The only reasonable hypothesis at this point is that one of the chips failed. This may or may not be the case. The suspect chips could be replaced with new chips and the board re-tested. If a functional test after replacing the chip(s) shows positive results, it can reasonably be determined that the suspect chip was at fault.

The Ocean Server IBPS is a COTS product that comes with all the drawbacks of COTS. Specifically, detailed circuit design and expected conditions are not always known. This can make troubleshooting errors very difficult. Although manufacturer support was fairly swift when IBPS board faults were experienced, support was not so good when general design questions were posed. When questions such as, “What is the efficiency of the DC to DC converter?” went unanswered, tests had to be devised to discover the answer. In that case it was easy, but in other cases it may not be so straightforward. Another inherent problem with a COTS product is that the heritage of the components used will never be fully known. This can be problematic if the manufacturer swaps out components without notice. However, a rigorous inspection and test program by the integration team can mitigate this hazard.

Another area of deliberation when considering using the IBPS is the cost tradeoff between using a terrestrial system and an ostensibly more robust space rated system. The single most expensive part of the EPS is the cost of the solar cells and the associated work to integrate them into a solar panel. A rough order of magnitude cost estimate for the cells prescribed in Chapter II, Section D is approximately \$9,000.<sup>s</sup> Assuming an integrated solar panel costs \$13,500, an IBPS based system with two “medium” batteries adds approximately \$600 to this cost while a CubeSat Power System adds about \$6,000 to this cost. Thus, an

---

<sup>s</sup> \$250 per cell for 36 cells. This cost does not include integration costs which could easily increase this figure by 50%.

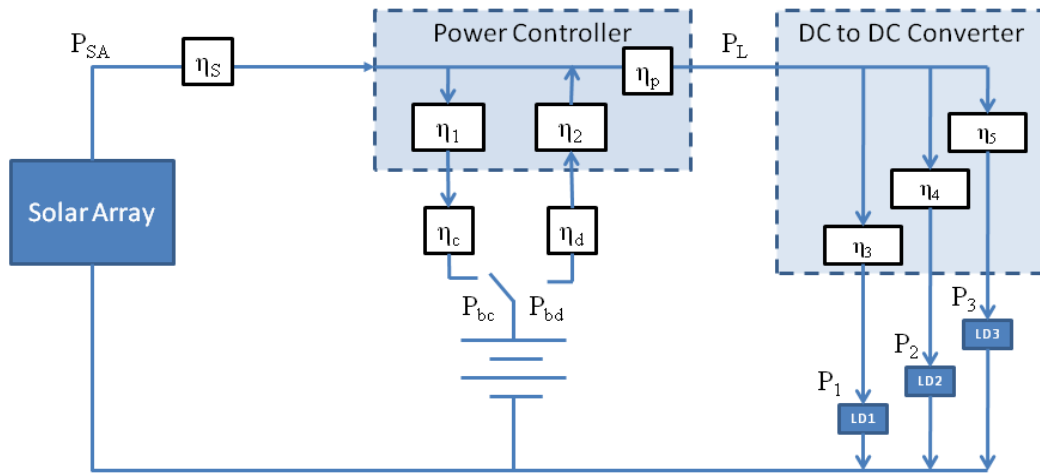
IBPS based system is about 28% cheaper overall. As this estimation is not sufficient to base a decision on, it is recommended that this area be studied further.

Given the problems associated with using a COTS product, the final decision to use one will always come down to the decision to accept a level of risk. One of the main purposes of this thesis was to increase understanding and attempt to quantify that risk so that an informed decision can be made.

## APPENDIX A. SOLAR ARRAY POWER EQUATION

The TINYSCOPE EPS is based on the single orbit energy balance equation, Equation 1, and the EPS equivalent circuit in Figure 5. These are repeated here for convenience.

$$P_{bd} \times T_d \leq P_{bc} \times T_c$$



Several additional efficiencies are included in Figure 5 that were not included in Figure 4. The efficiencies related to the power controller;  $\eta_1$ ,  $\eta_2$ , and  $\eta_p$ ; were included because distinct efficiencies were observed during hardware testing depending upon if the batteries were in a charge or discharge mode. The efficiencies related to the DC to DC converter are due to the fact that efficiencies are not uniform when converting one DC voltage to another DC voltage. A DC to DC converter has a higher efficiency when it is converting to a voltage that is close in magnitude and sign to its supply side voltage. Reference Chapter 4, Section B for additional details on the Ocean Server IBPS.

The power required by the load is supplied first by the solar array with any remaining power taken from the batteries. Thus the power taken from the batteries is the difference between what the load requires and what the solar array supplies. The power of the battery during discharge  $P_{bd}$  can be written as,

$$P_{bd} = \frac{P_L - P_{sa}\eta_s}{\eta_d\eta_2} \quad (26)$$

Note that Equation 26 allows for discharging of the batteries at anytime—during sunlight or eclipse.

The power supplied to the batteries during charging is the difference between the power collected by the solar array and what is required by the load. If the load uses all the power collected by the solar array, the batteries are not charged. The power going into the batteries during charge can be written as

$$P_{bc} = \left( P_{sa}\eta_s - \frac{P_L}{\eta_p} \right) \eta_l\eta_c \quad (27)$$

Equations 26 and 27 can now be substituted into the energy balance equation, Equation 1. The goal is to solve for the power required to be collected by the solar array  $P_{sa}$ .

$$\left[ \frac{P_L - P_{sa}\eta_s}{\eta_d\eta_2} \right] T_d \leq \left[ \left( P_{sa}\eta_s - \frac{P_L}{\eta_p} \right) \eta_l\eta_c \right] T_c \quad (28)$$

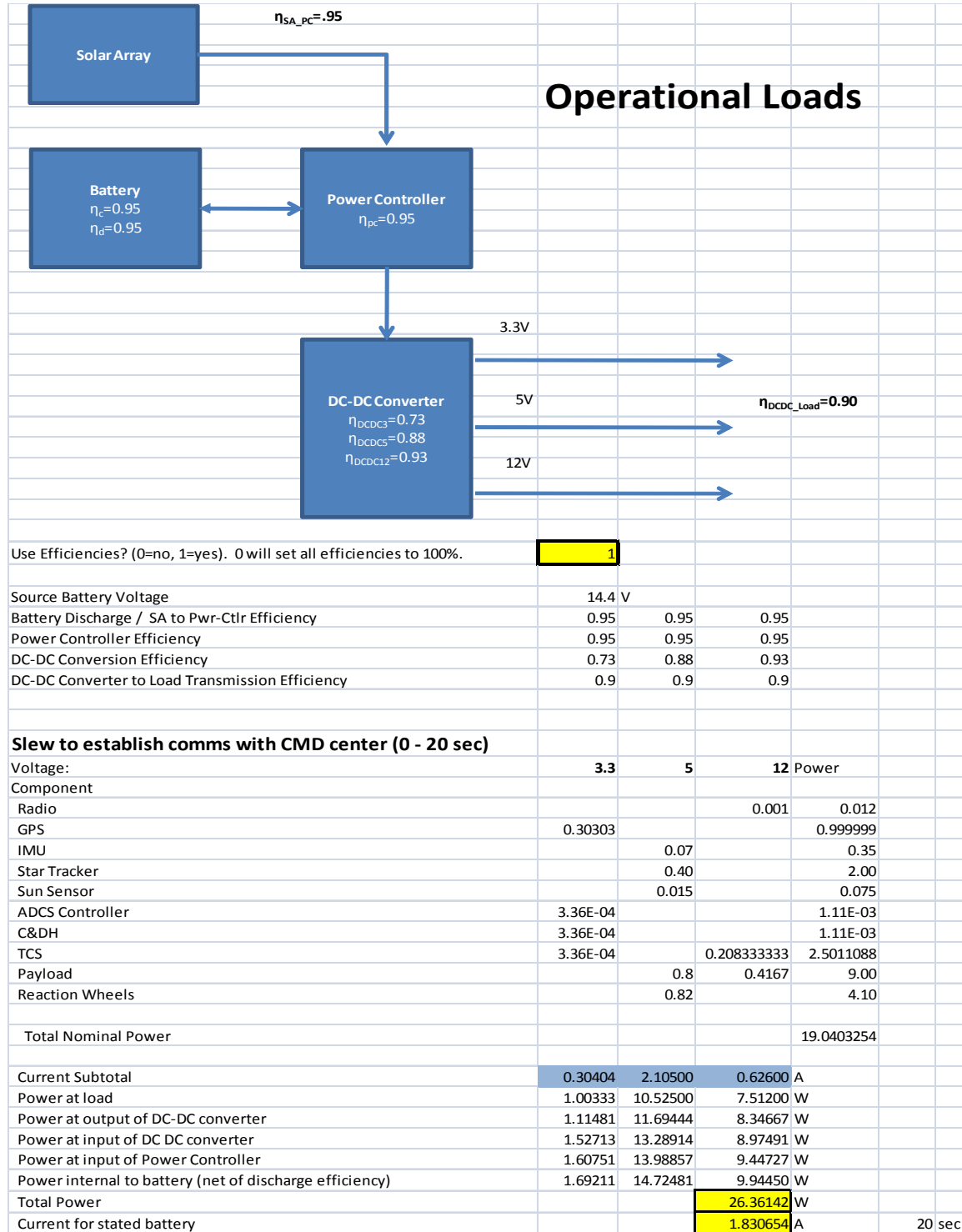
Rearranging and solving for  $P_{sa}$  results in Equation 6,

$$P_{sa} \geq \frac{P_L T_d}{\eta_p (\eta_s \eta_l \eta_c \eta_d \eta_2 T_c + \eta_s T_d)} + \frac{P_L T_c}{\eta_p \left( T_c + \frac{\eta_s}{\eta_l \eta_c \eta_d \eta_2} T_d \right)}; \quad \text{where } P_L = \frac{P_1}{\eta_3} + \frac{P_2}{\eta_4} + \frac{P_3}{\eta_5}$$

Equation 6 is much more difficult to interpret than Equation 5 but it gives an accurate expression for the amount of power that must be collected by the solar array. Additionally, one can gain insight into how each of the efficiencies affects the overall amount of power that is required. Note that Equation 6 allows for a regulated bus that has multiple efficiencies on the load lines. The number of efficiencies is based on the number of voltages supplied by the DC to DC converter in the EPS. In the case of TINYSCOPE, there are three voltages required by the load: 3.3 V, 5 V, and 12 V. However, any number may be included and used in Figure 5 and Equation 6.

## APPENDIX B. EPS LOAD DETAIL

### Operational Load Detail



<b>Comms (RWs to low rate slew) (20 - 90 sec)</b>			
Voltage:	3.3	5	12 Power
Component			
Radio		0.545	6.54
GPS	0.30303		0.999999
IMU		0.07	0.35
Star Tracker		0.4	2.00
Sun Sensor		0.015	0.075
ADCS Controller	3.36E-04		1.11E-03
C&DH	3.36E-04		1.11E-03
TCS	3.36E-04	0.208333333	2.5011088
Payload		0.8	9.00
Reaction Wheels		0.24	1.20
Total			22.668325
Current Subtotal	0.30404	1.52500	1.17000 A
Power at load	1.00333	7.62500	14.04000 W
Power at output of DC-DC converter	1.11481	8.47222	15.60000 W
Power at input of DC DC converter	1.52713	9.62753	16.77419 W
Power at input of Power Controller	1.60751	10.13424	17.65705 W
Power internal to battery (net of discharge efficiency)	1.69211	10.66762	18.58636 W
Total Power		30.94609	W
Current for stated battery		2.149034	A
			70 sec
<b>Slew to first image, comms (90 - 110 sec)</b>			
Voltage:	3.3	5	12 Power
Component			
Radio		0.545	6.54
GPS	0.30303		0.999999
IMU		0.07	0.35
Star Tracker		0.4	2.00
Sun Sensor		0.015	0.075
ADCS Controller	3.36E-04		1.11E-03
C&DH	3.36E-04		1.11E-03
TCS	3.36E-04	0.208333333	2.50E+00
Payload		0.8	9.00
Reaction Wheels		0.82	4.10
Total			25.56833
Current Subtotal	0.30404	2.10500	1.17000 A
Power at load	1.00333	10.52500	14.04000 W
Power at output of DC-DC converter	1.11481	11.69444	15.60000 W
Power at input of DC DC converter	1.52713	13.28914	16.77419 W
Power at input of Power Controller	1.60751	13.98857	17.65705 W
Power internal to battery (net of discharge efficiency)	1.69211	14.72481	18.58636 W
Total Power		35.00329	W
Current for stated battery		2.430784	A
			20 sec

<b>First Image, comms, RWs in low rate slew (110 - 115 sec)</b>			
Voltage:	3.3	5	12 Power
Component			
Radio		0.545	6.54
GPS	0.30303		0.999999
IMU		0.07	0.35
Star Tracker		0.4	2
Sun Sensor		0.015	0.075
ADCS Controller	3.36E-04		1.11E-03
C&DH	3.36E-04		1.11E-03
TCS	3.36E-04	0.208333333	2.50E+00
Payload		0.8	9.00
Reaction Wheels		0.24	1.2
Total			22.66833
Current Subtotal	0.30404	1.52500	1.17000 A
Power at load	1.00333	7.62500	14.04000 W
Power at output of DC-DC converter	1.11481	8.47222	15.60000 W
Power at input of DC DC converter	1.52713	9.62753	16.77419 W
Power at input of Power Controller	1.60751	10.13424	17.65705 W
Power internal to battery (net of discharge efficiency)	1.69211	10.66762	18.58636 W
Total Power		30.94609	W
Current for stated battery		2.149034	A
			5 sec
<b>Slew to second image, comms (115 - 135 sec)</b>			
Voltage:	3.3	5	12 Power
Component			
Radio		0.545	6.54
GPS	0.30303		0.999999
IMU		0.07	0.35
Star Tracker		0.4	2.00
Sun Sensor		0.015	0.075
ADCS Controller	3.36E-04		1.11E-03
C&DH	3.36E-04		1.11E-03
TCS	3.36E-04	0.208333333	2.50E+00
Payload		0.8	9.00
Reaction Wheels		0.82	4.10
Total			25.56833
Current Subtotal	0.30404	2.10500	1.17000 A
Power at load	1.00333	10.52500	14.04000 W
Power at output of DC-DC converter	1.11481	11.69444	15.60000 W
Power at input of DC DC converter	1.52713	13.28914	16.77419 W
Power at input of Power Controller	1.60751	13.98857	17.65705 W
Power internal to battery (net of discharge efficiency)	1.69211	14.72481	18.58636 W
Total Power		35.00329	W
Current for stated battery		2.430784	A
			20 sec

<b>Second Image, comms (135 - 140 sec)</b>			
Voltage:	3.3	5	12 Power
Component			
Radio		0.545	6.54
GPS	0.30303		0.999999
IMU		0.07	0.35
Star Tracker		0.4	2
Sun Sensor		0.015	0.075
ADCS Controller	3.36E-04		1.11E-03
C&DH	3.36E-04		1.11E-03
TCS	3.36E-04	0.208333333	2.50E+00
Payload		0.8	0.4167
Reaction Wheels		0.24	1.2
Total			22.66833
Current Subtotal	0.30404	1.52500	1.17000 A
Power at load	1.00333	7.62500	14.04000 W
Power at output of DC-DC converter	1.11481	8.47222	15.60000 W
Power at input of DC DC converter	1.52713	9.62753	16.77419 W
Power at input of Power Controller	1.60751	10.13424	17.65705 W
Power internal to battery (net of discharge efficiency)	1.69211	10.66762	18.58636 W
Total Power		30.94609	W
Current for stated battery		2.149034	A
			5 sec
<b>Slew to CMD Center, comms (140 - 160 sec)</b>			
Voltage:	3.3	5	12 Power
Component			
Radio		0.545	6.54
GPS	0.30303		0.999999
IMU		0.07	0.35
Star Tracker		0.4	2
Sun Sensor		0.015	0.075
ADCS Controller	3.36E-04		1.11E-03
C&DH	3.36E-04		1.11E-03
TCS	3.36E-04		1.11E-03
Payload			0.00
Reaction Wheels		0.82	4.1
Total			14.06833
Current Subtotal	0.30404	1.30500	0.54500 A
Power at load	1.00333	6.52500	6.54000 W
Power at output of DC-DC converter	1.11481	7.25000	7.26667 W
Power at input of DC DC converter	1.52713	8.23864	7.81362 W
Power at input of Power Controller	1.60751	8.67225	8.22486 W
Power internal to battery (net of discharge efficiency)	1.69211	9.12868	8.65775 W
Total Power		19.47855	W
Current for stated battery		1.352677	A
			20 sec

<b>Comms (160 - 620 sec)</b>					
Voltage:	<b>3.3</b>	<b>5</b>	<b>12</b>	Power	
Component					
Radio			0.545	6.54	
GPS	0.30303			0.999999	
IMU		0.07		0.35	
Star Tracker		0.4		2	
Sun Sensor		0.015		0.075	
ADCS Controller	3.36E-04			1.11E-03	
C&DH	3.36E-04			1.11E-03	
TCS	3.36E-04			1.11E-03	
Payload				0.00	
Reaction Wheels		0.24		1.2	
Total				11.16833	
Current Subtotal	<b>0.30404</b>	<b>0.72500</b>	<b>0.54500</b>	A	
Power at load	1.00333	3.62500	6.54000	W	
Power at output of DC-DC converter	1.11481	4.02778	7.26667	W	
Power at input of DC DC converter	1.52713	4.57702	7.81362	W	
Power at input of Power Controller	1.60751	4.81792	8.22486	W	
Power internal to battery (net of discharge efficiency)	1.69211	5.07149	8.65775	W	
Total Power			<b>15.42135</b>	W	
Current for stated battery			<b>1.070927</b>	A	460 sec
<b>Sun Pointing (620 - 3532 sec)</b>					
Voltage:	<b>3.3</b>	<b>5</b>	<b>12</b>	Power	
Component					
Radio			0.001	0.012	
GPS	0.30303			0.999999	
IMU		0.07		0.35	
Star Tracker		0.4		2	
Sun Sensor		0.015		0.075	
ADCS Controller	3.36E-04			1.11E-03	
C&DH	3.36E-04			1.11E-03	
TCS	3.36E-04			1.11E-03	
Payload				0.00	
Reaction Wheels		0.24		1.2	
Total				4.6403254	
Current Subtotal	<b>0.30404</b>	<b>0.72500</b>	<b>0.00100</b>	A	
Power at load	1.00333	3.62500	0.01200	W	
Power at output of DC-DC converter	1.11481	4.02778	0.01333	W	
Power at input of DC DC converter	1.52713	4.57702	0.01434	W	
Power at input of Power Controller	1.60751	4.81792	0.01509	W	
Power internal to battery (net of discharge efficiency)	1.69211	5.07149	0.01589	W	
Total Power			<b>6.77949</b>	W	
Current for stated battery			<b>0.470798</b>	A	2912 sec

<b>Eclipse (Maintain Attitude) (3532 - 5216)</b>			
Voltage:	3.3	5	12 Power
Component			
Radio		0.001	0.012
GPS	0.30303		0.999999
IMU		0.07	0.35
Star Tracker		0.4	2
Sun Sensor		0.015	0.075
ADCS Controller	3.36E-04		1.11E-03
C&DH	3.36E-04		1.11E-03
TCS	3.36E-04	0.208333333	2.50E+00
Payload			0.00
Reaction Wheels		0.24	1.2
Total			7.1403254
Current Subtotal	0.30404	0.72500	0.20933 A
Power at load	1.00333	3.62500	2.51200 W
Power at output of DC-DC converter	1.11481	4.02778	2.79111 W
Power at input of DC DC converter	1.52713	4.57702	3.00119 W
Power at input of Power Controller	1.60751	4.81792	3.15915 W
Power internal to battery (net of discharge efficiency)	1.69211	5.07149	3.32542 W
Total Power			10.08903 W
Current for stated battery			0.700627 A
			1684 sec
<b>Eclipse (Maintain Attitude &amp; Warmup) (5216 - 5676.8)</b>			
Voltage:	3.3	5	12 Power
Component			
Radio		0.001	0.012
GPS	0.30303		0.999999
IMU		0.07	0.35
Star Tracker		0.4	2
Sun Sensor		0.015	0.075
ADCS Controller	3.36E-04		1.11E-03
C&DH	3.36E-04		1.11E-03
TCS	3.36E-04	0.208333333	2.50E+00
Payload		0.8	0.416666667
Reaction Wheels		0.24	1.2
Total			16.1403254
Current Subtotal	0.30404	1.52500	0.62600 A
Power at load	1.00333	7.62500	7.51200 W
Power at output of DC-DC converter	1.11481	8.47222	8.34667 W
Power at input of DC DC converter	1.52713	9.62753	8.97491 W
Power at input of Power Controller	1.60751	10.13424	9.44727 W
Power internal to battery (net of discharge efficiency)	1.69211	10.66762	9.94450 W
Total Power			22.30423 W
Current for stated battery			1.548905 A
			460.8 sec

## Operational Load Summary

<b>Nominal Discharge @ 14.4V</b>		Current Load (A)	Time (s)	Time (h)	Capacity Used (Ah)	
1	Eclipse (Maintain Attitude) (3532 - 5216)	0.700627	1684	0.467778	0.327738	
2	Eclipse (Maintain Attitude & Warmup) (5216 - 5676.8)	1.548905	460.8	0.128000	0.198260	
3	Slew to establish comms with CMD center (0 - 20 sec)	1.830654	20	0.005556	0.010170	
4	Comms (RWs to low rate slew) (20 - 90 sec)	2.149034	70	0.019444	0.041787	
5	Slew to first image, comms (90 - 110 sec)	2.430784	20	0.005556	0.013504	
6	First Image, comms, RWs in low rate slew (110 - 115 sec)	2.149034	5	0.001389	0.002985	
7	Slew to second image, comms (115 - 135 sec)	2.430784	20	0.005556	0.013504	
8	Second Image, comms (135 - 140 sec)	2.149034	5	0.001389	0.002985	
9	Slew to CMD Center, comms (140 - 160 sec)	1.352677	20	0.005556	0.007515	
10	Comms (160 - 620 sec)	1.070927	460	0.127778	0.136841	
11	Sun Pointing (620 - 3532 sec)	0.470798	2912	0.808889		
Maximum Draw		2.430784				
Battery Load Time (not including "Sun Pointing" loads)			2764.8			
Total			5676.8		0.755288	
(4) Series Cells					2.60 Ah	
DOD for nominal orbit cycle					29.05%	
Estimated Number of Cycles						
(4) Series, (2) Parallel					5.2 Ah	
DOD for nominal orbit cycle					14.52%	
(4) Series, (4) Parallel					10.4 Ah	
DOD for nominal orbit cycle					2.79%	

## Launch and Checkout Detail

Launch and checkout			
Use Efficiencies? (0=no, 1=yes). 0 will set all efficiencies to 100%.	1		
Source Battery Voltage	14.4	V	
Battery Discharge / SA to Pwr-Ctrl Efficiency	0.95	0.95	0.95
Power Controller Efficiency	0.95	0.95	0.95
DC-DC Conversion Efficiency	0.73	0.88	0.93
DC-DC Converter to Load Transmission Efficiency	0.9	0.9	0.9
T-10 Minutes to Deployment			
Voltage:	3.3	5	12 Power
Component			
Radio			0
GPS			0
IMU		0	0
Star Tracker			0.00
Sun Sensor			0
ADCS Controller	0.00E+00		0
C&DH	0.00E+00		0
TCS	0.00E+00		0
Payload			0.00
Reaction Wheels			0.00
Total Nominal Power			0
Current Subtotal	0.00000	0.00000	0.00000 A
Power at load	0.00000	0.00000	0.00000 W
Power at output of DC-DC converter	0.00000	0.00000	0.00000 W
Power at input of DC DC converter	0.00000	0.00000	0.00000 W
Power at input of Power Controller	0.00000	0.00000	0.00000 W
Power internal to battery (net of discharge efficiency)	0.00000	0.00000	0.00000 W
Total Power			0.00000 W
Current for stated battery		0.00000 A	1200 sec

3-Axis Stabilization and Solar Panel Deployment					
Voltage:	3.3	5	12	Power	
Component				0.001	0.012
Radio				0.001	0.012
GPS	0.30303			0.999999	
IMU		0.07		0.35	
Star Tracker		0.40		2.00	
Sun Sensor		0.015		0.075	
ADCS Controller	3.36E-04			0.0011088	
C&DH	3.36E-04			0.0011088	
TCS	3.36E-04	0.208333333	2.5011088		
Payload				0.00	
Reaction Wheels		0.82		4.10	
Total Nominal Power				10.0403254	
Current Subtotal	0.30404	1.30500	0.20933	A	
Power at load	1.00333	6.52500	2.51200	W	
Power at output of DC-DC converter	1.11481	7.25000	2.79111	W	
Power at input of DC DC converter	1.52713	8.23864	3.00119	W	
Power at input of Power Controller	1.60751	8.67225	3.15915	W	
Power internal to battery (net of discharge efficiency)	1.69211	9.12868	3.32542	W	
Total Power			14.14622	W	
Current for stated battery			0.982376	A	5400 sec

## Launch and Checkout Summary

Discharge @ 14.4V					
	Current Load (A)	Time (s)	Time (h)	Capacity Used (Ah)	
1 T-10 Minutes to Deployment	0	1200	0.333333333	0	
2 3-Axis Stabilization and Solar Panel Deployment	0.982376317	5400	1.5	1.473564475	
Maximum Draw	0.982376317				
Total				1.473564475	
(4) Series Cells				2.60 Ah	
DOD for nominal orbit cycle				56.68%	
Estimated Number of Cycles					
(4) Series, (2) Parallel				5.2 Ah	
DOD for nominal orbit cycle				28.34%	
(4) Series, (4) Parallel				10.4 Ah	
DOD for nominal orbit cycle				14.17%	

## Contingency Operations Detail

Contingency Operations				
Use Efficiencies? (0=no, 1=yes). 0 will set all efficiencies to 100%.	1			
Source Battery Voltage	14.4	V		
Battery Discharge / SA to Pwr-Ctrl Efficiency	0.95	0.95	0.95	
Power Controller Efficiency	0.95	0.95	0.95	
DC-DC Conversion Efficiency	0.73	0.88	0.93	
DC-DC Converter to Load Transmission Efficiency	0.9	0.9	0.9	
Contingency Operations				
Voltage:	3.3	5	12	Power
Component				
Radio			0.095	1.14
GPS	0.30303			0.999999
IMU		0.07		0.35
Star Tracker		0.40		2.00
Sun Sensor		0.015		0.075
ADCS Controller	3.36E-04			0.0011088
C&DH	3.36E-04			0.0011088
TCS	3.36E-04		0.208333333	2.5011088
Payload				0.00
Reaction Wheels		0.06		0.30
Total Nominal Power				7.3683254
Current Subtotal	0.30404	0.54500	0.30333	A
Power at load	1.00333	2.72500	3.64000	W
Power at output of DC-DC converter	1.11481	3.02778	4.04444	W
Power at input of DC DC converter	1.52713	3.44066	4.34886	W
Power at input of Power Controller	1.60751	3.62174	4.57775	W
Power internal to battery (net of discharge efficiency)	1.69211	3.81236	4.81869	W
Total Power			10.32316	W
Current for stated battery			0.716886	A
				5400 sec

## Contingency Operations Summary

<b>Discharge @ 14.4V</b>				
	Current Load (A)	Time (s)	Time (h)	Capacity Used (Ah)
1 Contingency Operations	0.716886201	5400	1.5	1.075329301
Maximum Draw	0.716886201			
Total				1.075329301
(4) Series Cells				2.60 Ah
DOD for nominal orbit cycle				41.36%
Estimated Number of Cycles				
(4) Series, (2) Parallel				5.2 Ah
DOD for nominal orbit cycle				20.68%
(4) Series, (4) Parallel				10.4 Ah
DOD for nominal orbit cycle				10.34%

THIS PAGE INTENTIONALLY LEFT BLANK

## APPENDIX C. SOLAR CELL SPECIFICATION SHEETS

### ATJM Photovoltaic Cell

Advanced Triple-Junction with Monolithic Diode Solar Cell for Space Applications



SPACE PHOTOVOLTAICS



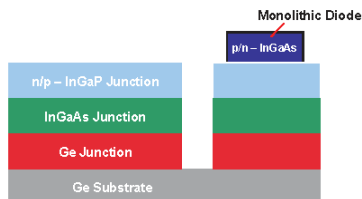
#### Typical Performance Data

Solar Cell Electrical Output Parameters	
Electrical Parameters @ AM0 (135.3 mW/cm <sup>2</sup> )	27%
V <sub>oc</sub>	2.575V
J <sub>sc</sub>	16.9 mA/cm <sup>2</sup>
V <sub>mp</sub>	2.285V
J <sub>mp</sub>	16.0 mA/cm <sup>2</sup>

Monolithic Diode Electrical Performance	
V <sub>fb</sub> < 2.0 V @ I <sub>sd</sub>	500 mA, 28°C
I <sub>sd</sub> < 50 μA @ V <sub>fb</sub>	2.5V (Dark), 28°C
I <sub>sd</sub> < 200 μA @ V <sub>fb</sub>	2.5V (Illuminated), 28°C
I <sub>sd</sub> < 10 μA @ V <sub>fb</sub>	2.5V (Dark), -150°C
I <sub>sd</sub> < 1 μA @ V <sub>fb</sub>	2.5V (Dark), +120°C

#### ATJM Cell Structure



Schematic Cross-Sectional View

### 27.0% Minimum Average Efficiency

#### Features & Characteristics

- Advanced Triple-Junction (ATJ) InGaP/InGaAs/Ge Solar Cells with n-on-p Polarity on 140-μm Uniform Thickness Substrate
- Fully space-qualified with proven flight heritage in LEO and GEO environments
- Fully Space-Qualified Monolithic Bypass Diode Protection
- Lowest solar cell mass of 84 mg/cm<sup>2</sup>
- Excellent radiation resistance with P/P<sub>0</sub> = 0.89 @ 1-MeV, 5E14 e/<sup>cm2</sup> fluence
- Excellent Mechanical Strength for Reduced Attrition during Assembly and Laydown
- Weldable or Solderable contacts
- Available at EPI, cell, CIC or panel configuration
- Standard and Custom Sizes Available

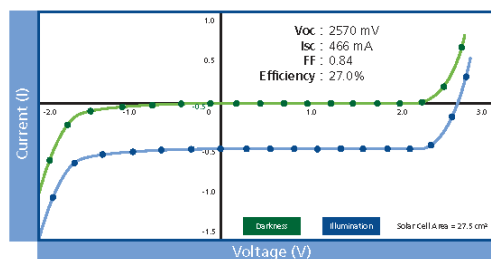
## ATJM Photovoltaic Cell

Advanced Triple-Junction with Monolithic Diode Solar Cell for Space Applications



### SPACE PHOTOVOLTAICS

#### Typical Current (I) / Voltage(V) Plot



#### Key Space Qualification Results

Test Performed	Industry Quality Standard	Typical Test Results
Metal Contact Thickness	4-10 µm	6 µm
Dark Current degradation after reverse bias	Δ Ispec <2%	<0.4%
Electrical performance after 2,000 thermal cycles -180°C to +95°C	<2%	<0.7%
High-Temperature Anneal at 200°C for >5,000 hrs	<2%	No measurable difference
Contact pull strength	>300 grams	>600 grams
Electrical performance degradation after 40 day humidity exposure at 60°C and 95% relative humidity	<1.5%	No measurable difference

For complete qualification results, please request EMCORE's ATJ Qual Report EWRP036

#### About EMCORE Corporation



Emcore Photovoltaics  
Albuquerque, NM

- Incorporated in 1984
- Appx. 900 Employees
- Nasdaq: EMKR

#### Radiation Performance at 1 MeV Electron Irradiation, EOL/BOL Ratios

Fluence (e/cm²)	Voc	Isc	Vmp	Imp	Pmp	Efficiency
5E 13	0.97	1.00	0.97	1.00	0.97	0.97
1E 14	0.96	1.00	0.96	1.00	0.96	0.96
5E 14	0.92	0.98	0.92	0.96	0.89	0.89
1E 15	0.90	0.96	0.90	0.94	0.85	0.85
3E 15	0.86	0.90	0.85	0.87	0.74	0.74

#### Temperature Coefficients

Fluence (e/cm²)	ΔVoc/ΔT (mV/°C)	Isc/ΔT <sup>(1)</sup> (µA/°C)	Vmp/ΔT (mW/°C)	Imp/ΔT <sup>(2)</sup> (µA/°C)
BOL	-5.48	+12	-5.93	+11
5E 13	-5.49	+10	-5.68	+7
1E 14	-5.46	+11	-5.66	+7
5E 14	-5.61	+12	-5.92	+12
1E 15	-5.77	+12	-6.14	+13

■ (1) Isc is the symbol for normalized Isc

■ (2) Imp is the symbol for normalized Imp

#### Regulatory



EMCORE CORPORATION  
ISO 9001 CERTIFIED



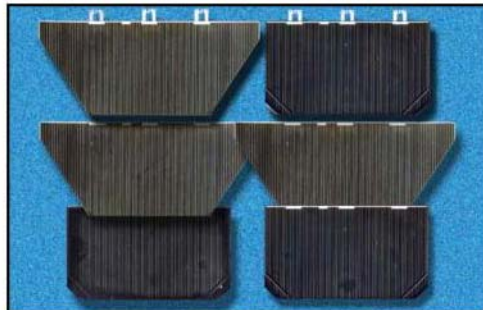
EMCORE PHOTOVOLTAICS  
AS9100 CERTIFIED



## 25.1% GaInP<sub>2</sub>/GaAs/Ge Triple Junction Solar Cells

### Features

- High efficiency n/p design
  - BOL: up to 26% minimum average efficiency (28°C, AM0)
  - EOL: up to 21% minimum average efficiency (28°C, AM0, 1E15 e/cm<sup>2</sup> 1 MeV equivalence)
- Integral bypass diode protection
- Transparent insertion into existing systems
- High volume production capability:
  - Currently delivering 24.5% min. avg. efficiency solar cells
  - 26% minimum average efficiency available in year 2000



### Product Description

Substrate	Germanium
Method of GaAs Growth	Metal Organic Vapor Phase Epitaxy
Device Design	Monolithic, two terminal triple junction. n/p GaInP <sub>2</sub> , GaAs, and Ge solar cells interconnected with two tunnel junctions
Sizes	Up To 30 cm <sup>2</sup>
Assembly Method	Multiple techniques including soldering, welding, thermocompression, or ultrasonic wire bonding
Integral Diode	Si diode integrated into recess on back side

Note: Other Variations Are Available Upon Request

### Heritage

- More than 2000 kW of multi-junction cells produced
- More than 675 kW of multi-junction arrays *on orbit*
- 1 MW annual capacity - cells, panels & arrays
- On orbit performance for multi-junction solar cells validated to ± 1.5% of ground test results



S P E C T R O L A B

A BOEING COMPANY

Spectrolab Inc. 12500 Gladstone Avenue, Sylmar, California 91342 USA • Phone: 818.365.4611 • Fax: 818.361.5102



[www.spectrolab.com](http://www.spectrolab.com)

### Typical Electrical Parameters

(AMO (135.3 mW/cm<sup>2</sup>) 28°C, Bare Cell)

J<sub>sc</sub>= 15.60 mA/cm<sup>2</sup>

J<sub>mp</sub>= 14.90 mA/cm<sup>2</sup>

J<sub>load min avg</sub>= 14.93 mA/cm<sup>2</sup>

V<sub>oc</sub>= 2.545 V

V<sub>mp</sub>= 2.275 V

V<sub>load</sub>= 2.220 V

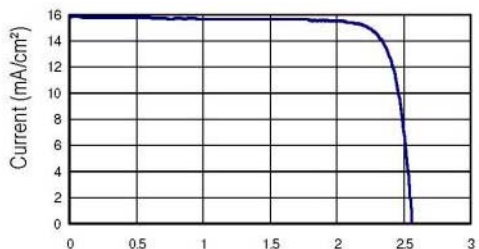
Cff= 0.85

Eff<sub>load</sub>= 24.5%

Eff<sub>mp</sub>= 25.1%

### Typical IV Characteristic

AMO (135.3 mW/cm<sup>2</sup>) 28°C, Bare Cell



### Radiation Degradation

(Fluence 1 MeV Electrons/cm<sup>2</sup>)

Parameters	1x10 <sup>14</sup>	3x10 <sup>14</sup>	1x10 <sup>15</sup>
I <sub>mp</sub> /I <sub>mp0</sub>	0.99	0.97	0.90
V <sub>mp</sub> /V <sub>mp0</sub>	0.97	0.95	0.92
P <sub>mp</sub> /P <sub>mp0</sub>	0.96	0.92	0.83

### Thermal Properties

Solar Absorptance= 0.92 (Ceria Doped Microsheet)

Emittance (Normal)= 0.85 (Ceria Doped Microsheet)

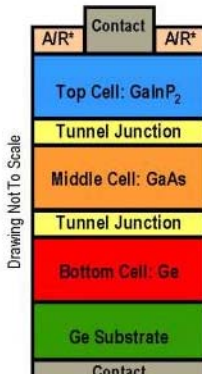
### Temperature Coefficients

Parameters	BOL	1x10 <sup>15</sup> (1 MeV e/cm <sup>2</sup> )
J <sub>mp</sub> (μA/cm <sup>2</sup> /°C)	6	14
J <sub>sc</sub> (μA/cm <sup>2</sup> /°C)	9	11
V <sub>mp</sub> (mV/°C)	-6.7	-7.2
V <sub>oc</sub> (mV/°C)	-6.4	-6.8

### Weight

84 mg/ cm<sup>2</sup> (Bare) @ 140 μm (5.5 mil) Thickness

Thickness of 175 μm typical with weight equivalence of a 140 μm thick cell.



\*A/R: Anti-Reflective Coating

S P E C T R O L A B

A BOEING COMPANY

**ISO9001:2000**  
REGISTERED

The information contained on this sheet is for reference only.  
Specifications subject to change without notice. 4/29/2008

**Spectrolab Inc. 12500 Gladstone Avenue, Sylmar, California 91342 USA • Phone: 818.365.4611 • Fax: 818.361.5102**

## APPENDIX D. SOLAR CELL PREDICTED TEMPERATURE

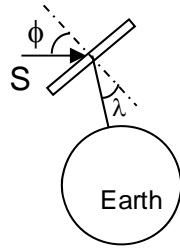


Figure 60. Solar Panel Configuration From [16]

Solar array					
	If back side of SA sees all of Earth Enter "1" else "0"	1			
Item	Equation	Symbol	SMAD	Source	
Altitude	-	h	500.0	Given	
Inclination	-	i	1.699950691	Given	
Solar/orbit angle	-	β	0	Given	
Orbit angle from SSP	-	vo	0	Given	
Radiator normal WRT Nadir	-	λ	0.785398163	Given	
Earth angular radius	asin(Re/Ro)	rho	1.187	calc	
Earth view factor	cos*(sinr)^2 or = "0"	Fe	0.6080	calc	
Albedo view factor	Fecosbcosno	Fa	0.608038453	calc	
Solar array temp:	T=[(αfScosφ+αbSa1Fa+εbEFe-ηfpScosφ)/(σ(ef+εb))]^0.25	Tsa			
Albedo	-	al	0.3	Given	
Emissivity solar cell side	-	ef	0.850	Given	
Emissivity back side	-	εb	0.92	Given	
Absorptivity front side	-	αf	0.92	Given	
Absorptivity back side	-	αb	0.17	Given	
Cell packing factor	-	fp	0.8	Given	
Cell efficiency	-	η	0.251	Given	
Max direct solar flux~W/m^2	-	S	1322	Given	
Solar incidence angle~rad	-	Phi	0	Given	
MaxEarth IR emission @ surface	-	E	326	Given	
Solar array temperature ~K	[(af'S*cos(phi)+ab'S*al*Fa+eb'E*Fe-h*fp*S*cos(phi))/[s(ef+eb)]]^0.25	Tsa	328.88	calc	

Solar array					
	If back side of SA sees all of Earth Enter "1" else "0"	1			
Item	Equation	Symbol	SMAD	Source	
Altitude	-	h	500.0	Given	
Inclination	-	i	1.699950691	Given	
Solar/orbit angle	-	β	0	Given	
Orbit angle from SSP	-	vo	0	Given	
Radiator normal WRT Nadir	-	λ	0.785398163	Given	
Earth angular radius	asin(Re/Ro)	rho	1.187	calc	
Earth view factor	cos*(sinr)^2 or = "0"	Fe	0.6080	calc	
Albedo view factor	Fecosbcosno	Fa	0.608038453	calc	
Solar array temp:	T=[(αfScosφ+αbSa1Fa+εbEFe-ηfpScosφ)/(σ(ef+εb))]^0.25	Tsa			
Albedo	-	al	0.3	Given	
Emissivity solar cell side	-	ef	0.850	Given	
Emissivity back side	-	εb	0.92	Given	
Absorptivity front side	-	αf	0.92	Given	
Absorptivity back side	-	αb	0.17	Given	
Cell packing factor	-	fp	0.8	Given	
Cell efficiency	-	η	0.251	Given	
Max direct solar flux~W/m^2	-	S	1414	Given	
Solar incidence angle~rad	-	Phi	0	Given	
MaxEarth IR emission @ surface	-	E	326	Given	
Solar array temperature ~K	[(af'S*cos(phi)+ab'S*al*Fa+eb'E*Fe-h*fp*S*cos(phi))/[s(ef+eb)]]^0.25	Tsa	333.61	calc	

Solar array					
Item	Equation	Symbol	SMAD	Source	
Altitude	-	h	500.0	Given	
Inclination	-	i	1.699950691	Given	
Solar/orbit angle	-	$\beta$	0	Given	
Orbit angle from SSP	-	$\omega_0$	0	Given	
Radiator normal WRT Nadir	-	$\lambda_n$	0.785398163	Given	
Earth angular radius	$\text{asin}(R_e/R_o)$	$r_{\text{ho}}$	1.187	calc	
Earth view factor	$\cos^*(\sin i)^2 \text{ or } = "0"$	$F_E$	0.6080	calc	
Albedo view factor	$F_{\text{ecosbcosn}}$	$F_a$	0.608038453	calc	
Solar array temp:	$T = \frac{[(\alpha f S \cos \beta + \alpha b S a l F_a + \epsilon b E F_e - \eta f p S \cos \beta) / (\sigma (e_f + \epsilon b))]^{0.25}}{S}$	$T_{\text{sa}}$			
Albedo	-	$a_l$	0.3	Given	
Emissivity solar cell side	-	$\epsilon_f$	0.850	Given	
Emissivity back side	-	$\epsilon_b$	0.92	Given	
Absorptivity front side	-	$\alpha_f$	0.92	Given	
Absorptivity back side	-	$\alpha_b$	0.17	Given	
Cell packing factor	-	$f_p$	0.8	Given	
Cell efficiency	-	$\eta$	0.27	Given	
Max direct solar flux~W/m <sup>2</sup>	-	S	1322	Given	
Solar incidence angle~rad	-	$\Phi$	0	Given	
MaxEarth IR emission @ surface	-	E	326	Given	
Solar array temperature ~K	$([a f S * \cos(\phi) + a b * S * a l * F_a + \epsilon b * E * F_e - h * f_p * S * \cos(\phi \cdot f)] / [S * (e_f + \epsilon b)])^{0.25}$	$T_{\text{sa}}$	327.47	calc	

Solar array					
Item	Equation	Symbol	SMAD	Source	
Altitude	-	h	500.0	Given	
Inclination	-	i	1.699950691	Given	
Solar/orbit angle	-	$\beta$	0	Given	
Orbit angle from SSP	-	$\omega_0$	0	Given	
Radiator normal WRT Nadir	-	$\lambda_n$	0.785398163	Given	
Earth angular radius	$\text{asin}(R_e/R_o)$	$r_{\text{ho}}$	1.187	calc	
Earth view factor	$\cos^*(\sin i)^2 \text{ or } = "0"$	$F_E$	0.6080	calc	
Albedo view factor	$F_{\text{ecosbcosn}}$	$F_a$	0.608038453	calc	
Solar array temp:	$T = \frac{[(\alpha f S \cos \beta + \alpha b S a l F_a + \epsilon b E F_e - \eta f p S \cos \beta) / (\sigma (e_f + \epsilon b))]^{0.25}}{S}$	$T_{\text{sa}}$			
Albedo	-	$a_l$	0.3	Given	
Emissivity solar cell side	-	$\epsilon_f$	0.850	Given	
Emissivity back side	-	$\epsilon_b$	0.92	Given	
Absorptivity front side	-	$\alpha_f$	0.92	Given	
Absorptivity back side	-	$\alpha_b$	0.17	Given	
Cell packing factor	-	$f_p$	0.8	Given	
Cell efficiency	-	$\eta$	0.27	Given	
Max direct solar flux~W/m <sup>2</sup>	-	S	1414	Given	
Solar incidence angle~rad	-	$\Phi$	0	Given	
MaxEarth IR emission @ surface	-	E	326	Given	
Solar array temperature ~K	$([a f S * \cos(\phi) + a b * S * a l * F_a + \epsilon b * E * F_e - h * f_p * S * \cos(\phi \cdot f)] / [S * (e_f + \epsilon b)])^{0.25}$	$T_{\text{sa}}$	332.16	calc	

## APPENDIX E. SUMMARY OF UNITED NATIONS T-TESTS

### Guidelines For Shipping, Handling, Storage & Disposal of Your Inspired Energy Lithium Ion Battery

UN T-Tests			
Test Title	Procedure	Test Sample Size	Pass Requirement
T1: Altitude Simulation	Store @ $\leq 11.6\text{kPa}$ or less for $\geq 6\text{hrs} @ 20\pm 5^\circ\text{C}$	4 batteries, cycle 1 fully charged	No mass loss, leakage, venting, rupture, disassembly, or fire & OCV after test $\geq 90\%$ OCV before test
		4 batteries, cycle 50 fully charged	No mass loss, leakage, venting, rupture, disassembly, or fire
		4 batteries, cycle 1 fully discharged	No mass loss, leakage, venting, rupture, disassembly, or fire
		4 batteries, cycle 50 fully discharged	No mass loss, leakage, venting, rupture, disassembly, or fire
T2: Thermal Shock (follows test 1)	Store for $\geq 6\text{hrs} @ 75\pm 2^\circ\text{C}$ , Store for $\geq 6\text{hrs} @ -40\pm 2^\circ\text{C}$ . Interval between extremes $\leq 30\text{mins}$ . Repeat 10 times.	Same 8 fully charged batteries	As above for fully charged batteries
		Same 8 fully discharged batteries	As above for fully discharged batteries
T3: Vibration (follows test 2)	Sinusoidal vibration, logarithmic sweep of 7Hz-200Hz-7Hz in 15minutes. Repeat 12 times in each of 3 perpendicular axes	Same 8 fully charged batteries	As above for fully charged batteries
		Same 8 fully discharged batteries	As above for fully discharged batteries
T4: Shock (follows test 3)	Half Sine shock of peak acceleration of 150G duration 6ms. 3 shocks in positive direction & 3 shocks in negative direction in each of 3 perpendicular axes: A total of 18	Same 8 fully charged batteries	As above for fully charged batteries
		Same 8 fully discharged batteries	As above for fully discharged batteries
T5: Short Circuit (follows test 4)	Stabilize the battery at $55\pm 2^\circ\text{C}$ . Short circuit the battery with $< 0.1\Omega$ for $\geq 1\text{hr}$ or until 1hr after the battery case has returned to $55\pm 2^\circ\text{C}$ . Observe for 6hrs.	Same 8 fully charged batteries	external temp $\leq 170^\circ\text{C}$ , no disassembly, no rupture, no fire within 6hrs of test.
		Same 8 fully discharged batteries	
T6: Impact Cell level test - done by Cell mfr. Not required if cell already has approval	15.8mm dia bar placed on the cell & 9.1kg mass dropped onto bar from a height of $61\pm 2.5\text{cm}$	Cylindrical cells used in batteries: 5 cells, cycle 1, 50% charged plus 5 cells, cycle 50, fully discharged.	external temp $\leq 170^\circ\text{C}$ , no disassembly, no rupture, no fire within 6hrs of test.
		Prismatic cells used in batteries: 10 cells, cycle 1, 50% charged plus 10 cells, cycle 50, fully discharged.	
T7: Overcharge Can follow test 5 if undamaged	Charge @ $20^\circ\text{C}\pm 5^\circ\text{C}$ @ twice the manufacturers recommended charge current.	4 new or undamaged batteries from 1-5, cycle 1 fully charged	No Disassembly & No Fire within 7 days of the test
		4 new or undamaged batteries from 1-5, cycle 50 fully charged	
T8: Forced Discharge Cell level test - done by Cell mfr. Not required if cell already has approval	@ $20^\circ\text{C}\pm 5^\circ\text{C}$ , connect each cell in series with a 12V DC power supply at an initial current equal to the manufacturers max rated discharge current for a time equal to the rated capacity divided by the initial test current.	Ten cells, Cycle 1, fully discharged Ten cells cycle 50 fully discharged	No Disassembly & No Fire within 7 days of the test

Inspired Energy 25440 NW 8<sup>th</sup> Place, Newberry, FL 32669  
 US toll free: 1-888-5-INSPIRE (1-888-546-7747) Tel: 352 472 4855, Fax: 352 472 4859  
[www.inspiredenergy.com](http://www.inspiredenergy.com)

Page 6 of 6

Copyright © Inspired Energy 2008

Shipping & Handling Li Ion Batteries 09-04-14.doc

THIS PAGE INTENTIONALLY LEFT BLANK

## APPENDIX F. EPS SIMULATION PARAMETER FILE

```
clear all
clc
format compact
format long
mu = 398600;
Re = 6378;
h = 500;

% Set beta angle
% 23.5 degrees for winter & summer solstice
% 0 degrees for vernal & autumnal equinox
beta = 0*pi/180;

rho = asin(Re/(Re+h));
orbit_period_sec = 2*pi/sqrt(mu)*(Re+h)^1.5
orbit_period_min = orbit_period_sec/60
time_in_eclipse_sec = orbit_period_sec*acos(cos(rho)/cos(beta))/pi
time_in_eclipse_min = time_in_eclipse_sec/60
time_in_sun_sec = orbit_period_sec - time_in_eclipse_sec
time_in_sun_min = time_in_sun_sec/60

% Set starting point of orbit
% -135 puts the satellite in eclipse for the first 320 seconds of the
% simulation.
nuo = -112*pi/180;

% Set the solar constant
% 1322 W/m^2 for summer solstice
% 1367 W/m^2 for vernal & autumnal equinox (mean value throughout the
year)
% 1414 W/m^2 for winter solstice
S = 1335;

% Loads
% 3.3V, 336uA (Texas Instruments MSP430; used formula on p.13 of data
sheet
% to calculate average current consumption).
cdh = [0          .0011088
       5676.8     .0011088];

% 3.3V, 336uA (TI MSP430)
adcs_ctlr = [0          .0011088
             5676.8     .0011088];

% 5V, .07A in normal mode (Analog Devices ADIS16400/ADIS16405)
imu = [0          .35
       5676.8     .35];
```

```

% Estimate: 5V, .4A (AeroAstro Miniature Star Tracker)
st = [0          2
      5676.8    2 ];

% 3.3V, .303A (Novatel OEMV -1/1G)
gps = [0          1
        5676.8    1 ];

% 5V, .015A at peak (Sinclair SS-411)
sun_sensor =[0          .075
              5676.8    .075 ];

% Sinclair 30mNm-sec; 5V. 2 at max (.4A), 1 at low speed steady state
% (.02A)
med = [0          4.1
        20         4.1
        20         1.2
        90         1.2
        90         4.1
        110        4.1
        110        1.2
        115        1.2
        115        4.1
        135        4.1
        135        1.2
        140        1.2
        140        4.1
        160        4.1
        160        1.2
        5676.8    1.2 ];

% Estimate MSP430 Controller on continuously and 2.5W for heating
during
% eclipse.  Uses Minco HK5951 commercial grade polyimide heater.
tcs_ctlr = [0          0.0011088
             140        0.0011088
             140        .0011088
             3532       .0011088
             3532       0.0011088
             5676.8    0.0011088];

tcs_heater = [0          2.5
               140        2.5
               140        0
               3532       0
               3532       2.5
               5676.8    2.5];

% 12V, .001A (Sleep) and 12V, .545A (TX & RX simultaneously)
% Used specs for n920 12V option because IP2421 says it uses from 9-
30VDC
% but doesn't have current or power specs. Reference email from Jeff
% stating that power consumption will be similar to n920. In future
can

```

```

% use actual measurements from radio.
comms = [ 0          .012
          20         .012
          20         6.54
          620        6.54
          620        .012
          5676.8     .012 ];

% 12V, .416667A. 10 minute pre-imaging warmup. Toshiba Teli
CleverDragon 12MP.
pyld_camera=[ 0          5
              140        5
              140        0
              5216.8     0
              5216.8     5
              5676.8     5  ];

% 5V, .8A. 10 minute pre-imaging warmup. Estimated from PC-104
version
% frame grabbers.
pyld_frame =[ 0          4
               140        4
               140        0
               5216.8     0
               5216.8     4
               5676.8     4  ];

% Power collection factor to account for not being able to collect
power
% when we're imaging. The satellite will not just be nadir pointing.
It
% could be up to 45 degrees off-nadir plus the impacts of beta for an
% equitorial orbit at the winter and summer solstices.
power_factor = [ 0          0
                  620        0
                  620        1
                  5676.8    1];

```

THIS PAGE INTENTIONALLY LEFT BLANK

## APPENDIX G. SOLAR INTENSITY VERSUS BETA MATLAB CODE

The following Matlab code creates a plot of solar Intensity versus TINYSOCPE's beta angle. The code was used to create Figure 19.

```

clear all;
close all;
clc;
format compact
format short g

% Representative solar intensity from Gilmore
% Maximum 1414 W/m^2 at winter solstice and minimum of 1322 W/m^2 at
% summer
% solstice. Average at equinoxes of approximately 1358W/m^2
x=linspace(0,2*pi,361);
y=-46*cos(x-pi/2)+1368;

% beta angle
day=0:1:360;      % days of year starting on March 21st
R=6378.135;        % Mean earth radius (km)
h=500;             % altitude (km)
u0=0;              % RA of sun in ecliptic
w0=0;              % RA of AN of orbit
i=97.402;          % inclination (degrees)
E=0;               % eccentricity
% nodal regression rate, wdot
wdot=-(9.96390003*(R/(R+h))^3.5*cos(i*pi/180))/(1-E^2)^2;
e=23.44241;        % earth axis tilt (degrees)
MSD=0.98564733;   % mean solar day
mu=398601.2;       % earth g constant
orb_rate=sqrt(mu/(R+h)^3);
orb_per=2*pi/orb_rate/60;
earth_ang_radius=asin(R/(R+h))*180/pi;
u=u0+MSD*day;
w=w0+wdot*day;
beta
=(180/pi)*asin(sin(u*pi/180).*sin(e*pi/180).*cos(i*pi/180)+cos(u*pi/180)
).*sin(i*pi/180).*sin(w*pi/180)-
sin(u*pi/180).*cos(e*pi/180).*sin(i*pi/180).*cos(w*pi/180));

% Calculate required inclination for 500km sun-synchronous orbit
% J2, below, is from table 4.3 of Curtis
J2=1.08263*10^(-3);
incl=180*acos((2*(-1.991*10^-7)*(R+h)^(7/2))/(3*sqrt(mu)*J2*R^2))/pi;

% Plot solar intensity and beta angle on same graph
h1 = line(x,y,'Color','r','linewidth',2);
ax1 = gca;
set(ax1,'XColor','r','YColor','r')

```

```

set(get(gca,'XLabel'), 'String', 'Season (Starting at Vernal
Equinox)', 'fontweight', 'bold')
set(get(gca,'YLabel'), 'String', 'Solar Intensity
(W/m^2)', 'fontweight', 'bold')
set(ax1,'XTick',[0 pi/2 pi 3/2*pi 2*pi]);
set(ax1,'XTickLabel','21 Mar|21 Jun|21 Sep|21 Dec|21
Mar', 'fontweight', 'bold');

ax2 = axes('Position',get(ax1,'Position'),...
            'XAxisLocation','top',...
            'YAxisLocation','right',...
            'Color','none',...
            'XColor','k','YColor','k','fontweight','bold');
set(get(gca,'XLabel'), 'String', 'Day of Year (Starting at Vernal
Equinox)', 'fontweight', 'bold')
set(get(gca,'YLabel'), 'String', 'Beta Angle
(Degrees)', 'fontweight', 'bold')
h12 = line(day,beta,'Color','k','Parent',ax2,'linewidth',2);
grid on;

```

## APPENDIX H. EFFICIENCY MEASUREMENTS

1	<b>All Loads Connected</b>	<b>Description</b>				
2	Power In from Ext DC Power Supply (BB, J7)					
3	Voltge	Measured	18.9000 V			
4	Current	Measured	0.7850 A			
5	Power	Line 3 * Line 4	14.8365 W			
6						
7	Measurements from BB to DC on J13					
8	Voltage	Measured	18.8 V			
9	Current 1	Measured	0.3550 A			
10	Current2	Measured	0.4050 A			
11	Total Current	Line 9 + Line 10	0.7600 A			
12	Power	Line 8 * Line 11	14.2880 W			
13	BB Efficiency	Line 12 / Line 5	<b>0.9630</b>			
14						
15	Power out at Load (J20 of DC)					
16			3.3V	5V	12V	-12V
17	Voltage	Measured	3.3100	4.9530	11.8180	-11.3950
18	Current	Measured	0.2810	0.6830	0.3540	-0.3370
19	Subtotal Power	Line 17 * Line 18	0.9301	3.3829	4.1836	3.8401
20	Total Power	Sum of Line 19	12.3367 W			
21	Overall Efficiency	Line 20 / Line 5	0.8315			
22						
23	<b>Only 3.3V Load Connected</b>					
24	Power In from Ext DC Power Supply (BB,J7)					
25	Voltge	Measured	18.9000 V			
26	Current	Measured	0.0710 A			
27	Power	Line 25 * Line 26	1.3419 W			
28						
29	Measurements from BB to DC on J13					
30	Voltage	Measured	18.9000 V			
31	Current 1	Measured	0.0340 A			
32	Current2	Measured	0.0320 A			
33	Total Current	Line 31 + Line 32	0.0660 A			
34	Power	Line 30 * Line 33	1.2474 W			
35	BB Efficiency	Line 34 / Line 27	<b>0.9296</b>			
36						
37	Power out at Load (J20 of DC)					
38			3.3V	5V	12V	-12V
39	Voltage	Measured	3.3100			
40	Current	Measured	0.2830			
41	Subtotal Power	Line 39 * Line 40	0.9367			
42	Total Power		0.9367 W			
43	DC-DC Converter Efficiency	Line 42 / Line 34	<b>0.7509</b>			
44	Overall Efficiency	Line 42 / Line 27	0.6981			

45						
46	<b>Only 5V Load Connected</b>					
47	Power In from Ext DC Power Supply (BB,J7)					
48	Voltge	Measured	18.9000	V		
49	Current	Measured	0.2120	A		
50	Power	Line 48 * Line 49	4.0068	W		
51						
52	Measurements from BB to DC on J13					
53	Voltage	Measured	18.9000	V		
54	Current 1	Measured	0.0950	A		
55	Current2	Measured	0.1100	A		
56	Total Current	Line 54 + Line 55	0.2050	A		
57	Power	Line 53 * Line 56	3.8745	W		
58	BB Efficiency	Line 57 / Line 50	0.9670			
59						
60	Power out at Load (J20 of DC)					
61			3.3V	5V	12V	-12V
62	Voltage	Measured		4.9530		
63	Current	Measured		0.6850		
64	Subtotal Power	Line 62 * Line 63		3.3928		
65	Total Power			3.3928	W	
66	DC-DC Converter Efficiency	Line 65 / Line 57	0.8757			
67	Overall Efficiency	Line 65 / Line 50	0.8468			
68						
69	<b>Only 12V Load Connected</b>					
70	Power In from Ext DC Power Supply (BB, J7)					
71	Voltge	Measured	18.9000	V		
72	Current	Measured	0.2450	A		
73	Power	Line 71 * Line 72	4.6305	W		
74						
75	Measurements from BB to DC on J13					
76	Voltage	Measured	18.9000	V		
77	Current 1	Measured	0.1090	A		
78	Current2	Measured	0.1210	A		
79	Total Current	Line 77 + Line 78	0.2300	A		
80	Power	Line 76 * Line 79	4.3470	W		
81	BB Efficiency	Line 80 / Line 73	0.9388			
82						
83	Power out at Load (J20 of DC)					
84			3.3V	5V	12V	-12V
85	Voltage	Measured		11.8950		
86	Current	Measured		0.3410		
87	Subtotal Power	Line 85 * Line 86		4.0562		
88	Total Power			4.0562	W	
89	DC-DC Converter Efficiency	Line 88 / Line 80	0.9331			
90	Overall Efficiency	Line 88 / Line 73	0.8760			

91						
92	<b>Only -12V Load Connected</b>					
93	Power In from Ext DC Power Supply (J7)					
94	Voltge	Measured	18.9000	V		
95	Current	Measured	0.3180	A		
96	Power	Line 94 * Line 95	6.0102	W		
97						
98	Measurements from BB to DC on J13					
99	Voltage	Measured	18.9000	V		
100	Current 1	Measured	0.1380	A		
101	Current2	Measured	0.1620	A		
102	Total Current	Line 100 + 101	0.3000	A		
103	Power	Line 99 * Line 102	5.6700	W		
104	BB Efficiency	Line 103 / Line 96	0.9434			
105						
106	Power out at Load (J20 of DC)					
107			3.3V	5V	12V	-12V
108	Voltage	Measured				-11.4580
109	Current	Measured				-0.3590
110	Subtotal Power	Line 108 * Line 109				4.1134
111	Total Power		4.1134	W		
112	DC-DC Converter Efficiency	Line 111 / Line 103	0.7255			
113	Overall Efficiency	Line 111 / Line 96	0.6844			
114						
115						
116	Average BB Efficiency	Average	0.9484			

1	<b>Charging Battery with no loads connected</b>	Description					
2	Power In From External DC Power Supply						
3	Voltage	Measured	18.9000	V			
4	Current	Measured	3.6700	A			
5	Power	Line 3 * Line 4	69.3630	W			
6							
7	Power Going into Battery						
8	Voltage	Measured	16.6100	V			
9	Current	Measured	3.8400	A			
10	Power	Line 8 * Line 9	63.7824	W			
11							
12	Efficiency		0.9195				
13							
14	<b>Charging Battery with all loads connected</b>						
15	Power In From External DC Power Supply						
16	Voltage	Measured	18.9000	V			
17	Current	Measured	3.8500	A			
18	Power	Line 16 * Line 17	72.7650	W			
19							
20	Power Going into Battery						
21	Voltage	Measured	16.5150	V			
22	Current	Measured	3.0500	A			
23	Power	Line 21 * Line 22	50.3708	W			
24							
25	Power Going into Loads						
26			3.3V	5V	12V	-12V	
27	Voltage	Measured	3.3100	4.4940	11.8430	-11.4100	
28	Current	Measured	0.3040	0.6980	0.3460	-0.3460	
29	Subtotal Power	Line 27 * Line 28	1.0062	3.1368	4.0977	3.9479	
30	Total Power	Sum of Line 29	12.1886				
31							
32	Efficiency	(Line 23 + Line 30) / Line 18	0.8597				
33							
34	Average Efficiency	Average of Lines 12 & 32	0.8896				

## **APPENDIX I. FUNCTIONAL TEST SOFTWARE & EQUIPMENT**

### **Software**

- Firebird Version 2.1.3 Database Management System. Must be installed to store data collected by OS\_Tester1.py.
- FlameRobin Version 0.9.3 Database Administration Tool. Used to interface with the Firebird database management system.
- Python Version 2.5 Object Oriented High Level Programming Language. Used as the platform for the two software programs below.
- OS\_Tester1.py Python Software to control baseline functional test (developed by Mr. Jim Horning)
- HH147.py temperature collection software. The Omega HH147 sends data via a serial RS-232 connection to the control computer with is stored in a comma separated value file by HH147.py.

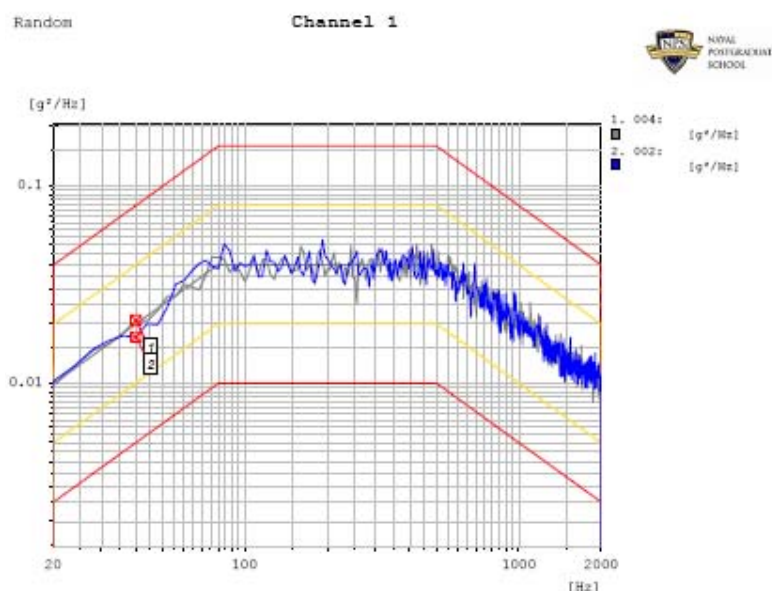
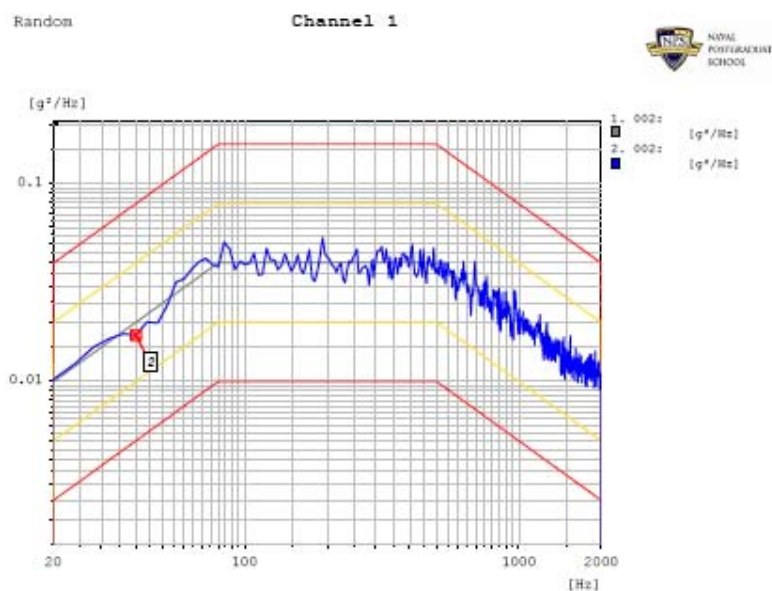
### **Hardware**

- One MASTECH MY64 Multimeter to measure battery voltages.
- Four Agilent 34410A 6 ½ Digit Multimeter controlled by OS-Tester1.py via LAN to monitor load voltages.
- One Agilent E3632A DC Power Supply controlled by OS\_Tester1.py via serial interface to power the base board.
- One Tektronix TDS 3034C Digital Phosphor Oscilloscope with Hall Effect sensor to measure battery current.
- One ZyXEL ES-2108 Router to route signals from the multimeters (used with loads).
- One Omega HH147 Four-Channel Handheld Data Logger Thermometer.
- One Tenney Model TJR Bench-Top Temperature Chamber.

THIS PAGE INTENTIONALLY LEFT BLANK

## APPENDIX J. VIBRATION TEST RESULTS

The plots below depict the GEVS random vibration tests conducted on the IBPS. The underlying black line is the test level while the yellow and red lines are warning and alarm levels. The blue line is the drive signal from the vibration software and the grey line is the error signal between the drive and the sense accelerometer on the DC to DC converter board.



THIS PAGE INTENTIONALLY LEFT BLANK

## APPENDIX K. THERMAL-VACUUM TEST PROCEDURES

### Test Setup Procedure

#### WARNING:

ENSURE NO ELECTRICAL POWER FROM BATTERIES OR EXTERNAL POWER SUPPLY IS CONNECTED TO EITHER BOARD OR ANY EXTERNAL CONNECTOR.

#### Setup Steps:

1. Turn on (4) multimeters.
2. Turn on (1) power supply. ENSURE THAT THAT THE OUTPUT IS SET TO "OFF".
3. Connect BB J10 to DC J10 with 10 pin flat ribbon cable.
4. Install temperature sensor equipment:
  - a. Install up to (4) temperature sensors on boards and internal walls of TVAC chamber.
  - b. Connect internal DB37 temperature sensor connector to TVAC temp. sensor connector.
  - c. Connect external temp sensor connectors to data logging device.
  - d. Connect serial DB9 connector from the Omega HH147 to a PC COM port.
  - e. Start HH147.py to begin logging temperatures.
  - f. Record which sensors correspond to HH147.py's data traces (T0, T1, T2, and T3).
5. Place BB and DC boards in TVAC chamber.
6. Ensure there are no metal or un-insulated wires touching any part of either board.
7. Connect Interim Connectors (ICs) DB15 and DB25 to respective DB15 and DB25 power board connectors.
8. Connect IC DB50 to TVAC chamber port (J23).
9. Install External Connector (EC) DB9 to J24. Connect J24 to computer serial port.
10. Install EC DB15 to J25.

POWER SUPPLY SHOULD ALREADY BE POWERED ON AND SET TO "OFF".

- a. EC DB15 Pin 1 goes to external power supply positive output (RED)
  - b. EC DB15 Pin 2 goes to external power supply return (BLACK)
  - c. EC DB15 Pins 3-9 are ganged to a DB9 connector that must be connected to the load bank.
11. Install EC DB25 to J26:
    - a. EC DB25 Pins 1-5 are ganged to a 5 pin AMP connector that goes to Battery 1. Do not connect battery 1.
    - b. EC DB25 Pins 9-13 are ganged to a 5 pin AMP connector that goes to Battery 2. Do not connect battery 2.
    - c. EC DB25 Pins 14-18 are ganged to a 5 pin AMP connector that goes to Battery 3. Do not connect battery 3.
    - d. EC DB25 Pins 21-25 are ganged to a 5 pin AMP connector that goes to Battery 4. Do not connect battery 4.
    - e. EC DB25 Pins 7 & 20 are ganged to an Ocean Server push button switch (yellow & black wire). Connect the Ocean Server switch.

Install multimeter probes across each resistor in the load bank.

## 28 October 2009 Test

### NOTES

Batteries must have less than 90% charge or they will not be charged by IBPS.

Battery charge percent of all four batteries should be close so that all batteries are charged and discharged during test.

### Procedure

1. Perform TVAC TEST SETUP procedure.
2. Before closing TVAC chamber door, perform functional test
  - a. Plug in batteries to 5 pin AMP connectors.
  - b. Double click "OS\_Tester1.py" on control computer desktop.
  - c. Maximize the main screen when it appears
  - d. Click "Enable Data Collection"
  - e. Wait 5 minutes.
  - f. Manually record voltage and current at terminals 1 & 5 of each battery.
  - g. Turn on loads via yellow and black push button switch.
  - h. Wait 5 minutes.
  - i. Manually record voltage and current at terminals 1 & 5 of each battery.
  - j. Click "Enable Power Supply".
  - k. Wait 5 minutes.
  - l. Manually record voltage and current at terminals 1 & 5 of each battery.
  - m. Click "Enable Data Collection" to remove check and disable data recording.
  - n. Turn off loads via yellow and black push button switch (must hold down for > 3 seconds).
  - o. Click "Enable Power Supply" to remove check and disable power supply.
  - p. Close OS\_Tester1.py.
  - q. Disconnect all batteries
3. Close TVAC chamber door.
4. Begin raising temperature and reducing pressure. Temperature should reach 70 degrees C. Reduce pressure to less than or equal to  $10^{-5}$  torr.

ALL EQUIPMENT MUST BE UNPOWERED BEFORE REDUCING PRESSURE OR DAMAGE MAY RESULT.
5. Once  $10^{-5}$  torr is reached:
  - a. Plug in batteries to 5 pin AMP connectors.
  - b. Double click "OS\_Tester1.py" on control computer desktop.
  - c. Maximize the main screen when it appears
  - d. Click "Enable Data Collection"
6. Once 70 degrees C AND pressure  $\leq 10^{-5}$  torr is reached:
  - a. Wait 60 minutes
  - b. Manually record voltage and current at terminals 1 & 5 of each battery.

- c. Turn on loads via yellow and black push button switch.
- d. Wait 5 minutes.
- e. Manually record voltage and current at terminals 1 & 5 of each battery.
- f. Click "Enable Power Supply".
- g. Wait 5 minutes.
- h. Manually record voltage and current at terminals 1 & 5 of each battery.
- i. Turn off loads via yellow and black push button switch (must hold down for > 3 seconds).
- j. Click "Enable Power Supply" to remove check and disable power supply.

DO NOT REMOVE POWER FROM THE BOARDS. BOARDS SHOULD NOW BE IN A QUIESCENT STATE I.E. USING APPROXIMATELY 25mA. CONTINUE TO COLLECT BASELINE DATA FROM THE BOARDS.

7. Reduce temperature to -30 degrees C.
  - a. Wait 60 minutes
  - b. Manually record voltage and current at terminals 1 & 5 of each battery.
  - c. Turn on loads via yellow and black push button switch.
  - d. Wait 5 minutes.
  - e. Manually record voltage and current at terminals 1 & 5 of each battery.
  - f. Click "Enable Power Supply".
  - g. Wait 5 minutes.
  - h. Manually record voltage and current at terminals 1 & 5 of each battery.
  - i. Turn off loads via yellow and black push button switch (must hold down for > 3 seconds).
  - j. Click "Enable Power Supply" to remove check and disable power supply.
8. If time permits, increase temperature to 70 degrees C and repeat steps 6 and 7.
9. Return temperature to starting ambient temperature.
  - a. Manually record voltage and current at terminals 1 & 5 of each battery.
  - b. Turn on loads via yellow and black push button switch.
  - c. Wait 5 minutes.
  - d. Manually record voltage and current at terminals 1 & 5 of each battery.
  - e. Click "Enable Power Supply".
  - f. Wait 5 minutes.
  - g. Manually record voltage and current at terminals 1 & 5 of each battery.
  - h. Click "Enable Data Collection" to remove check and disable data recording.
  - i. Turn off loads via yellow and black push button switch (must hold down for > 3 seconds).
  - j. Click "Enable Power Supply" to remove check and disable power supply.
  - k. Close OS\_Tester1.py.
  - l. Disconnect all batteries
10. Increase pressure to starting ambient pressure.

---

11. Open TVAC chamber door.
12. Run baseline functional test (steps 2a.-2q.)

## 17 November 2009 Test

### NOTES

Batteries must have less than 90% charge or they will not be charged by IBPS.

Battery charge percent of all four batteries should be close so that all batteries are charged and discharged during test.

### Procedure

1. Perform TVAC TEST SETUP procedure.
2. Close TVAC chamber door.
3. Begin dropping temperature and reducing pressure. Temperature should reach -30 degrees C. Reduce pressure to less than or equal to  $10^{-5}$  torr.

ALL EQUIPMENT MUST BE UNPOWERED BEFORE REDUCING PRESSURE OR DAMAGE  
MAY RESULT.
4. Once  $10^{-5}$  torr is reached:
  - a. Plug in batteries to 5 pin AMP connectors.
  - b. Double click "OS\_Tester1.py" on control computer desktop.
  - c. Maximize the main screen when it appears
  - d. Click "Enable Data Collection"
5. Once -30 degrees C AND pressure  $\leq 10^{-5}$  torr is reached:
  - a. Wait 60 minutes
  - b. Manually record voltage and current at terminals 1 & 5 of each battery.
  - c. Turn on loads via yellow and black push button switch.
  - d. Wait 5 minutes.
  - e. Manually record voltage and current at terminals 1 & 5 of each battery.
  - f. Click "Enable Power Supply".
  - g. Wait 5 minutes.
  - h. Manually record voltage and current at terminals 1 & 5 of each battery.
  - i. Turn off loads via yellow and black push button switch (must hold down for > 3 seconds).
  - j. Click "Enable Power Supply" to remove check and disable power supply.

DO NOT REMOVE POWER FROM THE BOARDS. BOARDS SHOULD NOW BE IN A QUIESCENT STATE I.E. USING APPROXIMATELY 25mA. CONTINUE TO COLLECT BASELINE DATA FROM THE BOARDS.

6. Return temperature to starting ambient temperature.
  - a. Manually record voltage and current at terminals 1 & 5 of each battery.
  - b. Turn on loads via yellow and black push button switch.
  - c. Wait 5 minutes.
  - d. Manually record voltage and current at terminals 1 & 5 of each battery.

- e. Click "Enable Power Supply".
  - f. Wait 5 minutes.
  - g. Manually record voltage and current at terminals 1 & 5 of each battery.
  - h. Click "Enable Data Collection" to remove check and disable data recording.
  - i. Turn off loads via yellow and black push button switch (must hold down for > 3 seconds).
  - j. Click "Enable Power Supply" to remove check and disable power supply.
  - k. Close OS\_Tester1.py.
  - l. Disconnect all batteries
7. Increase pressure to starting ambient pressure.
  8. Open TVAC chamber door.
  9. Run baseline functional test (steps 2a.-2q.)

THIS PAGE INTENTIONALLY LEFT BLANK

## APPENDIX L. THERMAL-VACUUM TEST NOTES

28 October 2009 Test

Time	Pressure (torr)	Tenney Temp (°C)	Bat1_V (V)	Bat1_I (mA)	Bat2_V (V)	Bat2_I (mA)	Bat3_V (V)	Bat3_I (mA)	Bat4_V (V)	Bat4_I (mA)	Notes (Steps refer to "TVAC TEST" Procedure)
0935	760	20	15.23	-9	15.3	-7	15.38	-1	15.28	-9	Began test, enabled data collection, took first measurements; step 2a
0941											Turned on loads; step 2g
0945	760	20	15.18	-150	15.22	-220	15.28	-340	15.21	-200	Step 2i
0946											Enabled power supply; step 2j
0949	760	20	15.32	340	15.37	260	15.44	163	15.37	285	Step 2l
0951											Enabled data collection; step 2m
1006											Began to raise temperature; 1006 is 1256749608 epoch seconds; step 4
1136											Board temps reached 790 C
1144	4.00E-05										
1202	2.70E-05										
1220	2.20E-05										
1250	1.80E-05										
1257											Connected batteries; brought up hyperterminal; all batteries working; step 5a
1258	1.70E-05										Brought up OS_Tester1.py; step 5b
1300			15.24	-12	15.3	-14.2	15.44	-25	15.28	-13	Boards are above 70 C and torr is near 1E-5; step 6b
1302											Turned on loads; step 6c
1306			15.18	-170	15.22	-237	15.3	-355	15.21	-215	Step 6e
1307											Enabled power supply; Step 6f
1314			15.33	505	15.42	440	15.42	-3	15.31	-3	Step 6h
1316											Turned off loads; step 6i
1318	1.80E-05										
1320											OS_Tester1.py is not responding to inputs.
1321											Disabled power supply thru OS_Tester1.py--it worked; closed OS_Tester1.py; opened hyperterminal; only batteries 1 and 2 showed up; data is reasonable; handheld multimeter shows good data across all four batteries.
1325											Restarted OS_Tester1.py; it reported only two batteries were working. Continue test with only 2 batteries
1327	1.70E-05										
1328											Turned on load; all loads worked off of batteries 1 and 2
1329											Turned off loads; turned on ambient cooling
1347	1.00E-05										
1352	8.60E-06										
1357	7.20E-06										
1400											Turned off ambient cooling; turned on sub-zero cooling
1401	6.20E-06										
1410	4.70E-06										
1421	4.50E-06										
1440	2.70E-06										
1500	2.00E-06										
1512	1.70E-06										
1534	1.40E-06										
1536			15.23	-60	15.24	-93					Step 7b
1537											Turned on loads; step 7c
1542			15.08	-548	15.1	-580					Step 7e
1542											Enabled power supply; step 7f
1547			15.34	453	15.36	420					
1555											Turned off data collection; closed OS_Tester1.py; started hyperterminal; unplugged batteries; plugged in batteries 3 & 4; IBPS got power but no data on batteries 3 & 4; plugged in batteries 1 & 2--their data showed up in hyperterminal
1555											Turned off sub-zero cooling; turned on "heat" and "door heat"
1557	1.30E-06										Closed hyperterminal; started OS_Tester1.py; enabled data collection; turned loads on to help with warming
1615	1.90E-06	42.7									Turned off loads; closed OS_Tester1.py; unplugged batteries
1617											Steps 8 through 10 were not performed as documented.

## 17 November 2009 Test

Time	Pressure (torr)	Tenney (°C)	Tenney								Notes (Steps refer to "COLD TVAC TEST" Procedure)
			Bat1_V (V)	Bat1_I (mA)	Bat2_V (V)	Bat2_I (mA)	Bat3_V (V)	Bat3_I (mA)	Bat4_V (V)	Bat4_I (mA)	
0905											Began test, enabled data collection, took first measurements
0925											Turned on sub-zero cooling
0935											"Lost" baseboard thermocouple
1005	4.00E-04	-46.2									
1029	3.20E-06	-57.5									
1040	3.20E-06	-65.1									
1041											
1144	1.90E-06	-76.5									
1244	1.50E-06	-77.9									
1315	1.50E-06	-77.8									
1344	1.40E-06	-77.1									
1400	1.50E-06	-73									
1409	1.40E-06	-72.6	15.07	-63	15.07	-71					Step 5
1411											Turned on loads; step 5c
1417			14.9	-573	14.9	-575					
1418											Enabled power supply; step 5f
1423			15.21	443	15.21	430					Step 5h
1423-											Continued to collect data in transit to ambient temperature and pressure; did not perform steps 6-9 as documented.
1513											Turned off thermocouples
1513											Turned off power supply
1514											Disabled data collection
1515											

## LIST OF REFERENCES

- [1] Allen Blocker, Chance Litton, Jason Hall, and Marcello Romano, "TINYSCOPE—The Feasibility of a 3-Axis Stabilized Earth Imaging Cubesat from LEO," in *AIAA/USU Conference on Small Satellites*, Logan, 2008, p. 10.
- [2] J. Allen Blocker, "TINYSCOPE: The Feasibility of a Tactically Useful, Three-Axis Stabilized, Earth-Imaging Nano-Satellite," Naval Postgraduate School, Monterey, Master's Thesis 2008.
- [3] C. Chance Litton, "TINYSCOPE: The Feasibility of a Tactically Useful Earth-Imaging Nanosatellite and a Preliminary Design of the Optical Payload," Naval Postgraduate School, Monterey, Master's Thesis 2009.
- [4] Susan K Mashiko, Results of 2009 DoD Space Experiments Review Board, 2009, Memorandum.
- [5] Christopher J. Ortona, "Systems Level Engineering of Advanced Experimental Nanosatellites," Naval Postgraduate School, Monterey, Master's Thesis 2009.
- [6] Patrick Hanrahan, "TINYSCOPE Payload," Naval Postgraduate School, Monterey, Master's Thesis 2009.
- [7] Jason Tuthill, "TINYSCOPE ADCS," Naval Postgraduate School, Monterey, Master's Thesis 2009.
- [8] California Polytechnic State University — San Luis Obispo. (2009, October) CubeSat Community Web site. [Online].  
[http://cubesat.atl.calpoly.edu/media/CDS\\_rev12.pdf](http://cubesat.atl.calpoly.edu/media/CDS_rev12.pdf), accessed Apr 09.
- [9] Hank Heidt, Jordi Puig-Suari, Augustus S. Moore, Shinichi Nakasuka, and Robert J. Twiggs, *CubeSat: A New Generation of Picosatellite for Education and Industry Low-Cost Space Experimentation*. Logan, United States of America: American Institute of Aeronautics and Astronautics / Utah State University, 2001.
- [10] Bryan Klofas, Jason Anderson, and Kyle Leveque, "A Survey of CubeSat Communications Systems," in *CubeSat Developer's Workshop*, San Luis Obispo, 2008, p. 36.
- [11] California Polytechnic Institute State University of San Luis Obispo. (2009, December) CubeSat.org. [Online]. <http://www.cubesat.org/>, accessed Apr 09.

- [12] Matthew Long et al., "A CubeSat Derived Design for a Unique Academic Research Mission in Earthquake Signature Detection," in *16th Annual/USU Conference on Small Satellites*, Logan, 2002, p. 17.
- [13] Thomas Bleier, Interview with Author, October 2006, Palo Alto, California.
- [14] QuakeFinder LLC. (2009, October) QuakeSat-1 Specs. [Online].  
<http://www.quakefinder.com/services/quakesat1specs.php>, accessed Mar 09.
- [15] Space Technology Library, *Space Mission Analysis and Design*, 3rd ed., James R. Wertz and Wiley J. Larson, Eds. Hawthorne, CA, USA: Microcosm Press & Springer, 1999.
- [16] Barry Leonard, AE3804 Thermal Control of Spacecraft Class Notes, 2008.
- [17] California Polytechnic State University — San Luis Obispo. (2007, August) CubeSat Community Website - Launch Providers. [Online].  
<http://cubesat.atl.calpoly.edu/media/P-POD%20Mk%20III%20ICD.pdf>, accessed Apr 09.
- [18] European Space Agency. (2009, November) SPENVIS. [Online].  
<http://www.spenvis.oma.be>
- [19] J. I. Vette. (2009, August) NASA Goddard Space Flight Center. [Online].  
<http://ccmc.gsfc.nasa.gov/modelweb/magnetas/aeap.html>, accessed Sep 09.
- [20] William O. Neel, Senior Engineering Specialist, August 2009, Interview with Author.
- [21] The Aerospace Corporation, *Spacecraft Thermal Control Handbook, Volume 1: Fundamental Technologies*, 2nd ed., David G. Gilmore, Ed. El Segundo, USA: Aerospace Press, 2002.
- [22] Ocean Server Technology, Inc. (2008, December) About Us. [Online].  
<http://www.ocean-server.com/aboutus.html>, accessed Sep 08.
- [23] Eric Anderson, Chris Dohan, and Aaron Sikora, "Solar Panel Peak Power Tracking System," Worcester Polytechnic Institute, Worcester, Major Qualifying Project MQP-SJB-1A03, 2003.
- [24] Ocean Server Technology, Inc. (2006, January) Downloads. [Online].  
<http://www.ocean-server.com/download/SOLARCHARGE.pdf>, accessed Sep 08.

- [25] The System Management Interface Forum, Inc. (2005, June) SMBus Specifications. [Online]. <http://smbus.org/specs/>, accessed Oct 09.
- [26] Inspired Energy. (2008, January) Shipping, Handling, & Transportation Guidelines. [Online].  
[http://www.inspiredenergy.com/Standard\\_Products/Shipping%20&%20Handling%20Li%20Ion%20Batteries%2009-04-14.pdf](http://www.inspiredenergy.com/Standard_Products/Shipping%20&%20Handling%20Li%20Ion%20Batteries%2009-04-14.pdf), accessed Oct 09.
- [27] Quallion, LLC. (2008, January) Quallion Home Page. [Online].  
<http://www.quallion.com/>, accessed Jul 09.
- [28] Saft, S.A. (2007, January) Saft Batteries Home Page. [Online].  
<http://www.saftbatteries.com/>, accessed Jul 09.
- [29] Chad William Melone, Interview with David Baggaley of Inspired Energy, Inc., 2009, Procedure for adjusting number of cycles relative to depth of discharge of lithium ion batteries.
- [30] David Halliday, Robert Resnick, and Jearl Walker, *Fundamentals of Physics*, 5th ed. New York, United States of America: John Wiley & Sons, Inc., 1997.
- [31] American Institute of Aeronautics and Astronautics, *Orbital Mechanics*, 3rd ed., Vladimir A Chobotov, Ed. Reston, USA: AIAA, 2002.
- [32] Ocean Server Technology, Inc. (2005, July) Downloads - Software Manual. [Online]. <http://www.ocean-server.com/download/swmanual.pdf>, accessed Mar 09.
- [33] Ocean Server Technology, Inc. (2008, June) Downloads - Hardware User's Guide. [Online]. <http://www.ocean-server.com/download/IBPSMANUAL.pdf>, accessed Mar 09.
- [34] Ocean Server Technology, Inc. (2008, September) Downloads - IBPS FAQ. [Online]. <http://www.ocean-server.com/download/FAQ.pdf>, accessed Mar 09.
- [35] AllPinouts.org. (2008, September) ATX Motherboard Power - 20 Pin (ver. 1.x) Connector Pinout. [Online].  
[http://www.allpinouts.org/index.php/ATX\\_Motherboard\\_Power\\_-\\_20\\_Pin\\_%28ver.\\_1.x%29](http://www.allpinouts.org/index.php/ATX_Motherboard_Power_-_20_Pin_%28ver._1.x%29), accessed May 09.
- [36] Chad William Melone, Interview with Small Satellite Laboratory Technician, 2009, Interview with Ron Phelps.
- [37] Roy Schmaus. (2005, February) Vacuum Technology Page. [Online].  
<http://www.ee.ualberta.ca/~schmaus/vacf/outgas.html>, accessed Oct 09.

- [38] Ocean Server Technology, Inc. (2006, January) Downloads - Solar Charging Application Note. [Online]. <http://www.ocean-server.com/download/SOLARCHARGE.pdf>, accessed Jun 09.
- [39] Power Film, Inc. (2008, January) Technical Specifications. [Online]. [http://www.powerfilmsolar.com/downloads/pdf/FoldableCharger\\_Flysheet\\_LOWRES.pdf](http://www.powerfilmsolar.com/downloads/pdf/FoldableCharger_Flysheet_LOWRES.pdf), accessed Mar 09.
- [40] Microhard Systems, Inc. (2008, January) Spectra 2420 Overview. [Online]. <http://www.microhardcorp.com/brochures/Spectra2420.Rev.3.0.pdf>, accessed Sep 08.
- [41] National Aeronautics and Space Administration Goddard Space Flight Center. (2005, April) General Environmental Verification Standard. [Online]. [http://www.goes-r.gov/procurement/flight\\_documents/GSFC-STD-7000.pdf](http://www.goes-r.gov/procurement/flight_documents/GSFC-STD-7000.pdf), accessed Oct 09.
- [42] The Aerospace Corporation. (2006, September) Test Requirements for Launch, Upper-Stage, and Space Vehicles. [Online]. [http://www.everspec.com/USAF/TORs/TR-2004%288583%29-1\\_REV\\_A\\_4984/](http://www.everspec.com/USAF/TORs/TR-2004%288583%29-1_REV_A_4984/), accessed Oct 09.
- [43] Brij N. Agrawal, Space Systems Laboratory Class Notes, 2008.
- [44] Chad W Melone, Jason Tuthill, Looyens Mike, and Ortiona Chris, "Final Project: TINYSCOPE Thermal Analysis," Naval Postgraduate School, Monterey, Class Project 2008.
- [45] Bleier Tom et al., "QuakeSat Lessons Learned: Notes from the Development of a Triple CubeSat," QuakeFinder, LLC, Palo Alto, 2004.
- [46] Felix Rossberg, "Simulation of the Deployment and Orbit Operations of the NPS-SCAT CubeSat," Naval Postgraduate School, Monterey, Master's Thesis 2008.
- [47] Gregory F. Hand, "Intermediate Design and Analysis of the PANSAT Electrical Power Subsystem," Naval Postgraduate School, Monterey, Masters Thesis 1994.
- [48] Lawrence Tyrone Dorn Jr., "NPS-SCAT; Electrical Power System," Naval Postgraduate School, Monterey, Master's Thesis 2009.
- [49] Brij N. Agrawal, *Design of Geosynchronous Spacecraft*. Englewood Cliffs, USA: Prentice-Hall, Inc., 1986.
- [50] System Management Interface Forum, Inc. (2005, February) Specs. [Online]. <http://www.smbus.org/specs/>, accessed Oct 09.

- [51] Molex. (2009, November) Data Sheet for Model Number 39012020. [Online].  
[http://www.molex.com/datasheets/pdf/0039012020\\_CRIMP\\_HOUSINGS.pdf](http://www.molex.com/datasheets/pdf/0039012020_CRIMP_HOUSINGS.pdf), accessed Nov 09.
- [52] Inspired Energy. (2007, January) Products. [Online].  
[http://www.inspiredenergy.com/Standard\\_Products/standard\\_products.htm](http://www.inspiredenergy.com/Standard_Products/standard_products.htm), accessed Mar 09.

THIS PAGE INTENTIONALLY LEFT BLANK

## **INITIAL DISTRIBUTION LIST**

1. Defense Technical Information Center  
Ft. Belvoir, Virginia
3. Dudley Knox Library  
Naval Postgraduate School  
Monterey, California
4. Professor Marcello Romano  
Naval Postgraduate School  
Monterey, California
5. Mr. Jim Horning  
Naval Postgraduate School  
Monterey, California
6. Professor Jim Newman  
Naval Postgraduate School  
Monterey, California